

NORSAR Scientific Report No. 1-97/98

Semiannual Technical Summary

1 April – 30 September 1997

Kjeller, November 1997

APPROVED FOR PUBLIC RELEASE, DISTRIBUTION UNLIMITED

REPORT DOCUMENTATION PAGE

1a. REPORT SECURITY CLASSIFICATION Unclassified			1b. RESTRICTIVE MARKINGS Not applicable		
2a. SECURITY CLASSIFICATION AUTHORITY Not Applicable			3. DISTRIBUTION / AVAILABILITY OF REPORT Approved for public release; distribution unlimited		
2b. DECLASSIFICATION / DOWNGRADING SCHEDULE			4. PERFORMING ORGANIZATION REPORT NUMBER(S) Scientific Rep.1-97/98		
4. PERFORMING ORGANIZATION REPORT NUMBER(S) Scientific Rep.1-97/98			5. MONITORING ORGANIZATION REPORT NUMBER(S) Scientific Rep. 1-97/98		
6a. NAME OF PERFORMING ORGANIZATION NFR/NORSAR.		6b. OFFICE SYMBOL (If applicable)	7a. NAME OF MONITORING ORGANIZATION HQ/AETAC/TTS		
6c. ADDRESS (City, State, and ZIP Code) Post Box 51 N-2007 Kjeller, Norway			7b. ADDRESS (City, State, and ZIP Code) Patrick AFB, FL 32925-6001		
8a. NAME OF FUNDING / SPONSORING ORGANIZATION Advanced Research Projects Agency/NTPO		8b. OFFICE SYMBOL (If applicable) NMRO/NTPO	9. PROCUREMENT INSTRUMENT IDENTIFICATION NUMBER Contract No. F08650-96-C-0001		
8c. ADDRESS (City, State, and ZIP Code) 1901 N. Moore St., Suite 609 Arlington, VA 22209			10. SOURCE OF FUNDING NUMBERS		
PROGRAM ELEMENT NO. R&D	PROJECT NO. NORSAR Phase 3	TASK NO. SOW Task 5.0	WORK UNIT ACCESSION NO. Sequence No. 004A2		
11. TITLE (Include Security Classification) Semiannual Technical Summary, 1 April - 30 September 1997					
12. PERSONAL AUTHOR(S)					
13a. TYPE OF REPORT Scientific Summary		13b. TIME COVERED FROM 1 APR 97 TO 30 SEP 97		14. DATE OF REPORT (Year, Month, Day) 1997 NOVEMBER	15. PAGE COUNT 141
16. SUPPLEMENTARY NOTATION					
17. COSATI CODES			18. SUBJECT TERMS (Continue on reverse if necessary and identify by block number)		
FIELD 8	GROUP 11.	SUB-GROUP	NORSAR, Norwegian Seismic Array		
19. ABSTRACT (Continue on reverse if necessary and identify by block number) This Semiannual Technical Summary describes the operation, maintenance and research activities at the Norwegian Seismic Array (NORSAR) , the Norwegian Regional Seismic Array (NORESS), the Arctic Regional Seismic Array (ARCESS) and the Spitsbergen Regional Array for the period 1 April - 30 September 1997. Statistics are also presented for additional seismic stations, which through cooperative agreements with institutions in the host countries provide continuous data to the NORSAR Data processing Center (NDPC). These stations comprise the Finnish Regional Seismic Array (FINESS), the German Regional Seismic Array (GERESS), the Hagfors array in Sweden and the regional seismic array in Apatity, Russia. (cont.)					
20. DISTRIBUTION / AVAILABILITY OF ABSTRACT <input type="checkbox"/> UNCLASSIFIED/UNLIMITED <input type="checkbox"/> SAME AS RPT. <input type="checkbox"/> DTIC USERS			21. ABSTRACT SECURITY CLASSIFICATION		
22a. NAME OF RESPONSIBLE INDIVIDUAL Mr. Michael C. Baker			22b. TELEPHONE (Include Area Code) (407) 494-4219	22c. OFFICE SYMBOL AETAC/TTS	

Abstract (cont.)

The NORSAR Detection Processing system has been operated throughout the period with an average uptime of 99.99%. A total of 2005 seismic events have been reported in the NORSAR monthly seismic bulletin for April through September 1997. The performance of the continuous alarm system and the automatic bulletin transfer to AFTAC has been satisfactory. Processing of requests for full NORSAR and regional array data on magnetic tapes has progressed according to established schedules.

This Semiannual Report also presents statistics from operation of the Regional Monitoring System (RMS). The RMS has been operated in a limited capacity, with continuous automatic detection and location and with analyst review of selected events of interest for GSETT-3. Data sources for the RMS have comprised all the regional arrays processed at NORSAR. The Generalized Beamforming (GBF) program is now used as a pre-processor to RMS.

On-line detection processing and data recording at the NORSAR Data Processing Center (NDPC) of NORESS, ARCESS, FINESS and GERESS data have been conducted throughout the period. Data from two small-aperture arrays at sites in Spitsbergen and Apatity, Kola Peninsula, as well as the Hagfors array in Sweden, have also been recorded and processed. Processing statistics for the arrays as well as results of the RMS analysis for the reporting period are given.

The operation of the regional arrays has proceeded normally in the period, except for an extended outage of the ARCESS array from 8 June to 29 August 1997. This outage was caused by an overvoltage from the commercial power line at the central array site. The Hub, the CIM and the UPS units were severely damaged, and had to be brought to NMC for repair.

Maintenance activities in the period comprise preventive/corrective maintenance in connection with all the NORSAR subarrays, NORESS and ARCESS. Other activities have involved repair of defective electronic equipment after thunderstorms in the array area, cable splicing and work in connection with the small-aperture array in Spitsbergen.

Summaries of seven scientific and technical contributions are presented in Chapter 7 of this report.

Section 7.1 summarizes the activities related to the GSETT-3 experiment and experience gained at the Norwegian NDC during the period 1 April - 30 September 1997. Norway has been contributing primary station data from three arrays: ARCESS, NORESS and NORSAR and one auxiliary array (Spitsbergen). Norway's NDC is also acting as a regional data center, forwarding data to the IDC from GSETT-3 primary and auxiliary stations in several countries. The work at the Norwegian NDC has continued to focus on operational aspects, like stable forwarding of data using the Alpha protocol, proper handling of outgoing and incoming messages, improvement to routines for dealing with failure of critical components, as well as implementation of other measures to ensure maximum reliability and robustness in providing data to the IDC. We will continue the efforts towards improvements and hardening of all critical data acquisition and data forwarding hardware and software components, so that requirements now established by the PrepCom related to operation of IMS stations can be met to the maximum extent possible. In line with recent PrepCom decisions, we envisage continuing the provision of

data from Norwegian IMS-designated stations without interruption to the PIDC, and later on, following certification, to the IDC in Vienna, via the new global communications infrastructure currently being elaborated by the PrepCom.

Section 7.2 gives a status report on the development and testing of the global Threshold Monitoring (TM) system at the Provisional International Data Center (PIDC), together with an outline of some ideas for future development of the system. During the reporting period we have been running successfully all the basic computational processes of the TM system on the PIDC testbed:

- Continuous calculation of short-term-averages (STAs) for all primary stations using the detection and feature extraction program (*DPX*) running in the Alpha processing pipeline.
- Continuous calculation of the three-station detection capability of the network for a set of 2562 globally distributed target areas, using the STAs calculated by *DFX*.
- Interpolation and reformatting of the three-station detection capability to facilitate map displays of the results.

We have verified that the basic computational processes of the TM system are now of sufficient quality to satisfy the requirements for transfer into the operational pipeline at the PIDC. Three types of products (plots) are available from the TM system. These products are designed to provide useful information to the international community on the performance and status of the primary seismic network used for CTBT monitoring. We plan in the near future to include in the TM system the bulk station magnitude corrections derived from the event station magnitudes reported in the Reviewed Event Bulletins (REBs). This will require little work, but it will significantly reduce the uncertainty associated with the estimated global detection capability.

Section 7.3 describes a new program, HYPOSAT, which has been developed for the purpose of utilizing the largest possible set of available information for locating events. Besides the usually used travel times and eventually azimuth information, this program also inverts for the observed ray parameters as well as for travel-time differences between phases observed at the same station. With this program all possible travel-time differences can be used as additional observations. Since all travel-time differences are dependent on the epicentral distance but not on the source time or systematic timing errors; the influence of such errors as well as velocity anomalies below the stations can be reduced by this approach. Examples are given applying various velocity models to locate the 16 August 1997 Kara Sea event using the HYPOSAT program.

Section 7.4 describes the current status of NORSAR large array processing at the IDC testbed, and includes as an appendix a summary of a memorandum to the IDC Configuration Control Board (CCB) recommending implementing NORSAR large-array processing in the operational pipeline. The section also gives a list of recommendations for the IDC based upon our experience from NORSAR testbed processing. In particular, care must be taken to include appropriate DC offset removal and tapering before applying digital filters. Some inconsistencies in the beamforming routines of the ARS station are pointed out, and corrective actions are suggested. Finally, recommendations are made for improved flexibility of the interactive f-k analysis.

Section 7.5 is a study of the seismic event near Novaya Zemlya on 16 August 1997. This event caused considerable interest, since initial analysis indicated that the seismic signals had characteristics similar to those of an explosion. The event provides a very useful case study of what might happen if an unusual seismic event is detected after a CTBT enters into force. It highlights the fact that even for a well-calibrated region like Novaya Zemlya, where numerous well-recorded underground nuclear explosions have been conducted, it is a difficult process to reliably locate and classify a seismic event of approximate $m_b=3.5$. We show that supplementary data from national networks can provide useful constraints on event location, especially if the azimuthal coverage of the monitoring network is inadequate. While the IDC processing functioned very well for this event, it should be taken due note of the fact that a second (smaller) event, not satisfying the current IDC event definition criteria, could be clearly singled out by detailed analysis of the IMS station at Spitsbergen. It might be useful to consider, for future processing, the possibility of the IDC carrying out routine searches for aftershocks in such cases of events of special interest. NORSAR's optimized threshold monitoring technique could provide a useful tool to help the analyst undertake such searches efficiently and easily.

Section 7.6 discusses P/S ratios for events near the Novaya Zemlya test site. The NORSAR large array has an extensive database of recordings from events near Novaya Zemlya, including some nuclear explosions of magnitudes similar to those of the 16 August 1997 event and the nearby earthquake of 1 August 1986. In this study we compare the P/S ratios for these events, as recorded by individual sensors in the array. We also make comparisons to observations from other available stations at regional distances. We find in particular that there is a remarkable and systematic increase in the NORSAR P/S ratio with increasing magnitude. This demonstrates that comparing the P/S ratios of large and small events could easily give misleading conclusions, and serves to suggest some caution in using data from large nuclear explosions to characterize the source of the small 16 August 1997 event.

Section 7.7 contains recommendations for improvements in IDC processing of the Matshushiro array (MJAR). We propose 1) To calculate the parameters to be used in the fk-analysis of MJAR data in accordance with the actual frequency content of each signal, 2) To modify the fk-analysis routine so that elevation differences between the array sites can be taken into account, and 3) To carry out an iterative search for the best frequency band, by choosing the analysis window around the maximum SNR value. In a longer perspective, a modification of the MJAR array configuration (i.e. minimum distance between sites, number of sites) is recommended, especially in order to improve the capability for estimating large slowness values at high frequencies. The definition of additional and well analyzed S onsets would improve the location of seismic events in the whole region surrounding MJAR.

AFTAC Project Authorization : T/6141/NORSAR
ARPA Order No. : 4138 AMD # 53
Program Code No. : 0F10
Name of Contractor : The Norwegian Research Council (NFR)
Effective Date of Contract : 1 Oct 1995
Contract Expiration Date : 30 Sep 1998
Project Manager : Frode Ringdal +47 63 80 59 00
Title of Work : The Norwegian Seismic Array
(NORSAR) Phase 3
Amount of Contract : \$ 2,958,528
Contract Period Covered by Report : 1 April - 30 September 1997

The views and conclusions contained in this document are those of the authors and should not be interpreted as necessarily representing the official policies, either expressed or implied, of the Advanced Research Projects Agency, the Air Force Technical Applications Center or the U.S. Government.

This research was supported by the Advanced Research Projects Agency of the Department of Defense and was monitored by AFTAC, Patrick AFB, FL32925, under contract no. F08650-96-C-0001.

NORSAR Contribution No. 627



Table of Contents

1	Summary.....	1
2	NORSAR Operation.....	4
2.1	Detection Processor (DP) operation.....	4
2.2	Array Communications.....	8
2.3	NORSAR Event Detection operation.....	15
3	Operation of Regional Arrays.....	20
3.1	Recording of NORESS data at NDPC, Kjeller.....	20
3.2	Recording of ARCESS data at NDPC, Kjeller.....	23
3.3	Recording of FINESS data at NDPC, Kjeller.....	26
3.4	Recording of Spitsbergen data at NDPC, Kjeller.....	29
3.5	Event detection operation.....	32
3.6	Regional Monitoring System operation.....	63
4	Improvements and Modifications.....	65
4.1	NORSAR.....	65
5	Maintenance Activities.....	68
6	Documentation Developed.....	73
7	Summary of Technical Reports / Papers Published.....	74
7.1	Status Report: Norway's participation in GSETT-3.....	74
7.2	Status of the global Threshold Monitoring (TM) system.....	83
7.3	HYPOSAT - A new routine to locate seismic events.....	94
7.4	NORSAR Large Array Processing at the IDC Testbed.....	103
7.5	The seismic event near Novaya Zemlya on 16 August 1997.....	110
7.6	P/S ratios for seismic events near Novaya Zemlya.....	120
7.7	Recommendations for improvements in the PIDC processing of Matsushiro (MJAR) array data.....	128



1 Summary

This Semiannual Technical Summary describes the operation, maintenance and research activities at the Norwegian Seismic Array (NORSAR), the Norwegian Regional Seismic Array (NORESS), the Arctic Regional Seismic Array (ARCESS) and the Spitsbergen Regional Array for the period 1 April - 30 September 1997. Statistics are also presented for additional seismic stations, which through cooperative agreements with institutions in the host countries provide continuous data to the NORSAR Data Processing Center (NPDC). These stations comprise the Finnish Regional Seismic Array (FINESS), the German Regional Seismic Array (GERESS), the Hagfors array in Sweden and the regional seismic array in Apatity, Russia.

The NORSAR Detection Processing system has been operated throughout the period with an average uptime of 99.99%. A total of 2005 seismic events have been reported in the NORSAR monthly seismic bulletin for April through September 1997. The performance of the continuous alarm system and the automatic bulletin transfer to AFTAC has been satisfactory. Processing of requests for full NORSAR and regional array data on magnetic tapes has progressed according to established schedules.

This Semiannual Report also presents statistics from operation of the Regional Monitoring System (RMS). The RMS has been operated in a limited capacity, with continuous automatic detection and location and with analyst review of selected events of interest for GSETT-3. Data sources for the RMS have comprised all the regional arrays processed at NORSAR. The Generalized Beamforming (GBF) program is now used as a pre-processor to RMS.

On-line detection processing and data recording at the NORSAR Data Processing Center (NDPC) of NORESS, ARCESS, FINESS and GERESS data have been conducted throughout the period. Data from two small-aperture arrays at sites in Spitsbergen and Apatity, Kola Peninsula, as well as the Hagfors array in Sweden, have also been recorded and processed. Processing statistics for the arrays as well as results of the RMS analysis for the reporting period are given.

The operation of the regional arrays has proceeded normally in the period, except for an extended outage of the ARCESS array from 8 June to 29 August 1997. This outage was caused by an overvoltage from the commercial power line at the central array site. The Hub, the CIM and the UPS units were severely damaged, and had to be brought to NMC for repair.

Maintenance activities in the period comprise preventive/corrective maintenance in connection with all the NORSAR subarrays, NORESS and ARCESS. Other activities have involved repair of defective electronic equipment after thunderstorms in the array area, cable splicing and work in connection with the small-aperture array in Spitsbergen.

Summaries of seven scientific and technical contributions are presented in Chapter 7 of this report.

Section 7.1 summarizes the activities related to the GSETT-3 experiment and experience gained at the Norwegian NDC during the period 1 April - 30 September 1997. Norway has been contributing primary station data from three arrays: ARCESS, NORESS and NORSAR and one auxiliary array (Spitsbergen). Norway's NDC is also acting as a regional data center, forwarding data to the IDC from GSETT-3 primary and auxiliary stations in several countries. The work at

the Norwegian NDC has continued to focus on operational aspects, like stable forwarding of data using the Alpha protocol, proper handling of outgoing and incoming messages, improvement to routines for dealing with failure of critical components, as well as implementation of other measures to ensure maximum reliability and robustness in providing data to the IDC. We will continue the efforts towards improvements and hardening of all critical data acquisition and data forwarding hardware and software components, so that requirements now established by the PrepCom related to operation of IMS stations can be met to the maximum extent possible. In line with recent PrepCom decisions, we envisage continuing the provision of data from Norwegian IMS-designated stations without interruption to the PIDC, and later on, following certification, to the IDC in Vienna, via the new global communications infrastructure currently being elaborated by the PrepCom.

Section 7.2 gives a status report on the development and testing of the global Threshold Monitoring (TM) system at the Provisional International Data Center (PIDC), together with an outline of some ideas for future development of the system. During the reporting period we have been running successfully all the basic computational processes of the TM system on the PIDC testbed:

- Continuous calculation of short-term-averages (STAs) for all primary stations using the detection and feature extraction program (*DPX*) running in the Alpha processing pipeline.
- Continuous calculation of the three-station detection capability of the network for a set of 2562 globally distributed target areas, using the STAs calculated by *DFX*.
- Interpolation and reformatting of the three-station detection capability to facilitate map displays of the results.

We have verified that the basic computational processes of the TM system are now of sufficient quality to satisfy the requirements for transfer into the operational pipeline at the PIDC. Three types of products (plots) are available from the TM system. These products are designed to provide useful information to the international community on the performance and status of the primary seismic network used for CTBT monitoring. We plan in the near future to include in the TM system the bulk station magnitude corrections derived from the event station magnitudes reported in the Reviewed Event Bulletins (REBs). This will require little work, but it will significantly reduce the uncertainty associated with the estimated global detection capability.

Section 7.3 describes a new program, HYPOSAT, which has been developed for the purpose of utilizing the largest possible set of available information for locating events. Besides the usually used travel times and eventually azimuth information, this program also inverts for the observed ray parameters as well as for travel-time differences between phases observed at the same station. With this program all possible travel-time differences can be used as additional observations. Since all travel-time differences are dependent on the epicentral distance but not on the source time or systematic timing errors; the influence of such errors as well as velocity anomalies below the stations can be reduced by this approach. Examples are given applying various velocity models to locate the 16 August 1997 Kara Sea event using the HYPOSAT program.

Section 7.4 describes the current status of NORSAR large array processing at the IDC testbed, and includes as an appendix a summary of a memorandum to the IDC Configuration Control Board (CCB) recommending implementing NORSAR large-array processing in the operational pipeline. The section also gives a list of recommendations for the IDC based upon our experience

from NORSAR testbed processing. In particular, care must be taken to include appropriate DC offset removal and tapering before applying digital filters. Some inconsistencies in the beam-forming routines of the ARS station are pointed out, and corrective actions are suggested. Finally, recommendations are made for improved flexibility of the interactive f-k analysis.

Section 7.5 is a study of the seismic event near Novaya Zemlya on 16 August 1997. This event caused considerable interest, since initial analysis indicated that the seismic signals had characteristics similar to those of an explosion. The event provides a very useful case study of what might happen if an unusual seismic event is detected after a CTBT enters into force. It highlights the fact that even for a well-calibrated region like Novaya Zemlya, where numerous well-recorded underground nuclear explosions have been conducted, it is a difficult process to reliably locate and classify a seismic event of approximate $m_b=3.5$. We show that supplementary data from national networks can provide useful constraints on event location, especially if the azimuthal coverage of the monitoring network is inadequate. While the IDC processing functioned very well for this event, it should be taken due note of the fact that a second (smaller) event, not satisfying the current IDC event definition criteria, could be clearly singled out by detailed analysis of the IMS station at Spitsbergen. It might be useful to consider, for future processing, the possibility of the IDC carrying out routine searches for aftershocks in such cases of events of special interest. NORSARs optimized threshold monitoring technique could provide a useful tool to help the analyst undertake such searches efficiently and easily.

Section 7.6 discusses P/S ratios for events near the Novaya Zemlya test site. The NORSAR large array has an extensive database of recordings from events near Novaya Zemlya, including some nuclear explosions of magnitudes similar to those of the 16 August 1997 event and the nearby earthquake of 1 August 1986. In this study we compare the P/S ratios for these events, as recorded by individual sensors in the array. We also make comparisons to observations from other available stations at regional distances. We find in particular that there is a remarkable and systematic increase in the NORSAR P/S ratio with increasing magnitude. This demonstrates that comparing the P/S ratios of large and small events could easily give misleading conclusions, and serves to suggest some caution in using data from large nuclear explosions to characterize the source of the small 16 August 1997 event.

Section 7.7 contains recommendations for improvements in IDC processing of the Matshushiro array (MJAR). We propose 1) To calculate the parameters to be used in the fk-analysis of MJAR data in accordance with the actual frequency content of each signal, 2) To modify the fk-analysis routine so that elevation differences between the array sites can be taken into account, and 3) To carry out an iterative search for the best frequency band, by choosing the analysis window around the maximum SNR value. In a longer perspective, a modification of the MJAR array configuration (i.e. minimum distance between sites, number of sites) is recommended, especially in order to improve the capability for estimating large slowness values at high frequencies. The definition of additional and well analyzed S onsets would improve the location of seismic events in the whole region surrounding MJAR.

Frode Ringdal

2 NORSAR Operation

2.1 Detection Processor (DP) operation

There was 1 break in the otherwise continuous operation of the NORSAR online system within the current 6-month reporting interval. The uptime percentage for the period is 99.99.

Fig. 2.1.1 and the accompanying Table 2.1.1 both show the daily DP downtime for the days between 1 April and 30 September 1997. The monthly recording times and percentages are given in Table 2.1.2.

The breaks can be grouped as follows:

a)	Hardware failure	1
b)	Stops related to program work or error	0
c)	Hardware maintenance stops	0
d)	Power jumps and breaks	0
e)	TOD error correction	0
f)	Communication lines	0

The total downtime for the period was 38 minutes. The mean-time-between-failures (MTBF) was 91.5 days.

J. Torstveit

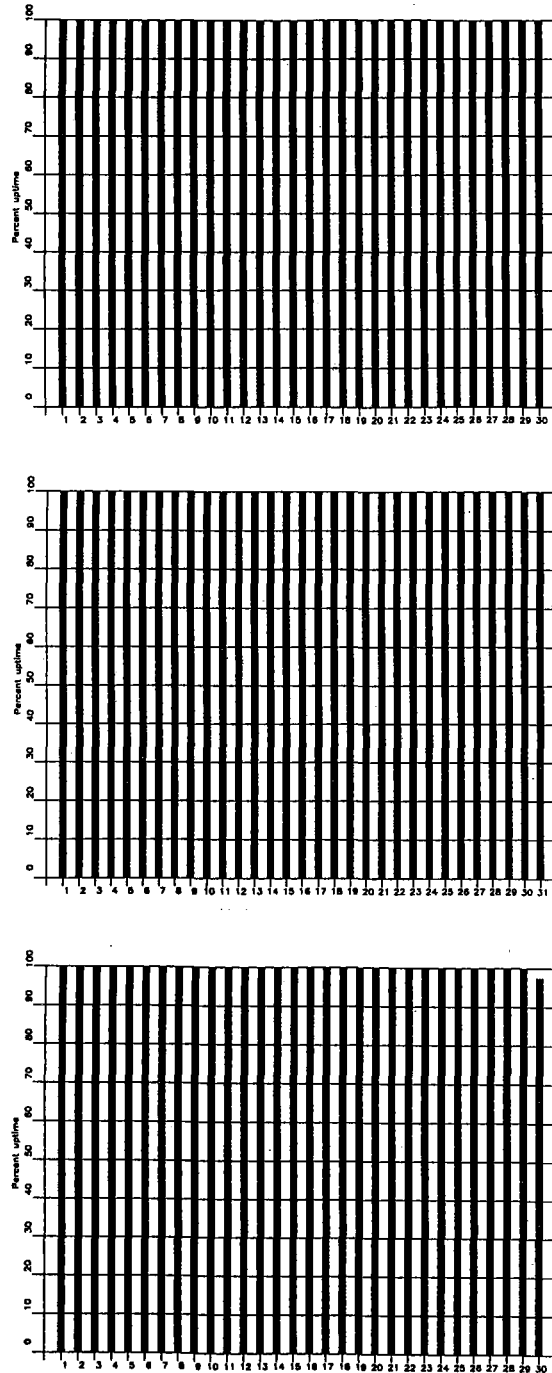


Fig. 2.1.1. Detection Processor uptime for April (top), May (middle) and June (bottom) 1997.

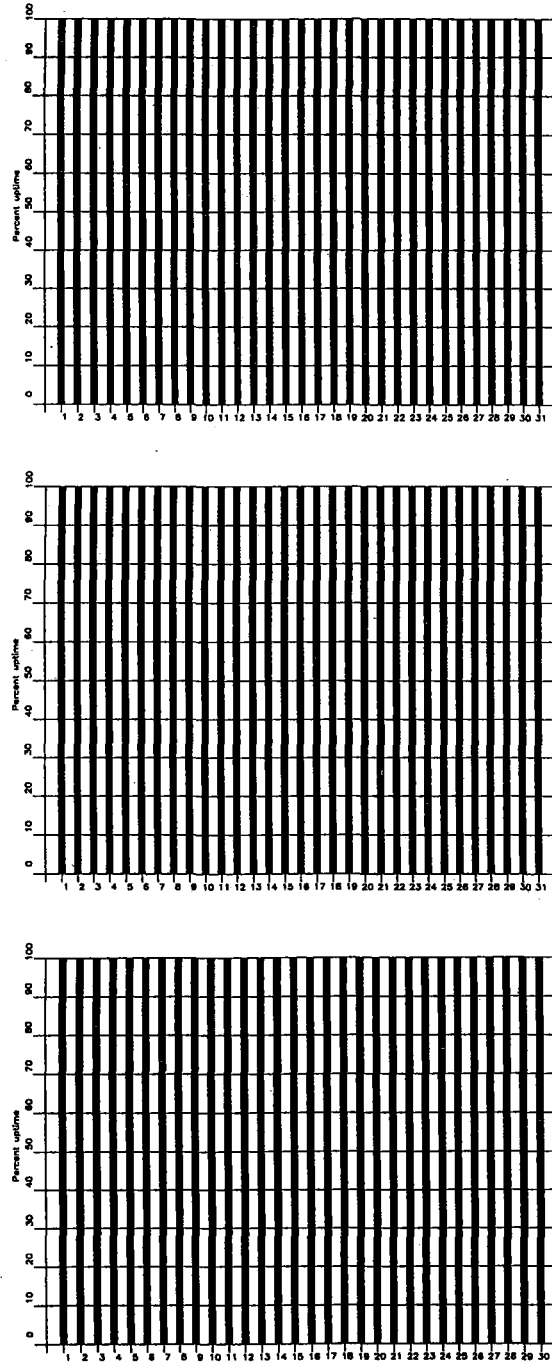


Fig. 2.1.1. Detection Processor uptime for July (top), August (middle) and September (bottom) 1997.

Date	Time	Cause
23 Jul	1041 - 1127	Software maintenance
23 Aug	1058 - 1128	Transmission line failure
16 Sep	1018 - 1320	Transmission line failure

Table 2.1.1. The major downtimes in the period 1 April - 30 September 1997.

Month	DP Uptime Hours	DP Uptime %	No. of DP Breaks	No. of Days with Breaks	DP MTBF* (days)
Apr 97	720.00	100	0	0	30.0
May	744.00	100	0	0	31.0
Jun	719.37	99.91	1	1	15.0
Jul	744.00	100	0	0	31.0
Aug	744.00	100	0	0	31.0
Sep	720.00	100	0	0	30.0
		99.99	1	1	

*Mean-time-between-failures = total uptime/no. of up intervals.

Table 2.1.2. Online system performance, 1 April - 30 September 1997.

2.2 Array Communications

After completion of the NORSAR refurbishment project, the operation of the subarray communication lines has proceeded normally.

For a complete description of the NORSAR refurbishment project, reference is made to Section 4.1 of the NORSAR Semiannual Technical Summary, 1 April - 30 September 1995.

From April through September 1997, there were no significant communications outages at any of the NORSAR subarrays.

A simplified daily summary of the communications performance for the seven individual subarray lines is summarized, on a month-by-month basis, in Table 2.2.1.

F. Ringdal

Table 2.2.1
NORSAR Communication Status Report
Month: April 1997

Day	Subarray						
	01A	01B	02B	02C	03C	04C	06C
01	X	X	X	X	X	X	X
02	X	X	X	X	X	X	X
03	X	X	X	X	X	X	X
04	X	X	X	X	X	X	X
05	X	X	X	X	X	X	X
06	X	X	X	X	X	X	X
07	X	X	X	X	X	X	X
08	X	X	X	X	X	X	X
09	X	X	X	X	X	X	X
10	X	X	X	X	X	X	X
11	X	X	X	X	X	X	X
12	X	X	X	X	X	X	X
13	X	X	X	X	X	X	X
14	X	X	X	X	X	X	X
15	X	X	X	X	X	X	X
16	X	X	X	X	X	X	X
17	X	X	X	X	X	X	X
18	X	X	X	X	X	X	X
19	X	X	X	X	X	X	X
20	X	X	X	X	X	X	X
21	X	X	X	X	X	X	X
22	X	X	X	X	X	X	X
23	X	X	X	X	X	X	X
24	X	X	X	X	X	X	X
25	X	X	X	X	X	X	X
26	X	X	X	X	X	X	X
27	X	X	X	X	X	X	X
28	X	X	X	X	X	X	X
29	X	X	X	X	X	X	X
30	X	X	X	X	X	X	X
31	-	-	-	-	-	-	-
Total hours normal operation	720	720	720	720	720	720	720
% normal operation	100	100	100	100	100	100	100

Legend:

- X : Normal operations
- A : All channels masked for more than 12 hours that day
- B : All SP channels masked for more than 12 hours that day
- C : All LP channels masked for more than 12 hours that day
- I : Communication outage for more than 12 hours

Table 2.2.1
NORSAR Communication Status Report
Month: May 1997

Day	Subarray						
	01A	01B	02B	02C	03C	04C	06C
01	X	X	X	X	X	X	X
02	X	X	X	X	X	X	X
03	X	X	X	X	X	X	X
04	X	X	X	X	X	X	X
05	X	X	X	X	X	X	X
06	X	X	X	X	X	X	X
07	X	X	X	X	X	X	X
08	X	X	X	X	X	X	X
09	X	X	X	X	X	X	X
10	X	X	X	X	X	X	X
11	X	X	X	X	X	X	X
12	X	X	X	X	X	X	X
13	X	X	X	X	X	X	X
14	X	X	X	X	X	X	X
15	X	X	X	X	X	X	X
16	X	X	X	X	X	X	X
17	X	X	X	X	X	X	X
18	X	X	X	X	X	X	X
19	X	X	X	X	X	X	X
20	X	X	X	X	X	X	X
21	X	X	X	X	X	X	X
22	X	X	X	X	X	X	X
23	X	X	X	X	X	X	X
24	X	X	X	X	X	X	X
25	X	X	X	X	X	X	X
26	X	X	X	X	X	X	X
27	X	X	X	X	X	X	X
28	X	X	X	X	X	X	X
29	X	X	X	X	X	X	X
30	X	X	X	X	X	X	X
31	X	X	X	X	X	X	X
Total hours normal operation	732.5	744	744	743	741.5	744	744
% normal operation	98.45	100	100	99.86	99.66	100	100

Legend:

- X : Normal operations
- A : All channels masked for more than 12 hours that day
- B : All SP channels masked for more than 12 hours that day
- C : All LP channels masked for more than 12 hours that day
- I : Communication outage for more than 12 hours

Table 2.2.1
NORSAR Communication Status Report
Month: June 1997

Day	Subarray						
	01A	01B	02B	02C	03C	04C	06C
01	X	X	X	X	X	X	X
02	X	X	X	X	X	X	X
03	X	X	X	X	X	X	X
04	X	X	X	X	X	X	X
05	X	X	X	X	X	X	X
06	X	X	X	X	X	X	X
07	X	X	X	X	X	X	X
08	X	X	X	X	X	X	X
09	X	X	X	X	X	X	X
10	X	X	X	X	X	X	X
11	X	X	X	X	X	X	X
12	X	X	X	X	X	X	X
13	X	X	X	X	X	X	X
14	X	X	X	X	X	X	X
15	X	X	X	X	X	X	X
16	X	X	X	X	X	X	X
17	X	X	X	X	X	X	X
18	X	X	X	X	X	X	X
19	X	X	X	X	X	X	X
20	X	X	X	X	X	X	X
21	X	X	X	X	X	X	X
22	X	X	X	X	X	X	X
23	X	X	X	X	X	X	X
24	X	X	X	X	X	X	X
25	X	X	X	X	X	X	X
26	X	X	X	X	X	X	X
27	X	X	X	X	X	X	X
28	X	X	X	X	X	X	X
29	X	X	X	X	X	X	X
30	X	X	X	X	X	X	X
31	-	-	-	-	-	-	-
Total hours normal operation	720	720	720	720	720	720	720
% normal operation	100	100	100	100	100	100	100

Legend:

- X : Normal operations
- A : All channels masked for more than 12 hours that day
- B : All SP channels masked for more than 12 hours that day
- C : All LP channels masked for more than 12 hours that day
- I : Communication outage for more than 12 hours

Table 2.2.1
NORSAR Communication Status Report
Month: July 1997

Day	Subarray						
	01A	01B	02B	02C	03C	04C	06C
01	A	X	A	X	X	X	X
02	X	X	A	X	X	X	X
03	X	X	A	X	X	X	X
04	X	X	X	X	X	X	X
05	X	X	X	X	X	X	X
06	X	X	X	X	X	X	X
07	X	X	X	X	X	X	X
08	X	X	X	X	X	X	X
09	X	X	X	X	X	X	X
10	X	X	X	X	X	X	X
11	X	X	X	X	X	X	X
12	X	X	X	X	X	X	X
13	X	X	X	X	X	X	X
14	X	X	X	X	X	X	X
15	X	X	X	X	X	X	X
16	X	X	X	X	X	X	X
17	X	X	X	X	X	X	X
18	X	X	X	X	X	X	X
19	X	X	X	X	X	X	X
20	X	X	X	X	X	X	X
21	X	X	X	X	X	X	X
22	X	X	X	X	X	X	X
23	X	X	X	X	X	X	X
24	X	X	X	X	X	X	X
25	X	X	X	X	X	X	X
26	X	X	X	X	X	X	X
27	X	X	X	X	X	X	X
28	X	X	X	X	X	X	X
29	X	X	X	X	X	X	X
30	X	X	X	X	X	X	X
31	X	X	X	X	X	X	X
Total hours normal operation	712	744	684	744	744	744	744
% normal operation	95.7	100	91.9	100	100	100	100

Legend:

- X : Normal operations
- A : All channels masked for more than 12 hours that day
- B : All SP channels masked for more than 12 hours that day
- C : All LP channels masked for more than 12 hours that day
- I : Communication outage for more than 12 hours

Table 2.2.1
NORSAR Communication Status Report
Month: August 1997

Day	Subarray						
	01A	01B	02B	02C	03C	04C	06C
01	X	X	X	X	X	X	X
02	X	X	X	X	X	X	X
03	X	X	X	X	X	X	X
04	X	X	X	X	X	X	X
05	X	X	X	X	X	X	X
06	X	X	X	X	X	X	X
07	X	X	X	X	X	X	X
08	X	X	X	X	X	X	X
09	X	X	X	X	X	X	X
10	X	X	X	X	X	X	X
11	X	X	X	X	X	X	X
12	X	X	X	X	X	X	X
13	X	X	X	X	X	X	X
14	X	X	X	X	X	X	X
15	X	X	X	X	X	X	X
16	X	X	X	X	X	X	X
17	X	X	X	X	X	X	X
18	X	X	X	X	X	X	X
19	X	X	X	X	X	X	X
20	X	X	X	X	X	X	X
21	X	X	X	X	X	X	X
22	X	X	X	X	X	X	X
23	X	X	X	X	X	X	X
24	X	X	X	X	X	X	X
25	X	X	X	X	X	X	X
26	X	X	X	X	X	X	X
27	X	X	X	X	X	X	X
28	X	X	X	X	X	X	X
29	X	X	X	X	X	X	X
30	X	X	X	X	X	X	X
31	X	X	X	X	X	X	X
Total hours normal operation	744	744	744	744	744	744	744
% normal operation	100	100	100	100	100	100	100

Legend:

- X : Normal operations
- A : All channels masked for more than 12 hours that day
- B : All SP channels masked for more than 12 hours that day
- C : All LP channels masked for more than 12 hours that day
- I : Communication outage for more than 12 hours

Table 2.2.1
NORSAR Communication Status Report
Month: September 1997

Day	Subarray						
	01A	01B	02B	02C	03C	04C	06C
01	X	X	X	X	X	X	X
02	X	X	X	X	X	X	X
03	X	X	X	X	X	X	X
04	X	X	X	X	X	X	X
05	X	X	X	X	X	X	X
06	X	X	X	X	X	X	X
07	X	X	X	X	X	X	X
08	X	X	X	X	X	X	X
09	X	X	X	X	X	X	X
10	X	X	X	X	X	X	X
11	X	X	X	X	X	X	X
12	X	X	X	X	X	X	X
13	X	X	X	X	X	X	X
14	X	X	X	X	X	X	X
15	X	X	X	X	X	X	X
16	X	X	X	X	X	X	X
17	X	X	X	X	X	X	X
18	X	X	X	X	X	X	X
19	X	X	X	X	X	X	X
20	X	X	X	X	X	X	X
21	X	X	X	X	X	X	X
22	X	X	X	X	X	X	X
23	X	X	X	X	X	X	X
24	X	X	X	X	X	X	X
25	X	X	X	X	X	X	X
26	X	X	X	X	X	X	X
27	X	X	X	X	X	X	X
28	X	X	X	X	X	X	X
29	X	X	X	X	X	X	X
30	X	X	X	X	X	X	X
31	-	-	-	-	-	-	-
Total hours normal operation	720	720	720	720	720	720	720
% normal operation	100	100	100	100	100	100	100

Legend:

- X : Normal operations
- A : All channels masked for more than 12 hours that day
- B : All SP channels masked for more than 12 hours that day
- C : All LP channels masked for more than 12 hours that day
- I : Communication outage for more than 12 hours

2.3 NORSAR Event Detection operation

In Table 2.3.1 some monthly statistics of the Detection and Event Processor operation are given. The table lists the total number of detections (DPX) triggered by the on-line detector, the total number of detections processed by the automatic event processor (EPX) and the total number of events accepted after analyst review (teleseismic phases, core phases and total).

	Total DPX	Total EPX	Accepted events		Sum	Daily
			P-phases	Core Phases		
Apr 97	9716	1056	295	86	381	12.7
May 97	7214	1301	293	79	372	12.0
Jun 97	5917	1301	134	72	306	10.2
Jul 97	7000	1655	285	55	340	11.0
Aug 97	5922	950	282	54	336	10.8
Sep 97	7916	670	205	65	270	9.0
			1594	411	2005	10.95

Table 2.3.1. Detection and Event Processor statistics, 1 April - 30 September 1997.

NORSAR Detections

The number of detections (phases) reported by the NORSAR detector during day 091, 1997, through day 273, 1997, was 43,685, giving an average of 239 detections per processed day (183 days processed). Table 2.3.2 shows daily and hourly distribution of detections for NORSAR.

B. Paulsen

NOA .DPX Hourly distribution of detections

Day	00	01	02	03	04	05	06	07	08	09	10	11	12	13	14	15	16	17	18	19	20	21	22	23	Sum	Date
91	21	11	18	20	19	6	0	2	2	12	3	16	14	11	19	8	36	12	24	25	13	18	28	14	352	Apr 01 Tuesday
92	19	17	20	23	15	11	0	0	7	24	5	9	5	12	9	13	16	10	32	21	13	13	14	14	322	Apr 02 Wednesday
93	15	17	18	10	17	7	17	6	9	8	7	8	11	13	19	17	18	17	11	13	17	14	19	21	329	Apr 03 Thursday
94	16	15	24	9	5	18	19	13	11	15	16	11	10	15	17	6	13	11	16	14	14	9	15	9	321	Apr 04 Friday
95	12	7	14	19	14	16	12	16	16	10	11	8	31	10	11	15	16	20	20	23	25	25	19	22	392	Apr 05 Saturday
96	19	20	15	16	23	26	36	23	13	18	16	17	17	16	12	11	13	19	14	13	7	6	11	9	390	Apr 06 Sunday
97	11	7	8	6	15	12	24	8	25	18	15	17	27	26	4	40	14	30	4	11	12	18	11	14	377	Apr 07 Monday
98	8	19	10	18	13	36	6	26	34	17	16	19	21	10	18	29	16	9	11	8	10	16	11	11	392	Apr 08 Tuesday
99	10	16	16	21	22	9	14	19	11	6	13	14	12	19	16	16	15	5	10	15	15	17	13	19	343	Apr 09 Wednesday
100	14	13	18	20	15	12	16	30	20	23	7	11	17	12	14	12	12	18	22	16	25	18	15	21	401	Apr 10 Thursday
101	8	17	13	17	13	17	6	6	0	21	21	5	22	5	11	11	18	10	14	11	15	13	16	12	302	Apr 11 Friday
102	20	18	24	20	19	19	19	16	17	19	24	19	8	14	14	21	9	18	22	9	24	21	12	14	421	Apr 12 Saturday
103	17	21	16	12	15	16	19	15	20	38	8	13	16	13	15	17	9	29	15	23	24	15	22	13	421	Apr 13 Sunday
104	9	10	17	14	11	4	5	12	19	1	12	12	1	2	5	6	12	2	14	9	9	12	13	20	231	Apr 14 Monday
105	31	13	22	19	22	10	6	12	12	8	14	9	18	14	14	7	14	15	20	10	19	15	14	15	353	Apr 15 Tuesday
106	22	30	10	13	4	4	16	14	30	22	2	21	23	12	11	15	15	5	9	12	10	10	10	12	332	Apr 16 Wednesday
107	18	20	12	21	11	17	16	16	15	15	15	13	28	5	11	8	12	10	9	17	19	16	21	18	363	Apr 17 Thursday
108	24	19	19	20	13	8	6	3	5	11	9	9	10	10	12	12	9	6	10	21	28	25	22	12	323	Apr 18 Friday
109	12	20	19	17	14	17	12	10	10	11	11	15	6	5	9	22	11	5	14	17	17	19	18	7	318	Apr 19 Saturday
110	17	8	8	4	10	30	17	9	10	5	9	10	11	16	12	7	8	12	12	20	16	25	21	16	315	Apr 20 Sunday
111	12	13	17	22	18	6	8	9	3	17	9	7	52	25	21	19	9	16	17	18	24	17	19	18	396	Apr 21 Monday
112	20	15	29	31	14	13	18	8	8	18	20	11	19	7	11	7	16	13	13	12	11	21	20	20	362	Apr 22 Tuesday
113	24	10	12	19	12	4	2	6	15	8	3	15	5	8	6	13	13	9	2	12	16	14	12	10	250	Apr 23 Wednesday
114	10	14	12	14	7	4	6	2	8	8	8	10	10	16	16	15	12	4	6	16	12	15	16	13	254	Apr 24 Thursday
115	17	26	14	30	10	15	16	10	9	0	11	7	8	5	15	12	13	7	24	2	10	14	8	12	295	Apr 25 Friday
116	12	18	13	2	10	24	12	18	9	15	19	4	12	5	10	7	8	9	14	13	18	10	15	16	293	Apr 26 Saturday
117	17	18	15	14	16	9	16	10	7	4	6	3	3	3	22	2	1	12	21	1	6	15	10	5	236	Apr 27 Sunday
118	18	16	6	21	7	9	1	9	8	6	8	5	13	19	21	11	6	11	1	4	10	16	18	13	257	Apr 28 Monday
119	12	16	18	13	13	2	0	5	10	3	7	4	10	12	8	0	5	15	2	4	11	8	7	15	200	Apr 29 Tuesday
120	12	5	5	9	0	14	1	1	7	8	12	14	4	15	3	4	1	4	13	6	10	19	8	11	186	Apr 30 Wednesday
121	10	16	13	19	9	15	8	13	5	11	8	9	5	7	14	7	16	14	18	24	17	19	22	24	323	May 01 Thursday
122	18	21	15	14	8	11	10	13	3	7	6	21	11	2	6	9	6	2	8	7	17	16	7	8	246	May 02 Friday
123	5	6	10	11	10	10	5	3	6	4	6	11	14	2	5	9	6	20	5	9	17	16	14	15	219	May 03 Saturday
124	19	19	6	15	22	14	13	10	6	12	5	5	5	4	1	9	7	5	19	9	16	12	19	16	268	May 04 Sunday
125	15	12	22	17	16	10	3	8	1	8	1	3	1	16	13	15	17	13	3	10	9	15	7	17	252	May 05 Monday
126	12	24	16	21	9	6	5	5	6	4	7	6	4	8	4	4	5	11	18	4	11	5	13	8	216	May 06 Tuesday
127	0	7	5	13	3	8	0	3	5	4	0	10	7	7	2	9	22	2	1	1	1	0	1	3	114	May 07 Wednesday
128	2	1	2	8	5	4	11	1	6	0	7	17	3	10	12	1	8	3	4	6	10	3	7	13	144	May 08 Thursday
129	7	5	5	10	4	8	4	2	3	13	4	9	0	2	12	3	4	15	9	7	3	5	6	5	145	May 09 Friday
130	3	5	2	6	12	10	8	2	24	10	13	4	1	7	13	5	0	7	2	13	3	7	5	11	173	May 10 Saturday
131	2	6	0	1	5	2	5	12	4	4	3	3	1	9	6	8	5	4	21	5	7	9	16	11	149	May 11 Sunday
132	10	4	3	19	10	1	7	4	3	9	1	15	32	58	40	20	10	16	1	6	6	4	10	15	304	May 12 Monday
133	10	15	8	11	6	17	8	8	8	2	8	28	2	19	23	46	16	4	26	12	5	14	20	22	338	May 13 Tuesday
134	27	8	17	29	25	21	19	9	13	24	29	17	16	9	46	85	82	28	7	5	13	26	13	20	588	May 14 Wednesday
135	9	6	11	8	22	4	6	15	12	12	27	4	22	6	0	8	20	13	16	1	0	1	2	0	225	May 15 Thursday
136	6	2	0	3	0	0	4	8	2	9	9	22	8	9	14	2	14	4	12	2	7	7	20	10	174	May 16 Friday
137	11	26	27	25	15	1	8	1	0	4	3	3	4	3	11	21	32	22	2	2	5	8	7	4	245	May 17 Saturday
138	1	20	10	11	16	31	4	7	1	8	22	5	6	12	57	99	37	15	7	14	4	11	16	22	436	May 18 Sunday
139	6	5	15	10	10	4	8	10	3	11	16	16	8	22	13	15	11	13	19	12	17	8	17	13	282	May 19 Monday
140	19	18	9	13	20	4	4	5	1	4	7	12	14	4	5	14	4	15	8	11	6	21	10	11	239	May 20 Tuesday
141	22	14	22	12	8	7	3	14	33	9	34	8	19	24	19	4	8	7	2	5	8	4	4	40	330	May 21 Wednesday
142	26	3	10	9	1	5	3	11	40	7	5	9	11	15	20	15	2	11	2	6	6	6	5	12	240	May 22 Thursday
143	14	10	8	11	6	7	0	11	7	5	10	13	5	15	3	9	2	12	27	12	21	9	7	14	238	May 23 Friday
144	7	4	4	10	7	12	3	5	6	2	1	15	1	9	2	2	1	6	5	8	2	4	3	3	122	May 24 Saturday
145	1	1	20	14	0	4	2	2	1	2	3	5	9	0	11	12	3	6	8	14	5	10	11	17	161	May 25 Sunday
146	22	18	10	6	6	28	4	2	10	7	3	7	7	2	5	8	15	23	0	3	1	5	4	11	207	May 26 Monday

Table 2.3.2 (Page 1 of 4)

NQA .DPX Hourly distribution of detections

Day	00	01	02	03	04	05	06	07	08	09	10	11	12	13	14	15	16	17	18	19	20	21	22	23	Sum	Date
147	9	7	17	11	4	14	9	9	13	7	8	9	33	9	1	11	6	5	3	3	6	6	13	14	227	May 27 Tuesday
148	9	3	10	4	7	10	11	3	1	16	10	16	14	29	53	5	6	12	24	2	1	6	11	7	270	May 28 Wednesday
149	14	9	5	7	6	10	3	4	3	0	8	6	16	17	5	6	1	7	7	6	1	2	7	3	153	May 29 Thursday
150	3	10	0	7	1	0	0	3	16	8	16	6	1	12	0	4	0	2	7	17	6	8	5	6	138	May 30 Friday
151	1	4	1	1	0	7	0	2	0	1	7	0	0	6	1	1	0	2	5	9	4	8	2	15	77	May 31 Saturday
152	2	1	8	0	1	3	2	4	2	1	12	7	4	3	4	5	1	5	5	4	5	7	8	1	95	Jun 01 Sunday
153	6	4	4	13	7	1	1	5	8	8	8	4	5	7	16	9	17	5	9	20	4	14	3	6	184	Jun 02 Monday
154	9	16	7	3	4	5	6	3	10	5	1	10	7	9	2	14	3	6	6	6	13	7	5	16	173	Jun 03 Tuesday
155	6	6	3	9	7	9	10	14	14	9	18	18	15	5	16	12	16	7	8	1	0	11	2	4	220	Jun 04 Wednesday
156	10	2	2	5	2	11	8	10	6	12	6	12	11	13	18	2	4	1	16	2	8	8	6	8	183	Jun 05 Thursday
157	16	6	13	23	16	0	2	5	2	1	10	5	7	0	1	3	1	3	2	3	13	4	11	5	152	Jun 06 Friday
158	5	5	16	9	5	8	9	6	5	5	5	13	10	7	3	6	6	10	9	9	10	3	9	10	183	Jun 07 Saturday
159	9	7	8	11	2	7	6	18	1	2	2	1	4	5	6	2	4	2	5	1	9	4	5	0	121	Jun 08 Sunday
160	2	6	5	12	0	6	0	7	1	3	12	6	4	8	32	10	5	4	4	0	7	3	7	0	144	Jun 09 Monday
161	1	5	0	2	1	4	4	5	2	16	3	9	10	3	20	3	7	1	5	0	2	0	3	4	110	Jun 10 Tuesday
162	11	15	0	3	6	3	3	16	2	12	7	16	11	17	11	4	5	9	4	19	8	2	0	2	186	Jun 11 Wednesday
163	8	4	0	0	1	10	6	2	2	15	7	12	9	1	16	0	5	0	10	6	0	1	3	0	118	Jun 12 Thursday
164	6	5	3	2	0	6	5	4	0	9	15	12	13	5	5	6	1	7	6	3	2	1	1	8	125	Jun 13 Friday
165	4	12	2	5	12	1	0	2	2	6	18	10	16	3	8	7	3	17	8	8	3	6	4	5	162	Jun 14 Saturday
166	7	18	11	9	11	11	10	11	9	12	21	7	6	9	11	13	7	15	9	6	8	4	5	5	235	Jun 15 Sunday
167	6	5	8	13	3	2	2	0	7	9	15	18	9	12	21	16	18	9	4	2	7	4	11	10	211	Jun 16 Monday
168	7	4	3	5	3	6	3	2	4	8	12	15	2	15	14	2	1	5	4	3	7	27	17	13	182	Jun 17 Tuesday
169	9	2	10	2	1	0	2	11	10	2	11	7	12	6	13	15	17	11	1	20	4	9	13	8	196	Jun 18 Wednesday
170	12	2	0	12	2	3	4	8	19	15	15	11	4	5	8	13	10	9	2	2	3	17	28	37	241	Jun 19 Thursday
171	12	7	14	9	3	8	2	7	9	11	7	12	4	18	6	19	10	3	0	9	16	1	12	8	207	Jun 20 Friday
172	11	7	7	10	16	0	6	3	19	28	42	16	29	14	18	20	12	12	6	24	13	11	18	23	365	Jun 21 Saturday
173	19	19	11	14	18	11	15	15	22	12	9	15	16	17	23	12	11	13	16	11	10	14	11	9	343	Jun 22 Sunday
174	6	12	9	3	6	10	2	9	3	3	2	11	10	2	8	6	16	4	3	11	4	5	8	3	156	Jun 23 Monday
175	11	10	10	14	13	14	15	7	6	29	12	15	31	23	26	15	5	18	7	10	18	10	12	20	351	Jun 24 Tuesday
176	18	9	13	12	15	8	12	15	13	17	18	5	26	14	11	11	7	6	10	24	10	17	13	9	313	Jun 25 Wednesday
177	6	7	7	5	5	13	8	21	27	5	12	18	11	7	10	7	13	6	8	10	13	12	10	14	255	Jun 26 Thursday
178	9	11	12	9	14	17	2	9	4	12	11	8	13	5	24	14	24	11	2	5	7	2	3	4	232	Jun 27 Friday
179	2	4	10	4	6	4	18	2	13	3	7	2	6	6	8	3	5	1	12	15	4	4	9	1	149	Jun 28 Saturday
180	5	2	1	7	14	0	0	3	4	2	2	0	2	1	4	2	2	11	1	3	24	4	4	4	102	Jun 29 Sunday
181	0	0	0	0	0	0	0	0	0	0	0	0	0	0	0	0	0	0	0	0	22	19104101			246	Jun 30 Monday
182	138	18	7	8	7	2	1	0	5	2	5	13	5	2	4	7	3	11	27	9	14	78	29	9	404	Jul 01 Tuesday
183	3	5	4	12	22	16	26	15	3	5	11	5	2	1	3	3	0	2	6	1	1	2	1	1	150	Jul 02 Wednesday
184	1	5	3	2	0	5	3	8	1	0	4	10	21	12	2	6	4	1	8	0	2	2	0	1	101	Jul 03 Thursday
185	1	6	2	1	0	3	0	0	0	0	7	12	6	16	1	4	1	2	11	3	0	3	1	6	86	Jul 04 Friday
186	13	0	0	1	0	1	5	11	1	3	0	0	0	5	1	0	1	0	0	2	6	4	4	9	67	Jul 05 Saturday
187	5	0	6	3	2	0	4	0	5	6	6	1	9	3	7	2	0	1	4	15	14	5	8	0	106	Jul 06 Sunday
188	5	2	4	1	2	1	8	3	3	0	12	33	12	11	3	0	9	1	5	3	4	11	2	3	138	Jul 07 Monday
189	3	5	18	2	2	1	5	4	5	5	4	9	23	10	7	7	6	9	0	4	6	7	6	1	149	Jul 08 Tuesday
190	8	11	5	2	4	1	2	4	8	20	14	3	9	13	14	7	2	22	0	15	8	4	9	3	188	Jul 09 Wednesday
191	0	5	5	10	9	3	7	0	9	7	4	11	9	3	21	12	8	4	12	8	4	7	1	14	173	Jul 10 Thursday
192	6	11	7	8	4	2	3	5	7	20	19	5	10	18	13	18	2	1	1	3	0	0	4	0	167	Jul 11 Friday
193	5	12	1	0	9	1	1	0	0	3	1	1	0	3	2	1	3	7	8	0	8	0	1	10	77	Jul 12 Saturday
194	8	8	3	1	0	3	1	0	1	0	0	1	2	1	6	4	8	2	4	7	4	0	5	3	72	Jul 13 Sunday
195	8	10	2	1	2	5	5	1	1	8	9	18	9	10	11	8	14	1	1	1	1	0	6	3	135	Jul 14 Monday
196	3	1	1	3	7	3	2	4	3	0	13	6	3	7	9	4	2	4	3	2	3	7	0	1	91	Jul 15 Tuesday
197	1	1	8	0	0	0	1	5	2	13	18	23	7	10	7	0	2	4	4	9	0	8	1	2	126	Jul 16 Wednesday
198	8	5	3	8	6	0	0	6	2	5	9	5	14	8	9	19	11	0	6	5	0	1	2	4	136	Jul 17 Thursday
199	9	4	7	6	5	1	8	12	4	12	5	22	44	29	18	21	1	12	17	16	9	8	6	8	284	Jul 18 Friday
200	8	4	5	8	6	3	6	6	5	2	11	8	10	7	13	3	13	6	6	5	6	11	4	12	168	Jul 19 Saturday
201	10	17	7	18	5	14	5	4	10	15	21	2	6	11	8	6	10	11	6	8	6	7	4	7	218	Jul 20 Sunday
202	4	8	12	7	13	7	0	1	1	16	17	17	56	188	53	92	49	15	4	3	1	5	1	4	574	Jul 21 Monday

Table 2.3.2. (Page 2 of 4)

NOA .DPX Hourly distribution of detections

Day	00	01	02	03	04	05	06	07	08	09	10	11	12	13	14	15	16	17	18	19	20	21	22	23	Sum	Date		
203	9	6	4	3	4	0	0	0	7	10	55	49	50	69	37	12	33	13	5	7	6	3	17	9	408	Jul 22	Tuesday	
204	9	5	12	11	0	3	4	2	6	7	82	55	50	34	60	52	42	35	19	20	8	6	7	6	535	Jul 23	Wednesday	
205	14	10	6	9	11	5	15	11	4	8	33	25	14	28	21	12	39	38	4	4	6	10	7	9	343	Jul 24	Thursday	
206	10	8	17	9	11	7	1	2	4	16	16	46	131	68	26	30	13	20	5	3	8	3	2	4	460	Jul 25	Friday	
207	9	3	13	5	12	6	19	11	8	17	12	6	26	28	25	38	49	46	22	28	14	18	8	14	437	Jul 26	Saturday	
208	13	9	19	8	9	5	11	12	12	7	21	19	20	20	25	28	15	21	13	20	16	18	12	18	371	Jul 27	Sunday	
209	10	14	11	11	8	13	14	11	11	9	16	15	12	5	7	13	14	3	14	6	15	11	13	11	267	Jul 28	Monday	
210	8	6	10	14	9	5	4	9	7	7	6	15	8	12	12	7	4	8	2	13	9	5	8	200	Jul 29	Tuesday		
211	7	3	11	19	5	11	6	9	7	2	5	7	4	7	11	10	9	10	7	18	10	10	12	6	206	Jul 30	Wednesday	
212	11	7	15	8	8	5	5	2	2	5	3	10	9	5	12	4	24	6	7	3	4	6	37	6	204	Jul 31	Thursday	
213	5	2	6	1	2	2	4	3	3	7	11	5	13	2	3	10	5	5	4	11	14	13	12	5	148	Aug 01	Friday	
214	19	7	11	7	5	6	6	10	1	3	2	8	1	3	4	6	7	6	2	7	7	8	7	7	150	Aug 02	Saturday	
215	10	9	6	15	10	9	19	4	12	7	14	5	5	3	2	9	9	4	11	6	10	6	7	13	205	Aug 03	Sunday	
216	9	11	14	11	11	7	0	13	11	13	2	20	14	5	6	6	13	9	5	8	7	9	5	8	217	Aug 04	Monday	
217	3	12	11	8	4	11	5	10	6	12	5	26	8	17	15	11	18	11	3	8	11	17	6	10	248	Aug 05	Tuesday	
218	21	9	8	7	8	6	6	10	9	11	7	23	4	14	5	22	7	4	2	2	1	1	2	2	191	Aug 06	Wednesday	
219	11	10	4	5	7	4	9	6	11	0	13	24	9	14	6	6	3	5	8	2	2	2	2	4	0	165	Aug 07	Thursday
220	3	9	16	11	3	4	4	15	9	5	12	9	5	8	6	6	7	18	15	13	17	20	14	22	251	Aug 08	Friday	
221	20	18	22	12	23	18	18	9	15	3	10	10	9	9	11	12	7	14	6	6	6	6	3	3	270	Aug 09	Saturday	
222	6	9	7	10	13	16	15	12	12	23	4	5	6	14	17	13	6	5	8	4	7	9	18	9	248	Aug 10	Sunday	
223	11	20	10	11	4	6	8	5	2	13	6	11	7	5	4	4	16	3	0	7	4	7	6	3	173	Aug 11	Monday	
224	8	18	13	4	7	5	6	6	17	8	2	15	8	12	5	13	9	1	9	6	12	1	4	4	193	Aug 12	Tuesday	
225	13	5	9	6	9	6	3	6	14	4	6	3	6	5	15	2	17	5	7	0	5	5	3	10	164	Aug 13	Wednesday	
226	8	8	8	4	4	6	7	9	4	2	0	5	13	8	7	1	8	6	8	14	3	3	3	3	142	Aug 14	Thursday	
227	7	10	6	1	6	5	4	3	0	1	7	5	17	1	1	3	18	2	8	15	6	4	4	6	140	Aug 15	Friday	
228	11	14	13	12	4	8	1	9	0	12	3	3	2	6	6	4	3	0	3	3	5	4	3	5	134	Aug 16	Saturday	
229	9	7	8	7	7	15	19	10	13	11	4	18	5	10	5	8	4	3	5	6	10	4	3	17	208	Aug 17	Sunday	
230	7	11	3	9	5	2	5	3	6	9	2	11	15	2	12	3	15	4	5	5	1	0	3	1	139	Aug 18	Monday	
231	8	3	3	11	4	12	0	2	6	10	8	14	4	11	7	10	8	6	14	5	4	4	4	4	162	Aug 19	Tuesday	
232	2	1	3	0	0	9	0	12	0	0	9	9	14	4	14	11	9	3	2	6	1	5	11	11	136	Aug 20	Wednesday	
233	6	9	8	6	7	5	1	2	8	0	4	3	17	17	5	11	7	4	12	6	18	15	23	9	203	Aug 21	Thursday	
234	15	14	9	14	13	1	5	1	6	11	6	12	11	6	15	10	14	9	10	11	16	12	11	14	246	Aug 22	Friday	
235	21	10	21	24	22	20	20	13	14	16	14	12	12	3	11	10	19	10	13	18	15	12	13	5	348	Aug 23	Saturday	
236	17	14	17	21	7	9	12	11	11	13	8	14	13	15	7	10	14	8	6	10	8	15	11	7	278	Aug 24	Sunday	
237	16	15	14	10	9	3	3	8	1	0	5	12	15	15	8	1	13	7	4	6	2	8	11	9	195	Aug 25	Monday	
238	21	8	1	10	1	2	1	1	10	10	15	5	11	16	0	13	8	4	1	0	9	11	6	0	164	Aug 26	Tuesday	
239	4	8	7	6	0	1	1	18	5	2	4	7	9	12	20	8	0	0	2	3	9	4	4	9	143	Aug 27	Wednesday	
240	13	11	12	11	2	0	6	3	3	3	1	11	13	3	5	3	1	8	10	10	10	10	11	11	170	Aug 28	Thursday	
241	15	7	14	7	9	5	4	3	12	12	6	3	6	5	19	14	12	9	5	13	12	6	3	10	211	Aug 29	Friday	
242	7	6	9	21	9	25	11	8	5	9	4	6	8	4	6	3	6	7	9	5	1	10	13	3	195	Aug 30	Saturday	
243	8	1	2	2	1	12	0	10	6	1	5	10	2	7	11	1	3	0	1	2	3	2	3	4	97	Aug 31	Sunday	
244	10	4	4	9	5	3	0	6	2	2	6	5	13	5	7	4	2	4	5	4	11	3	5	9	128	Sep 01	Monday	
245	21	12	11	6	12	0	0	8	9	0	6	2	12	15	5	10	10	0	7	4	5	0	4	6	165	Sep 02	Tuesday	
246	3	1	4	3	3	0	4	0	3	7	2	0	2	7	2	1	8	1	1	10	8	6	18	10	104	Sep 03	Wednesday	
247	16	11	16	10	20	9	7	5	4	2	1	8	6	6	7	10	5	8	8	17	9	11	13	12	221	Sep 04	Thursday	
248	10	15	17	11	8	5	5	6	4	8	8	11	8	4	7	15	9	10	12	13	14	12	10	16	238	Sep 05	Friday	
249	14	17	13	16	9	13	18	13	9	12	7	18	4	8	7	5	14	19	5	9	14	4	2	20	270	Sep 06	Saturday	
250	16	9	15	8	10	11	11	12	11	6	22	13	14	22	25	13	21	12	19	31	20	25	19	24	389	Sep 07	Sunday	
251	20	23	22	24	24	17	14	13	12	11	14	13	9	13	11	13	16	12	15	8	6	17	12	19	358	Sep 08	Monday	
252	15	12	10	8	15	15	5	7	7	6	4	1	1	7	8	11	17	10	14	13	15	8	12	16	237	Sep 09	Tuesday	
253	9	16	19	20	18	7	13	11	11	12	4	10	11	17	13	13	5	9	9	8	17	16	17	15	300	Sep 10	Wednesday	
254	17	18	19	10	12	2	1	1	0	4	8	3	4	13	8	12	13	5	6	9	15	16	12	15	223	Sep 11	Thursday	
255	13	14	19	15	8	2	4	4	5	9	13	2	13	2	5	16	17	17	6	17	12	15	11	13	252	Sep 12	Friday	
256	9	10	16	17	10	11	14	14	10	14	13	7	15	13	11	11	9	21	18	21	11	15	12	9	311	Sep 13	Saturday	
257	18	16	20	19	24	20	24	26	20	17	22	16	13	18	19	16	18	25	14	19	18	13	19	16	450	Sep 14	Sunday	
258	26	26	12	12	16	12	14	9	9	10	11	10	10	18	14	16	16	15	21	21	17	13	19	12	359	Sep 15	Monday	

Table 2.3.2. (Page 3 of 4)

NOA .DPX Hourly distribution of detections

Day	00	01	02	03	04	05	06	07	08	09	10	11	12	13	14	15	16	17	18	19	20	21	22	23	Sum	Date
259	18	15	17	18	11	5	8	7	7	11	7	5	15	25	3	6	6	18	11	11	14	10	7	16	271	Sep 16 Tuesday
260	10	8	11	17	13	7	9	7	7	9	9	5	7	11	9	26	6	9	13	12	8	17	9	21	260	Sep 17 Wednesday
261	18	11	14	22	15	12	14	10	7	13	8	7	12	12	11	16	5	7	17	11	15	19	22	16	314	Sep 18 Thursday
262	12	11	22	18	14	8	3	11	5	9	6	10	9	7	7	8	13	8	10	11	20	10	15	13	260	Sep 19 Friday
263	10	18	12	29	21	13	14	12	14	14	10	18	15	15	12	33	19	18	20	17	22	19	16	16	407	Sep 20 Saturday
264	22	22	19	19	22	20	17	15	12	10	9	13	16	13	18	14	15	10	18	19	12	14	27	17	393	Sep 21 Sunday
265	12	9	11	9	9	2	9	10	2	7	5	4	9	2	16	8	8	10	15	6	12	10	13	14	212	Sep 22 Monday
266	12	7	12	22	8	5	3	14	28	5	3	3	24	13	8	9	8	6	5	4	25	4	9	11	248	Sep 23 Tuesday
267	13	16	15	18	6	2	2	3	14	7	5	6	2	6	12	11	3	5	7	3	6	4	11	6	183	Sep 24 Wednesday
268	9	10	5	10	5	13	3	4	11	1	16	8	14	7	8	8	7	5	6	11	12	7	8	15	203	Sep 25 Thursday
269	13	12	9	13	20	3	1	5	7	15	14	11	11	7	14	7	20	9	8	8	18	4	20	9	258	Sep 26 Friday
270	5	6	9	6	9	14	11	12	13	7	11	7	5	13	5	6	1	8	8	6	13	9	9	11	204	Sep 27 Saturday
271	11	15	9	10	5	3	7	12	16	5	4	6	6	3	11	6	7	0	7	12	5	6	22	17	205	Sep 28 Sunday
272	17	15	19	14	6	3	8	11	8	0	4	10	9	10	16	7	6	17	11	7	24	14	7	11	254	Sep 29 Monday
273	13	14	10	16	15	5	18	6	9	9	8	0	8	3	10	7	5	11	8	8	15	11	21	14	244	Sep 30 Tuesday
NOA	00	01	02	03	04	05	06	07	08	09	10	11	12	13	14	15	16	17	18	19	20	21	22	23		
Sum	1900	1998	1484	1438	1598	1965	2177	2130	1707	1687	1809	2002														
	2137	1907	1645	1331	1499	1853	2204	2194	1964	1663	1806	1965	44063	Total sum												
183	12	10	10	11	9	8	7	8	8	9	10	11	12	12	12	12	11	9	9	9	10	10	11	11	241	Total average
128	12	10	10	11	8	7	6	7	8	9	10	12	13	13	12	12	11	9	9	8	9	10	11	11	237	Average workdays
55	10	11	11	11	10	11	10	9	9	9	10	9	9	9	11	11	10	11	10	11	11	10	11	11	244	Average weekends

Table 2.3.2. Daily and hourly distribution of NORSAR detections. For each day is shown number of detections within each hour of the day and number of detections for that day. The end statistics give total number of detections distributed for each hour and the total sum of detections during the period. The averages show number of processed days, hourly distribution and average per processed day. (Page 4 of 4)

3 Operation of Regional Arrays

3.1 Recording of NORESS data at NDPC, Kjeller

The average recording time was 99.83% as compared to 99.54% during the previous reporting period.

Table 3.1.1 lists the main outage times and reasons.

Date	Time	Cause
30 Jul	1206 - 1233	Hardware failure due to thunderstorm
15 Aug	0858 - 0925	CE maintenance
16 Aug	1936 - 2114	Transmission line failure
17 Aug	1731 - 1747	Transmission line failure
17 Aug	1825 - 2158	Transmission line failure

Table 3.1.1. Interruptions in recording of NORESS data at NDPC, 1 April - 30 September 1997.

Monthly uptimes for the NORESS on-line data recording task, taking into account all factors (field installations, transmissions line, data center operation) affecting this task were as follows:

April 97	:	99.97
May	:	99.99
June	:	99.99
July	:	99.93
August	:	99.13
September	:	99.99

Fig. 3.1.1 shows the uptime for the data recording task, or equivalently, the availability of NORESS data in our tape archive, on a day-by-day basis, for the reporting period.

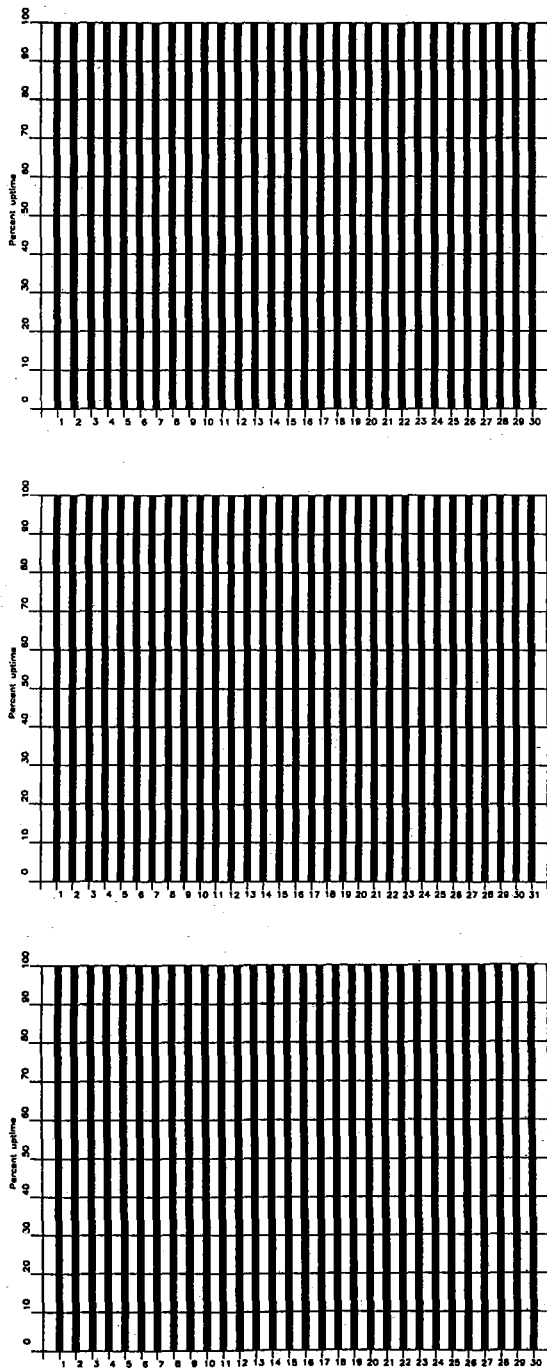


Fig. 3.1.1. NORESS data recording uptime for April (top), May (middle) and June (bottom) 1997.

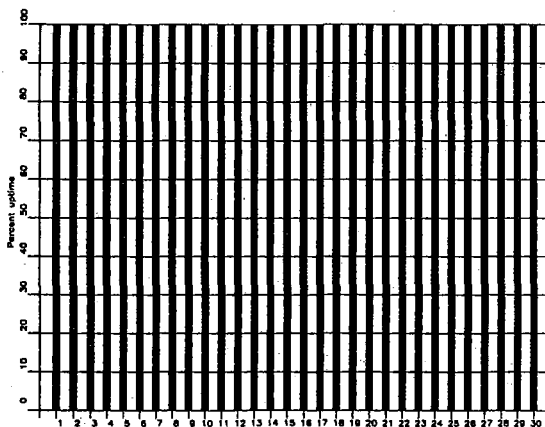
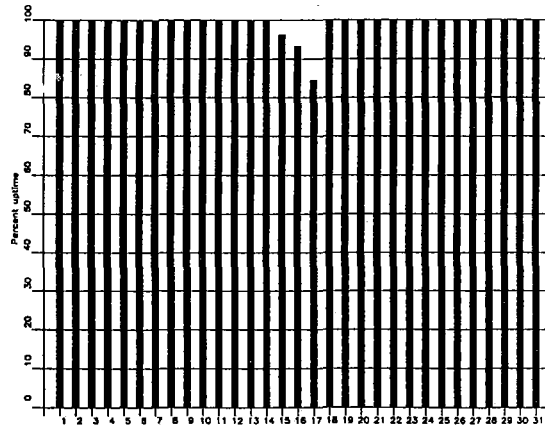
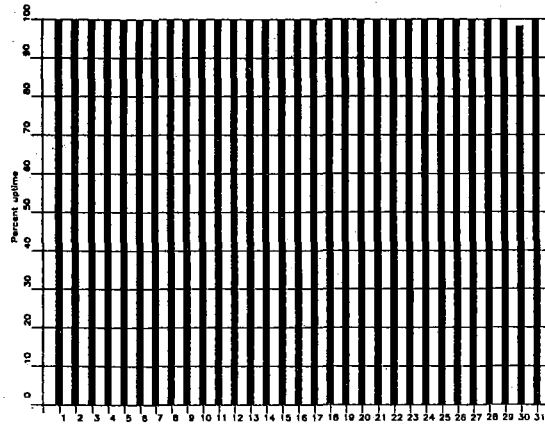


Fig. 3.1.1. (cont.) NORESS data recording uptime for July(top), August (middle) and September (bottom) 1997.

3.2 Recording of ARCESS data at NDPC, Kjeller

The average recording time was 53.53% as compared to 99.02% for the previous reporting period. The reason for this low uptime of ARCESS is an extended outage from 8 June to 29 August, caused by an overvoltage from the commercial power line. This caused severe damage to both the Hub, the CIM and the UPS units, which all had to be brought to NMC for repair. The array equipment was reinstalled on 29 August, and has functioned well since then.

Table 3.2.1 lists the main outage times and reasons.

Date	Time	Cause
27 Apr	1622 -	Hardware failure Hub
28 Apr	- 1534	
27 May	2221 -	Power failure Hub
28 May	- 1852	
08 Jun	2347 -	Hardware failure Hub
29 Aug	- 0950	
02 Sep	0621 -	Power failure Hub
03 Sep	- 1601	
15 Sep	1244 - 1933	Power failure Hub
22 Sep	0255 - 1728	Power failure Hub, UPS repaired

Table 3.2.1. The main interruptions in recording of ARCESS data at NDPC, 1 April - 30 September 1997.

Monthly uptimes for the ARCESS on-line data recording task, taking into account all factors (field installations, transmissions line, data center operation) affecting this task were as follows:

April 97	:	96.78%
May	:	97.17%
June	:	26.63%
July	:	0.0%
August	:	8.31%
September	:	92.30%

Fig. 3.2.1. shows the uptime for the data recording task, or equivalently, the availability of ARCESS data in our tape archive, on a day-by-day basis, for the reporting period.

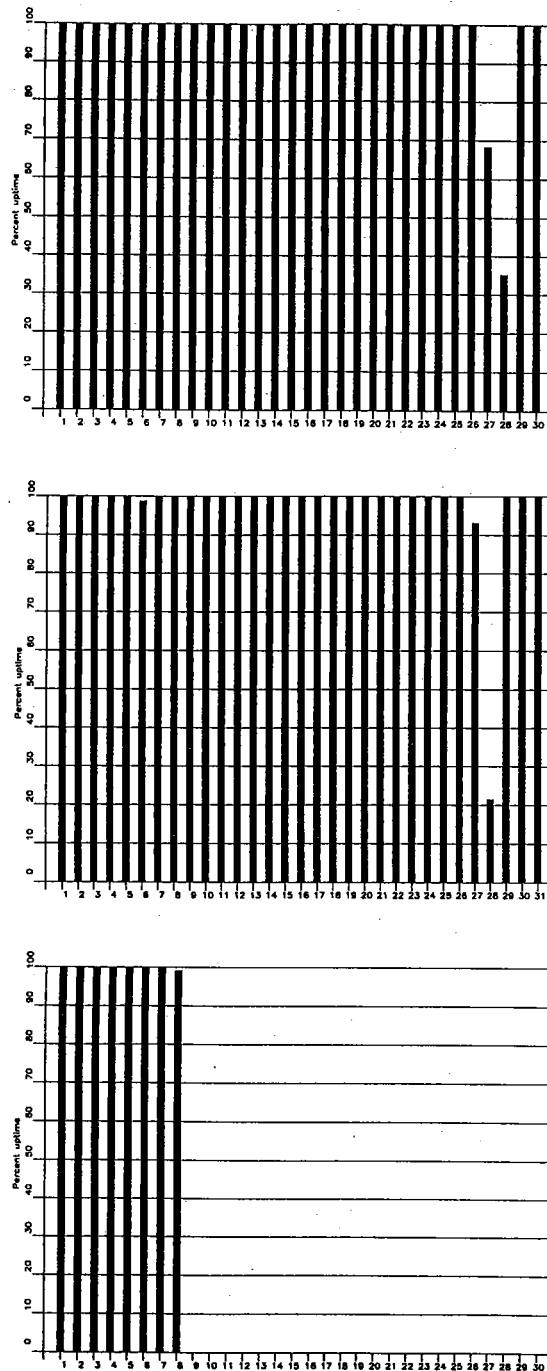


Fig. 3.2.1. ARCESS data recording uptime for April (top), May (middle) and June (bottom) 1997.

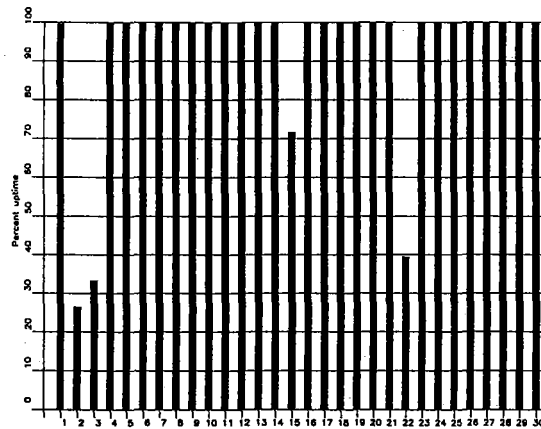
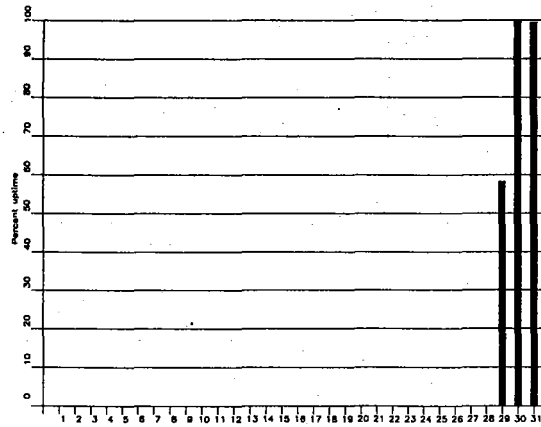


Fig. 3.2.1. (cont.) ARCESS data recording uptime for August (top) and September (bottom) 1997. Note that ARCESS was out of operation for all of July

3.3 Recording of FINESS data at NDPC, Kjeller

The average recording time was 99.44% as compared to 99.49% for the previous reporting period.

Date	Time	Cause
02 Jun	0050 - 0550	Transmission line failure
04 Jul	1227 - 1240	Transmission line failure
05 Jul	1346 - 1406	Hardware failure Helsinki
06 Jul	0805 - 0858	Transmission line failure
07 Jul	2204 - 2354	Transmission line failure
08 Jul	1503 - 1549	Transmission line failure
09 Jul	2216 - 2251	Transmission line failure
25 Aug	1747 -	Transmission line failure
26 Aug	- 0330	

Table 3.3.1. The main interruptions in recording of FINESS data at NDPC, 1 April - 30 September 1997.

Monthly uptimes for the FINESS on-line data recording task, taking into account all factors (field installations, transmission lines, data center operation) affecting this task were as follows:

April 97	:	100.00%
May	:	100.00%
June	:	99.30%
July	:	98.94%
August	:	98.48%
September	:	99.92%

Fig. 3.3.1 shows the uptime for the data recording task, or equivalently, the availability of FINESS data in our tape archive, on a day-by-day basis, for the reporting period.

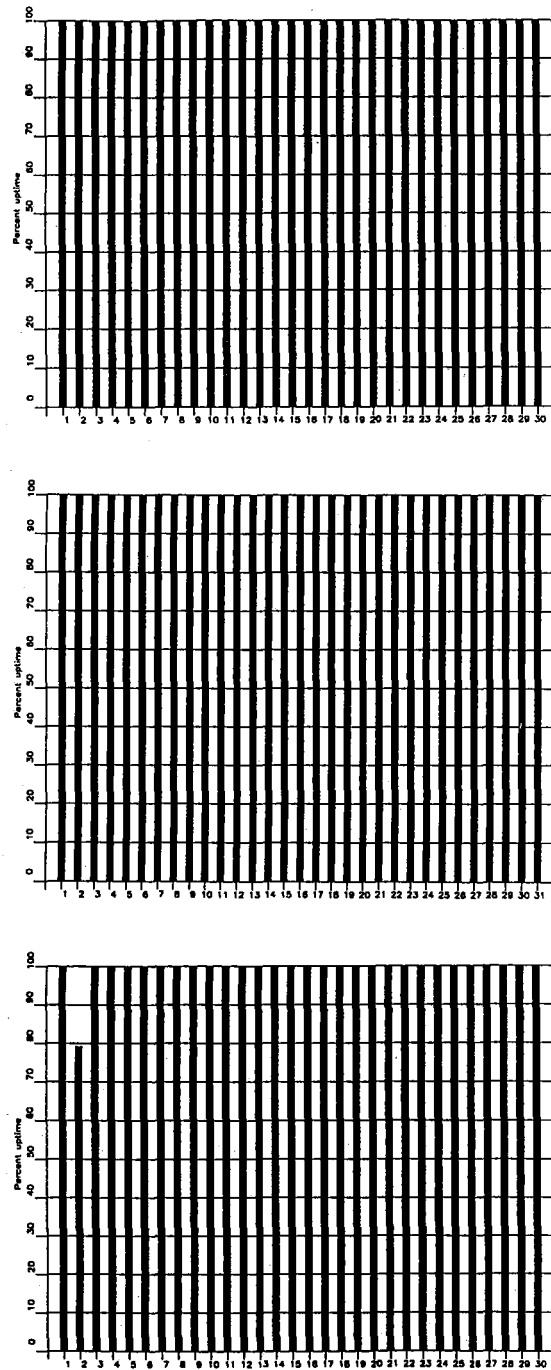


Fig. 3.3.1. FINESS data recording uptime for April (top), May (middle) and June (bottom) 1997.

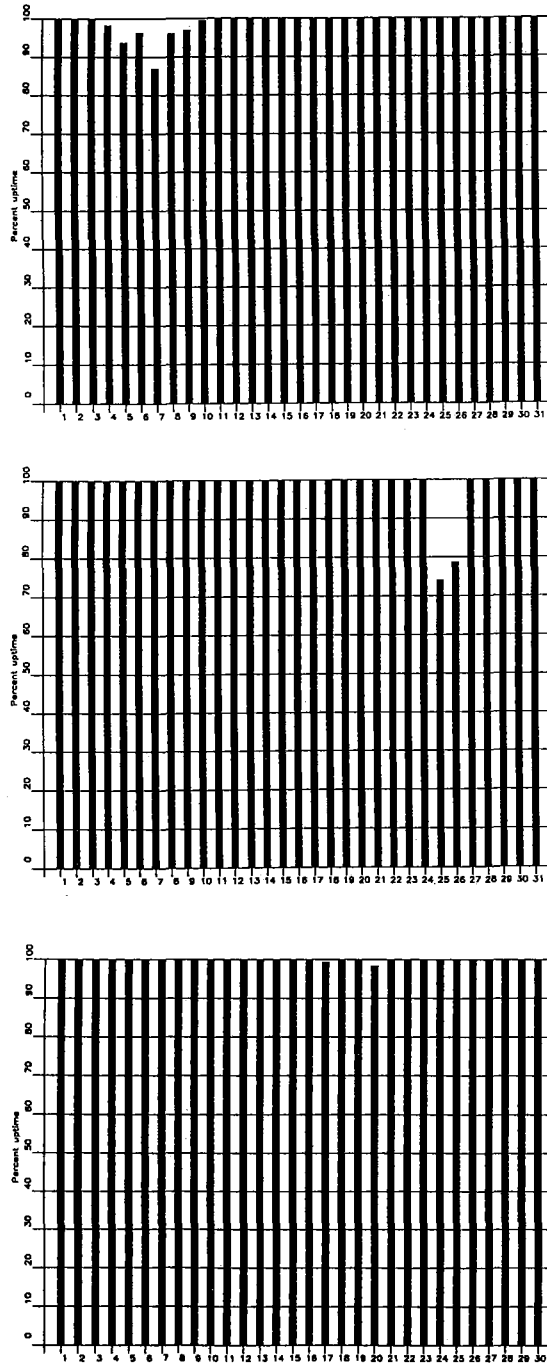


Fig. 3.3.1. (cont.) FINESS data recording uptime for July (top), August (middle) and September (bottom) 1997.

3.4 Recording of Spitsbergen data at NDPC, Kjeller

The average recording time was 98.66% as compared to 98.91% for the previous reporting period.

The main reasons for downtime follow:

Date	Time	Cause
25 Apr	1818 -	Software problem NDC
26 Apr	- 1031	
08 May	1354 - 1846	Software problem NDC
15 Jul	0106 - 0120	Transmission line failure
26 Jul	1452 - 1744	Software problem NDC
25 Aug	0021 - 0802	Software problem NDC
30 Aug	0255 - 0310	Transmission line failure
30 Aug	0322 - 0536	Transmission line failure
31 Aug	0847 - 1328	Transmission line failure
31 Aug	1712 -	Transmission line failure
01 Sep	- 0839	
03 Sep	1549 - 1753	Transmission line failure

Table 3.4.1. The main interruptions in recording of Spitsbergen data at NDPC, 1 April - 30 September 1997.

Monthly uptimes for the Spitsbergen online data recording task, taking into account all factors (field installations, transmission line, data center operation) affecting this task were as follows:

April 97	:	97.64%
May	:	99.34%
June	:	99.96%
July	:	99.56%
August	:	96.92%
September	:	98.51%

Fig. 3.4.1 shows the uptime for the data recording task, or equivalently, the availability of Spitsbergen data in our tape archive, on a day-by-day basis for the reporting period.

J. Torstveit

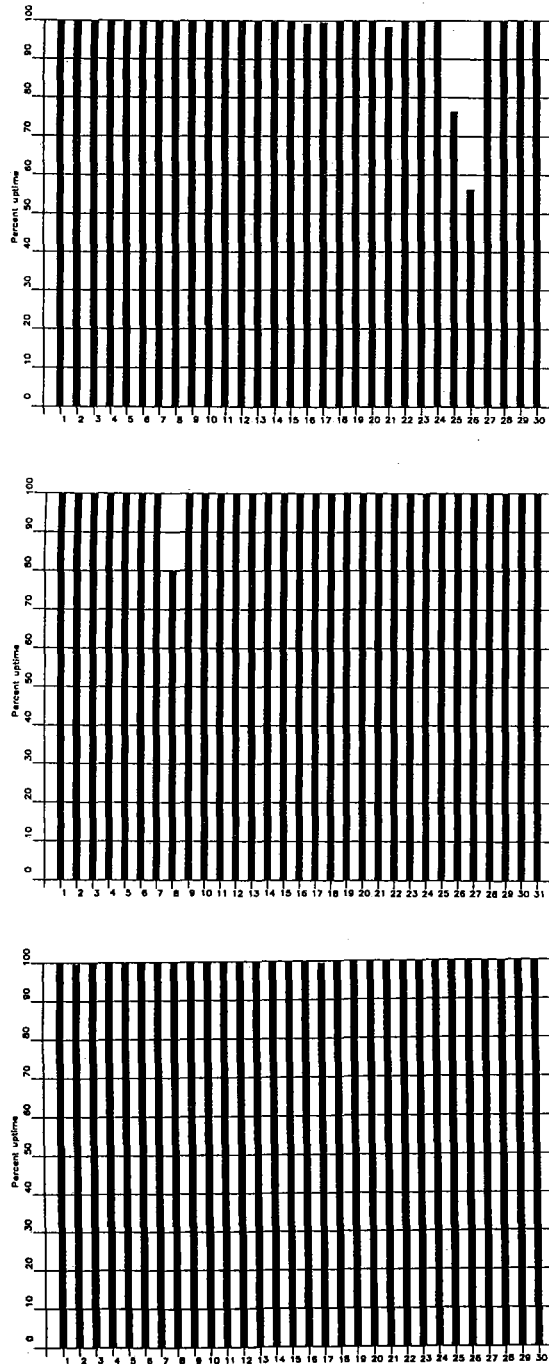


Fig. 3.4.1. Spitsbergen data recording uptime for April (top), May (middle) and June (bottom) 1997.

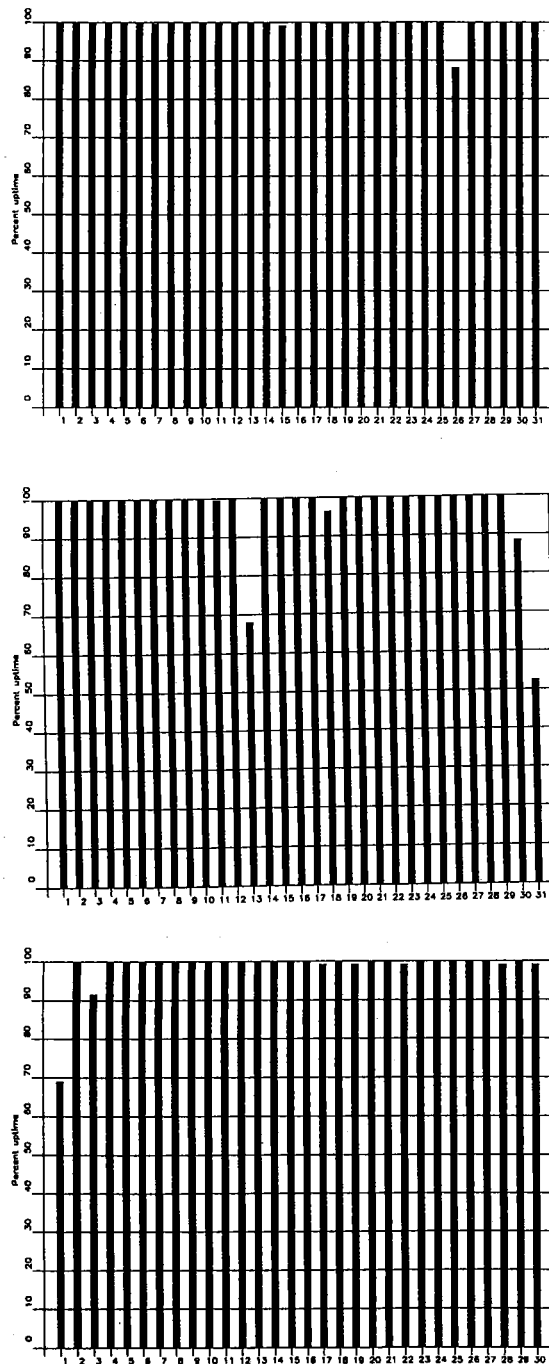


Fig. 3.4.1. (cont.) Spitsbergen data recording uptime for July (top), August (middle) and September (bottom) 1997.

3.5 Event detection operation

This section reports results from one-array automatic processing using signal processing recipes and "ronapp" recipes for the ep program (NORSAR Sci. Rep. No 2-88/89).

Three systems are in parallel operation to associate detected phases and locate events:

1. The ep program with "ronapp" recipes is operated independently on each array to obtain simple one-array automatic solutions.
2. The Generalized Beamforming method (GBF) (see F. Ringdal and T. Kværna (1989), A multichannel processing approach to real time network detection, phase association and threshold monitoring, BSSA Vol 79, no 6, 1927-1940) processes the four arrays jointly and presents locations of regional events.
3. The RMS system (Regional Monitoring System; previously referred to as the IMS system (Intelligent Monitoring System) system) is operated on the same set of arrivals as ep and GBF and reports also teleseismic events in addition to regional ones.

RMS results are reported in section 3.6.

NORESS detections

The number of detections (phases) reported from day 091, 1997, through day 273, 1997, was 40,975, giving an average of 225 detections per processed day (182 days processed).

Table 3.5.1 shows daily and hourly distribution of detections for NORESS.

Events automatically located by NORESS

During days 091, 1997, through 273, 1997, 2532 local and regional events were located by NORESS, based on automatic association of P- and S-type arrivals. This gives an average of 13.9 events per processed day (182 days processed). 69% of these events are within 300 km, and 90% of these events are within 1000 km.

ARCESS detections

The number of detections (phases) reported during day 091, 1997, through day 273, 1997, was 41,518, giving an average of 407 detections per processed day (102 days processed).

Table 3.5.2 shows daily and hourly distribution of detections for ARCESS.

Events automatically located by ARCESS

During days 091, 1997, through 273, 1997, 2982 local and regional events were located by ARCESS, based on automatic association of P- and S-type arrivals. This gives an average of 29.2 events per processed day (102 days processed). 55% of these events are within 300 km, and 86% of these events are within 1000 km.

FINESS detections

The number of detections (phases) reported during day 091, 1997, through day 273, 1997, was 43,708, giving an average of 239 detections per processed day (183 days processed).

Table 3.5.3 shows daily and hourly distribution of detections for FINESS.

Events automatically located by FINESS

During days 091, 1997, through 273, 1997, 2720 local and regional events were located by FINESS, based on automatic association of P- and S-type arrivals. This gives an average of 15.2 events per processed day (183 days processed). 79% of these events are within 300 km, and 91% of these events are within 1000 km.

GERESS detections

The number of detections (phases) reported from day 091, 1997, through day 273, 1997, was 42,425, giving an average of 232 detections per processed day (183 days processed).

Table 3.5.4 shows daily and hourly distribution of detections for GERESS.

Events automatically located by GERESS

During days 091, 1997, through 273, 1997, 4747 local and regional events were located by GERESS, based on automatic association of P- and S-type arrivals. This gives an average of 25.4 events per processed day (183 days processed). 71% of these events are within 300 km, and 90% of these events are within 1000 km.

Apatity array detections

The number of detections (phases) reported from day 091, 1997, through day 273, 1997, was 61,167, giving an average of 338 detections per processed day (181 days processed).

As described in earlier reports, the data from the Apatity array are transferred by one-way (simplex) radio links to Apatity city. The transmission suffers from radio disturbances that occasionally result in a large number of small data gaps and spikes in the data. In order for the communication protocol to correct such errors by requesting retransmission of data, a two-way radio link would be needed (duplex radio). However, it should be noted that noise from cultural activities and from the nearby lakes cause most of the unwanted detections. These unwanted detections are "filtered" in the signal processing, as they give seismic velocities that are outside accepted limits for regional and teleseismic phase velocities.

Table 3.5.5 shows daily and hourly distribution of detections for the Apatity array.

Events automatically located by the Apatity array

During days 091, 1997, through 273, 1997, 651 local and regional events were located by the Apatity array, based on automatic association of P- and S-type arrivals. This gives an average of 3.6 events per processed day (181 days processed). 60% of these events are within 300 km, and 79% of these events are within 1000 km.

Spitsbergen array detections

The number of detections (phases) reported from day 091, 1997, through day 273, 1997, was 143,458, giving an average of 784 detections per processed day (183 days processed).

Table 3.5.6 shows daily and hourly distribution of detections for the Spitsbergen array.

Events automatically located by the Spitsbergen array

During days 091, 1997, through 273, 1997, 11,557 local and regional events were located by the Spitsbergen array, based on automatic association of P- and S-type arrivals. This gives an average of 63.2 events per processed day (183 days processed). 47% of these events are within 300 km, and 73% of these events are within 1000 km.

Hagfors array detections

The number of detections (phases) reported from day 091, 1997, through day 273, 1997, was 43,164, giving an average of 236 detections per processed day (183 days processed).

Table 3.5.7 shows daily and hourly distribution of detections for the Hagfors array

Events automatically located by the Hagfors array

During days 091, 1997, through 273, 1997, 1876 local and regional events were located by the Hagfors array, based on automatic association of P- and S-type arrivals. This gives an average of 10.3 events per processed day (183 days processed). 40% of these events are within 300 km, and 80% of these events are within 1000 km

U. Baadshaug

NRS .FKX Hourly distribution of detections

Day	00	01	02	03	04	05	06	07	08	09	10	11	12	13	14	15	16	17	18	19	20	21	22	23	Sum	Date
259	6	11	11	3	4	5	8	1	11	11	13	4	11	21	9	6	13	20	21	21	14	11	18	14	267	Sep 16 Tuesday
260	13	20	6	12	7	9	5	8	6	8	14	6	17	16	18	16	28	12	12	19	14	14	23	22	325	Sep 17 Wednesday
261	34	26	12	22	9	2	6	6	6	11	14	3	17	16	7	10	4	15	7	8	4	3	3	7	252	Sep 18 Thursday
262	3	20	8	2	3	3	5	3	8	3	13	9	14	8	6	5	7	10	18	14	4	5	5	11	187	Sep 19 Friday
263	8	10	3	4	2	11	7	10	9	9	7	13	11	12	17	20	18	16	11	2	10	21	5	4	240	Sep 20 Saturday
264	5	4	3	10	3	6	3	11	5	5	5	6	8	11	6	2	16	2	9	2	5	9	5	12	153	Sep 21 Sunday
265	18	8	7	9	7	1	2	7	3	10	5	16	18	10	10	11	8	21	16	6	5	5	5	7	215	Sep 22 Monday
266	5	21	5	13	6	4	4	11	22	7	8	11	24	21	5	10	17	7	10	19	8	2	8	16	264	Sep 23 Tuesday
267	7	24	4	8	12	6	6	5	13	7	10	9	20	14	24	10	8	5	6	5	16	7	8	5	239	Sep 24 Wednesday
268	4	31	3	11	7	5	2	6	21	9	11	10	19	14	11	13	32	13	19	25	10	7	9	6	298	Sep 25 Thursday
269	12	23	1	5	15	3	5	11	3	13	9	13	9	9	10	6	18	9	26	5	4	16	13	4	242	Sep 26 Friday
270	6	6	4	5	13	4	6	15	8	12	15	13	8	42	103	116	49	8	5	8	38	5	4	7	500	Sep 27 Saturday
271	3	8	12	10	4	3	5	3	11	5	4	8	13	7	10	28	108	15	4	3	2	2	7	32	307	Sep 28 Sunday
272	14	9	24	11	7	8	13	9	8	13	9	7	15	16	21	12	16	16	18	5	7	6	10	5	279	Sep 29 Monday
273	7	23	6	5	9	5	14	2	3	5	10	9	24	14	10	10	59	30	19	3	20	6	10	17	320	Sep 30 Tuesday
NRS	00	01	02	03	04	05	06	07	08	09	10	11	12	13	14	15	16	17	18	19	20	21	22	23		
Sum	2245	1524	1654	1566	1772	2004	2154	1747	1513	1742	1201	1487	1622	1530	1341	1547	1474	2025	2595	1789	1985	1871	1260	1327	40975	Total sum
182	9	12	8	8	7	9	9	9	8	10	11	11	14	12	10	10	11	8	10	10	7	7	7	8	225	Total average
127	9	14	8	8	6	9	9	9	8	11	12	12	17	13	10	10	11	8	11	10	6	6	6	8	233	Average workdays
55	9	9	9	10	10	10	8	8	7	7	8	8	7	9	9	9	10	8	8	8	9	8	9	9	206	Average weekends

Table 3.5.1. (Page 4 of 4) Daily and hourly distribution of NORESS detections. For each day is shown number of detections within each hour of the day, and number of detections for that day. The end statistics give total number of detections distributed for each hour and the total sum of detections during the period. The averages show number of processed days, hourly distribution and average per processed day.

ARC .FKX Hourly distribution of detections

Day	00	01	02	03	04	05	06	07	08	09	10	11	12	13	14	15	16	17	18	19	20	21	22	23	Sum	Date
259	16	6	15	15	17	21	26	36	34	18	28	22	15	16	19	28	21	9	17	11	7	8	20	15	440	Sep 16 Tuesday
260	12	7	5	7	13	7	20	24	20	13	19	28	23	23	19	37	17	14	21	14	19	13	17	19	411	Sep 17 Wednesday
261	16	14	5	4	3	18	17	18	17	33	22	20	20	11	13	14	17	13	12	12	5	10	17	12	343	Sep 18 Thursday
262	6	10	11	12	16	22	21	35	26	60	30	29	35	22	19	26	25	10	17	23	16	15	17	19	522	Sep 19 Friday
263	8	5	13	22	12	9	19	32	22	18	21	21	14	11	13	28	11	10	10	7	23	14	11	16	370	Sep 20 Saturday
264	8	5	4	13	5	15	29	24	18	18	8	9	14	23	12	10	6	25	16	15	14	22	24	22	359	Sep 21 Sunday
265	10	11	9	0	0	0	0	0	0	0	0	0	0	0	0	0	0	20	21	13	18	19	17	22	160	Sep 22 Monday
266	21	16	17	14	7	11	32	19	22	28	25	27	27	16	33	21	16	21	22	22	27	4	18	19	485	Sep 23 Tuesday
267	8	6	9	8	19	25	38	38	19	15	43	37	36	31	16	28	30	23	22	17	15	10	24	23	540	Sep 24 Wednesday
268	8	7	6	8	6	20	25	19	16	22	36	33	23	23	53	26	27	19	13	34	18	11	7	19	479	Sep 25 Thursday
269	16	3	9	12	17	13	18	15	18	38	21	38	31	41	20	19	10	8	11	5	21	6	17	15	422	Sep 26 Friday
270	3	20	18	10	5	10	29	21	19	15	15	20	30	15	21	3	8	15	13	13	13	14	10	21	361	Sep 27 Saturday
271	4	8	7	4	6	11	10	29	20	10	26	27	12	20	17	16	17	9	14	4	12	6	25	22	336	Sep 28 Sunday
272	11	5	7	8	18	9	26	30	13	14	17	13	17	12	19	14	10	11	15	27	24	21	26	25	392	Sep 29 Monday
273	18	4	26	29	12	7	33	38	17	32	20	19	19	24	12	36	15	20	8	8	20	11	20	27	475	Sep 30 Tuesday
ARC	00	01	02	03	04	05	06	07	08	09	10	11	12	13	14	15	16	17	18	19	20	21	22	23		
Sum	1090	1210	1374	1879	2029	2405	1955	1908	1714	1575	1354	2184	1143	1130	1408	1768	1921	2268	2151	1905	1831	1861	1523	1932	41518	Total sum
102	11	11	11	12	14	13	17	18	19	20	22	24	21	19	19	19	18	17	18	15	15	13	19	21	407	Total average
69	11	11	10	11	14	14	18	20	20	21	24	26	24	20	20	21	19	18	19	16	15	13	19	21	427	Average workdays
33	11	10	12	13	12	12	15	15	17	17	18	19	16	17	16	14	15	14	15	13	14	13	18	22	358	Average weekends

Table 3.5.2. (Page 4 of 4) Daily and hourly distribution of ARCESS detections. For each day is shown number of detections within each hour of the day, and number of detections for that day. The end statistics give total number of detections distributed for each hour and the total sum of detections during the period. The averages show number of processed days, hourly distribution and average per processed day.

FIN .FKX Hourly distribution of detections

Day	00	01	02	03	04	05	06	07	08	09	10	11	12	13	14	15	16	17	18	19	20	21	22	23	Sum	Date
259	11	2	10	4	1	2	3	7	7	11	9	11	17	13	16	12	7	8	3	5	5	1	6	3	174	Sep 16 Tuesday
260	7	0	2	2	1	17	1	5	5	14	10	14	12	8	8	23	21	5	4	5	2	7	5	6	184	Sep 17 Wednesday
261	2	5	1	5	2	3	9	5	10	27	12	7	12	6	11	9	4	5	7	0	10	4	8	8	172	Sep 18 Thursday
262	8	9	11	9	8	1	5	7	5	10	11	12	10	7	6	4	6	4	3	10	5	13	21	28	213	Sep 19 Friday
263	30	41	38	31	35	34	34	26	36	19	12	6	3	3	5	5	11	2	4	0	8	2	4	3	392	Sep 20 Saturday
264	0	1	1	2	2	4	0	4	2	1	3	30	25	2	0	9	14	3	6	4	5	4	5	5	132	Sep 21 Sunday
265	2	1	1	2	0	5	21	5	1	16	10	19	16	4	6	11	4	6	10	1	2	10	5	1	159	Sep 22 Monday
266	2	7	2	3	0	2	4	5	22	14	9	9	19	4	7	14	2	7	2	3	11	2	4	5	159	Sep 23 Tuesday
267	4	4	1	2	4	0	4	3	6	15	15	8	12	12	9	6	5	7	6	1	5	4	8	2	143	Sep 24 Wednesday
268	7	10	3	2	3	10	10	8	15	10	9	31	19	19	24	32	19	23	26	18	19	12	10	11	350	Sep 25 Thursday
269	14	13	5	3	8	1	3	12	9	19	22	23	15	6	10	8	15	1	9	4	11	3	2	2	218	Sep 26 Friday
270	3	6	4	6	7	8	2	6	17	6	5	9	9	5	5	1	3	5	1	2	3	2	2	4	121	Sep 27 Saturday
271	2	4	7	1	3	2	0	13	22	32	34	19	4	11	17	6	17	19	27	30	32	34	32	20	388	Sep 28 Sunday
272	7	1	6	12	2	1	14	16	10	11	5	11	8	7	4	6	3	7	3	6	4	5	14	7	170	Sep 29 Monday
273	6	5	1	2	1	3	8	15	11	13	8	19	13	20	20	12	9	2	3	4	11	3	11	6	206	Sep 30 Tuesday
FIN	00	01	02	03	04	05	06	07	08	09	10	11	12	13	14	15	16	17	18	19	20	21	22	23		
Sum	1961	1805	1462	1629	2359	2462	1851	1806	1547	1576	1624	1865														
	1840	1809	1536	1353	2101	2468	2053	1895	1675	1382	1687	1962	43708	Total sum												
183	10	11	10	10	8	8	7	9	11	13	13	13	11	10	10	10	9	8	8	9	9	9	11	10	239	Total average
128	9	10	9	8	7	7	6	9	12	14	16	15	13	11	11	10	9	8	7	8	9	8	10	9	234	Average workdays
55	12	13	13	14	12	10	10	9	10	9	8	8	7	8	9	9	9	9	9	10	11	10	11	12	243	Average weekends

Table 3.5.3. (Page 4 of 4) Daily and hourly distribution of FINESS detections. For each day is shown number of detections within each hour of the day, and number of detections for that day. The end statistics give total number of detections distributed for each hour and the total sum of detections during the period. The averages show number of processed days, hourly distribution and average per processed day.

GER .FKX Hourly distribution of detections

Day	00	01	02	03	04	05	06	07	08	09	10	11	12	13	14	15	16	17	18	19	20	21	22	23	Sum	Date
259	2	6	43	3	5	2	5	17	24	15	47	40	24	42	29	14	7	15	5	3	2	4	4	0	358	Sep 16 Tuesday
260	7	3	9	2	8	7	26	27	19	24	35	17	39	15	43	22	1	7	1	8	1	4	1	8	334	Sep 17 Wednesday
261	5	25	10	12	9	2	7	3	19	29	40	19	23	19	13	14	7	5	6	1	7	4	5	8	292	Sep 18 Thursday
262	3	7	24	4	6	5	4	24	18	28	21	21	18	9	15	15	9	4	1	8	3	1	4	4	256	Sep 19 Friday
263	2	4	2	9	3	2	6	4	10	13	10	10	9	14	6	9	8	9	14	2	4	3	3	1	157	Sep 20 Saturday
264	5	0	2	2	3	6	3	5	6	8	4	5	5	4	4	2	4	5	8	4	9	13	10	9	126	Sep 21 Sunday
265	19	13	8	6	5	7	8	13	8	22	23	14	21	9	14	9	8	2	4	11	5	2	4	2	237	Sep 22 Monday
266	8	11	6	7	2	16	15	5	30	35	33	30	22	8	5	16	7	8	2	1	7	3	4	2	283	Sep 23 Tuesday
267	5	12	8	8	5	5	2	11	16	25	23	30	26	14	12	7	11	2	7	7	2	1	3	3	245	Sep 24 Wednesday
268	5	1	2	7	3	4	7	16	14	24	28	19	18	9	13	5	5	2	5	7	7	2	0	6	209	Sep 25 Thursday
269	20	19	29	7	39	9	16	24	24	36	32	34	28	34	31	14	22	12	17	22	19	12	13	21	534	Sep 26 Friday
270	5	6	18	15	19	14	18	20	23	16	29	11	11	15	12	11	17	16	14	20	10	1	3	4	328	Sep 27 Saturday
271	6	15	22	7	14	7	7	8	9	7	5	23	12	5	6	4	14	11	2	7	2	11	11	12	227	Sep 28 Sunday
272	19	5	13	18	9	20	20	23	16	31	30	29	13	14	9	10	12	11	5	4	6	17	10	4	348	Sep 29 Monday
273	5	7	21	4	14	10	30	19	46	44	21	24	13	14	14	2	1	3	5	4	4	0	7	10	322	Sep 30 Tuesday
GER	00	01	02	03	04	05	06	07	08	09	10	11	12	13	14	15	16	17	18	19	20	21	22	23		
Sum	1110	1258	1202	2094	3815	3595	2345	1571	1021	1311	966	849														
	1019	1263	1140	1530	2838	4447	2796	2118	1175	1039	1034	889	42425	Total sum												
183	6	6	7	7	6	7	8	11	16	21	24	20	15	13	12	9	6	6	6	7	6	5	5	5	232	Total average
128	6	7	7	7	6	7	9	14	19	26	31	24	17	14	14	10	7	6	5	6	5	5	5	5	262	Average workdays
55	4	5	6	7	6	5	6	6	8	9	8	10	10	10	6	6	5	5	7	9	6	6	5	5	158	Average weekends

Table 3.5.4. (Page 4 of 4) Daily and hourly distribution of GERESS detections. For each day is shown number of detections within each hour of the day, and number of detections for that day. The end statistics give total number of detections distributed for each hour and the total sum of detections during the period. The averages show number of processed days, hourly distribution and average per processed day.

APA .FKX Hourly distribution of detections

Table with columns: Day, 00-23 (hours), Sum, Date. Rows show hourly detection counts for days 91 to 146, including day and month names (e.g., Tuesday, Wednesday).

Table 3.5.5 (Page 1 of 4)

APA .FKX Hourly distribution of detections

Day	00	01	02	03	04	05	06	07	08	09	10	11	12	13	14	15	16	17	18	19	20	21	22	23	Sum	Date
259	6	8	15	31	24	46	28	23	28	21	40	21	27	20	22	31	27	24	22	5	17	8	8	5	507	Sep 16 Tuesday
260	0	24	14	19	30	49	51	42	31	41	18	35	32	24	19	36	21	17	16	9	6	8	8	14	564	Sep 17 Wednesday
261	8	6	19	24	17	51	52	37	33	21	45	42	30	38	31	15	24	15	12	1	11	6	6	9	553	Sep 18 Thursday
262	6	12	12	20	23	31	37	40	32	17	30	34	37	28	20	15	21	7	19	27	16	2	2	0	488	Sep 19 Friday
263	10	8	17	19	17	19	21	15	10	9	17	26	21	17	6	13	34	20	14	10	5	4	5	11	348	Sep 20 Saturday
264	8	2	9	16	4	15	27	23	14	9	14	11	6	15	17	16	13	13	10	6	2	8	5	3	266	Sep 21 Sunday
265	7	11	12	7	9	40	35	21	28	12	26	39	21	34	17	18	12	19	4	17	8	2	0	7	406	Sep 22 Monday
266	10	14	9	24	13	27	36	33	13	20	23	27	30	17	27	12	19	13	11	10	7	4	4	0	403	Sep 23 Tuesday
267	1	11	18	8	26	41	47	43	43	23	37	31	38	34	16	33	14	16	7	12	2	11	4	4	520	Sep 24 Wednesday
268	7	9	18	14	33	57	51	41	26	29	37	50	23	26	21	27	7	19	8	6	12	0	4	2	527	Sep 25 Thursday
269	11	15	15	20	19	35	42	27	28	30	28	60	35	20	34	32	30	25	20	14	7	5	2	6	560	Sep 26 Friday
270	2	6	14	20	9	12	30	6	16	16	23	12	19	27	17	14	29	16	18	12	15	4	6	12	355	Sep 27 Saturday
271	2	5	6	9	6	9	6	20	14	6	2	6	9	16	12	15	19	12	14	2	5	2	1	10	208	Sep 28 Sunday
272	5	8	17	14	7	24	47	42	28	24	29	31	21	23	27	18	6	26	3	6	5	1	1	5	418	Sep 29 Monday
273	7	3	11	21	41	24	57	30	15	13	29	33	22	14	27	43	19	24	7	4	16	9	15	5	489	Sep 30 Tuesday
APA	00	01	02	03	04	05	06	07	08	09	10	11	12	13	14	15	16	17	18	19	20	21	22	23		
Sum	1266	2490	4423	3892	3400	4076	3237	2479	2127	1496	1162	964														
	1013	2124	2678	4395	3777	3901	3478	2864	1982	1680	1324	939	61167	Total sum												
181	6	7	12	14	15	24	24	22	21	19	22	23	19	18	16	14	11	12	9	8	7	6	5	5	338	Total average
126	5	8	13	15	17	30	29	27	25	23	26	28	23	22	19	16	12	13	10	9	8	7	5	5	392	Average workdays
55	6	5	10	10	10	12	12	9	11	10	12	10	10	9	9	8	9	10	7	7	6	6	5	6	209	Average weekends

Table 3.5.5.(Page 4 of 4) Daily and hourly distribution of Apatity array detections. For each day is shown number of detections within each hour of the day, and number of detections for that day. The end statistics give total number of detections distributed for each hour and the total sum of detections during the period. The averages show number of processed days, hourly distribution and average per processed day.

SPI .FKX Hourly distribution of detections

Day	00	01	02	03	04	05	06	07	08	09	10	11	12	13	14	15	16	17	18	19	20	21	22	23	Sum	Date
259	34	30	12	20	35	27	25	33	28	23	19	30	28	34	47	39	41	44	62	47	52	54	44	26	834	Sep 16 Tuesday
260	35	45	70	50	60	43	59	63	49	60	43	32	62	50	53	48	76	48	59	41	38	36	14	39	1173	Sep 17 Wednesday
261	34	32	35	41	23	33	46	36	53	42	36	36	29	22	35	27	36	35	34	30	24	26	29	19	793	Sep 18 Thursday
262	37	35	22	29	36	40	32	22	39	40	25	16	32	22	23	22	23	31	40	33	33	23	35	35	725	Sep 19 Friday
263	37	27	45	25	36	52	48	41	43	48	47	34	46	28	40	48	43	29	33	46	48	58	66	48	1016	Sep 20 Saturday
264	31	31	48	46	39	33	32	34	24	22	32	32	30	27	26	22	34	34	39	13	21	21	38	43	752	Sep 21 Sunday
265	26	28	31	21	18	20	29	19	15	25	27	11	24	23	19	48	42	34	40	51	59	37	31	18	696	Sep 22 Monday
266	32	24	25	27	42	32	35	38	72	46	44	28	48	16	36	36	26	26	42	50	48	58	62	70	963	Sep 23 Tuesday
267	65	84	60	61	102	117	94	90	89	88	81	62	102	72	62	86	115	92	69	81	72	85	77	69	1975	Sep 24 Wednesday
268	46	43	39	57	70	60	66	43	43	35	47	54	60	61	26	33	42	57	51	39	34	65	41	43	1155	Sep 25 Thursday
269	70	53	48	21	31	29	28	42	28	43	28	59	25	43	23	38	47	32	32	38	44	31	21	24	878	Sep 26 Friday
270	48	25	43	38	40	54	46	35	34	29	23	39	31	39	36	45	40	43	44	46	41	38	34	56	947	Sep 27 Saturday
271	42	61	58	43	39	27	38	25	42	26	31	15	33	18	50	45	47	45	29	32	41	31	43	48	909	Sep 28 Sunday
272	48	39	42	34	32	43	52	44	38	42	44	33	45	56	43	23	28	58	47	52	67	53	56	44	1063	Sep 29 Monday
273	31	46	47	52	39	68	39	51	22	29	16	26	23	24	19	23	41	31	24	26	28	9	25	29	768	Sep 30 Tuesday
SPI	00	01	02	03	04	05	06	07	08	09	10	11	12	13	14	15	16	17	18	19	20	21	22	23		
Sum	5879	6013	5838	5847	5802	5891	5919	5826	5811	5853	6022	6394														
	6151	6106	5854	6210	5771	5918	6422	5962	5651	5986	6043	6289	143458	Total sum												
183	34	32	33	33	32	32	34	32	32	32	32	32	35	32	33	32	31	32	33	32	33	33	34	35	784	Total average
128	33	31	33	34	32	33	34	33	33	33	34	32	35	31	32	32	31	32	34	32	34	34	35	35	794	Average workdays
55	36	34	35	29	31	30	32	30	28	28	28	32	35	34	33	32	29	31	31	31	31	30	32	34	755	Average weekends

Table 3.5.6. (Page 4 of 4) Daily and hourly distribution of Spitsbergen array detections.
 For each day is shown number of detections within each hour of the day, and number of detections for that day. The end statistics give total number of detections distributed for each hour and the total sum of detections during the period. The averages show number of processed days, hourly distribution and average per processed day.

HFS .FKX Hourly distribution of detections

Day	00	01	02	03	04	05	06	07	08	09	10	11	12	13	14	15	16	17	18	19	20	21	22	23	Sum	Date
259	3	6	5	23	2	6	8	10	8	8	6	8	10	38	13	4	12	16	12	4	6	1	2	3	214	Sep 16 Tuesday
260	3	3	2	6	5	2	1	6	6	5	11	7	15	10	14	17	4	4	18	2	2	7	5	3	158	Sep 17 Wednesday
261	5	4	7	4	1	3	7	6	1	9	11	3	9	16	10	13	4	7	7	6	2	2	1	5	143	Sep 18 Thursday
262	2	2	7	4	2	0	7	1	2	11	15	4	16	0	3	3	12	4	3	4	5	5	2	7	121	Sep 19 Friday
263	5	0	3	5	3	3	9	4	5	8	1	7	1	13	14	18	14	3	15	0	7	2	6	2	148	Sep 20 Saturday
264	2	4	10	4	0	4	6	8	3	3	2	2	2	3	1	5	4	1	13	4	3	7	10	6	107	Sep 21 Sunday
265	2	0	8	0	5	4	6	4	3	6	6	7	12	11	13	7	3	12	16	8	2	4	4	1	144	Sep 22 Monday
266	5	1	12	8	4	5	15	22	32	15	6	6	25	14	7	10	9	8	5	1	15	3	2	2	232	Sep 23 Tuesday
267	9	6	9	6	2	6	9	4	23	8	6	9	7	8	14	12	6	7	4	5	2	3	5	5	175	Sep 24 Wednesday
268	3	11	6	2	4	16	8	1	23	5	4	4	16	17	22	13	22	4	2	2	3	2	1	7	198	Sep 25 Thursday
269	12	3	5	2	9	2	1	9	5	28	11	8	9	12	16	4	10	4	9	1	11	6	9	3	189	Sep 26 Friday
270	9	4	5	3	5	12	4	10	9	4	19	1	7	9	11	8	6	8	9	8	9	11	13	36	220	Sep 27 Saturday
271	14	8	28	10	13	6	5	7	7	8	7	12	17	3	16	10	15	13	10	10	4	14	27	14	278	Sep 28 Sunday
272	12	1	9	8	11	7	14	8	8	9	7	9	3	11	21	8	6	14	4	2	5	3	3	3	186	Sep 29 Monday
273	5	3	2	4	14	3	18	3	1	4	7	9	17	16	6	3	9	8	2	1	8	4	8	3	158	Sep 30 Tuesday

HFS 00 01 02 03 04 05 06 07 08 09 10 11 12 13 14 15 16 17 18 19 20 21 22 23

Sum	1130	1502	1475	1690	2247	2551	2953	2243	1841	1401	1154	1281														
	1151	1342	1461	1750	2027	2338	2777	2706	1976	1698	1339	1131	43164	Total sum												
183	6	6	7	8	8	8	10	9	11	12	13	14	15	16	15	12	11	10	9	8	7	6	6	7	236	Total average
128	6	6	6	8	8	8	9	9	11	12	13	15	16	17	15	12	11	10	9	7	6	6	5	6	230	Average workdays
55	7	7	9	9	8	8	10	9	11	12	11	10	12	13	13	13	10	10	10	9	9	7	8	9	236	Average weekends

Table 3.5.7. (Page 4 of 4) Daily and hourly distribution of Hagfors array detections. For each day is shown number of detections within each hour of the day, and number of detections for that day. The end statistics give total number of detections distributed for each hour and the total sum of detections during the period. The averages show number of processed days, hourly distribution and average per processed day

3.6 Regional Monitoring System operation

The Regional Monitoring System (RMS) was installed at NORSAR in December 1989 and was operated at NORSAR from 1 January 1990 for automatic processing of data from ARCESS and NORESS. A second version of RMS that accepts data from an arbitrary number of arrays and single 3-component stations was installed at NORSAR in October 1991, and regular operation of the system comprising analysis of data from the 4 arrays ARCESS, NORESS, FINESS and GERESS started on 15 October 1991. As opposed to the first version of RMS, the one in current operation also has the capability of locating events at teleseismic distance.

Data from the Apatity array were included on 14 December 1992, and from the Spitsbergen array on 12 January 1994. Detections from the Hagfors array were available to the analysts and could be added manually during analysis from 6 December 1994. After 2 February 1995, Hagfors detections were also used in the automatic phase association.

The operational stability of RMS has been very good during the reporting period. In fact the RMS event processor (pipeline) has had no downtime of its own; i.e., all data available to RMS have been processed by RMS.

Phase and event statistics

Table 3.6.1 gives a summary of phase detections and events declared by RMS. From top to bottom the table gives the total number of detections by the RMS, the number of detections that are associated with events automatically declared by the RMS, the number of detections that are not associated with any events, the number of events automatically declared by the RMS, the total number of events defined by the analyst, and finally the number of events accepted by the analyst without any changes (i.e., from the set of events automatically declared by the RMS).

Due to reductions in the FY94 funding for RMS activities (relative to previous years), new criteria for event analysis were introduced from 1 January 1994. Since that date, only regional events in areas of special interest (e.g, Spitsbergen, since it is necessary to acquire new knowledge in this region) or other significant events (e.g, felt earthquakes and large industrial explosions) were thoroughly analyzed. Teleseismic events were analyzed as before.

To further reduce the workload on the analysts and to focus on regional events in preparation for Gamma-data submission during GSETT-3, a new processing scheme was introduced on 2 February 1995. The GBF (Generalized Beamforming) program is used as a pre-processor to RMS, and only phases associated to selected events in northern Europe are considered in the automatic RMS phase association. All detections, however, are still available to the analysts and can be added manually during analysis.

There is one exception to the new rule for automatic phase association: all detections from the Spitsbergen array are passed directly on to the RMS. This allows for thorough analysis of all events in the Spitsbergen region.

	Apr 97	May 97	Jun 97	Jul 97	Aug 97	Sep 97	Total
Phase detections	55661	62709	54731	52616	76033	9136	393386
- Associated phases	5864	6670	3896	3598	5244	6743	32015
- Unassociated phases	49797	56039	50835	49018	70789	84893	361371
Events automatically declared by RMS	1363	1608	1043	1085	1625	2051	8775
No. of events defined by the analyst	277	281	236	164	164	274	1396
No. of events accepted without modifications	0	0	0	1	0	0	1

Table 3.6.1. RMS phase detections and event summary.

U. Baadshaug

B.Kr. Hokland

B. Paulsen

4 Improvements and Modifications

4.1 NORSAR

NORSAR instrumentation

During this reporting period, 3 AIM24 digitizers, 24 Brick amplifiers and 1 KS54000P have been repaired and reinstalled. Work has continued to try to reduce the lightning problems reported in the previous Semiannual Technical Summary.

A block diagram of the remote sensor site components can be found in NORSAR Sci. Rep. No. 1-95/96.

NORSAR data acquisition

The Science Horizons XAVE data acquisition system has been operating satisfactorily during the reporting period. A block diagram of the digitizer and communication controller components is found in NORSAR Sci. Rep No 2-94/95.

NORSAR detection processing and feature extraction

The NORSAR detection processor has been running satisfactorily. To maintain consistent detection capability, the NORSAR beam tables have remained unchanged.

Detection statistics for the NORSAR array are given in section 2.

A description of the NORSAR beamforming techniques can be found in NORSAR Sci. Rep. 2-95/96.

NORSAR event processing

The automatic routine processing of NORSAR events as described in NORSAR Sci. Rep. No. 2-93/94, has been running satisfactorily. The analyst tools for reviewing and updating the solutions have been continuously modified to simplify operations and improve results.

Configuration files for IDC implementation

We have carried out considerable work to create a systematic set of NORSAR configuration files for use in the operational implementation at the IDC (see Section 7.4). The following configuration files from the testbed are necessary to implement NOA processing in operations. They should be installed in the corresponding subdirectories in the OPS tree.

Under the directory /nmrd/ops/net/idc/static/DFX:

- DFX-site-detection.par
- beam/NOA-beam.par
- beam/detection/NOA-beam.par
- beam/originbeam/NOA-beam.par

- beam/tdcorr/NOA.tdcorr
- fk/NOA-fk.par
- fk/fkgrid/NOA.BMFK.maxslow0.1
- fk/fkgrid/NOA.BMFK.maxslow0.3
- det/NOA-det.par
- qc/larray-qc.par
- polar/NOA-polar.par
- scheme/DFX-detection.scm

Under the directory /nmsrd/ops/net/idc/static/XfkDisplay:

- arrays/NOA_fk.par
- recipes/NOA.par

Under the directory /nmsrd/ops/net/idc/static/stations:

- NOA.par

Under the directory /nmsrd/rel/scheme:

- scheme/DFXdefault.scm

Under the directory /nmsrd/rel/bin:

- DFX

The following par files are necessary for optional subarray processing. They are used if the analyst chooses to create subarray origin beam(s) using ARS. It is recommended that these files be included in any case.

Under the directory /nmsrd/ops/net/idc/static/DFX:

- beam/NAO-beam.par, NBO-beam.par, NB2-beam.par, NC2-beam.par, NC3-beam.par, NC4-beam.par, NC6-beam.par
- beam/detection/NAO-beam.par, NBO-beam.par, NB2-beam.par, NC2-beam.par, NC3-beam.par, NC4-beam.par, NC6-beam.par
- beam/originbeam/NAO-beam.par, NBO-beam.par, NB2-beam.par, NC2-beam.par, NC3-beam.par, NC4-beam.par, NC6-beam.par

The following par files are optional for subarray processing. They are needed if one chooses to perform detection processing on a subarray as one station. The beam/detection/<subarray>-beam.par files specified above do not include subarray detection processing.

Under the directory /nmsrd/ops/net/idc/static/DFX:

- fk/NAO-fk.par, NBO-fk.par, NB2-fk.par, NC2-fk.par, NC3-fk.par, NC4-fk.par, NC6-fk.par

The following par files are necessary for optional subarray processing. They are needed if an analyst chooses to use XfkDisplay to do subarray F/K analysis and to create subarray fkb beams from XfkDisplay.

Under the directory /nmsrd/ops/net/idc/static/XfkDisplay:

- arrays/NAO_fk.par, NBO_fk.par, NB2_fk.par, NC2_fk.par, NC3_fk.par, NC4_fk.par, NC6_fk.par
- recipes/NAO.par, NBO.par, NB2.par, NC2.par, NC3.par, NC4.par, NC6.par
- XfkDisplay.par

The /nmrd/ops/net/idc/static/XfkDisplay/XfkDisplay.par file needs the following edits:

```
array_list="... NOA NAO NB2 NBO NC2 NC3 NC4 NC6 ..."  
NOA_par=$(OPSDIR)/static/XfkDisplay/arrays/NOA_fk.par  
NAO_par=$(OPSDIR)/static/XfkDisplay/arrays/NAO_fk.par  
NB2_par=$(OPSDIR)/static/XfkDisplay/arrays/NB2_fk.par  
NBO_par=$(OPSDIR)/static/XfkDisplay/arrays/NBO_fk.par  
NC2_par=$(OPSDIR)/static/XfkDisplay/arrays/NC2_fk.par  
NC3_par=$(OPSDIR)/static/XfkDisplay/arrays/NC3_fk.par  
NC4_par=$(OPSDIR)/static/XfkDisplay/arrays/NC4_fk.par  
NC6_par=$(OPSDIR)/static/XfkDisplay/arrays/NC6_fk.par  
recipe_list="... NOA NAO NB2 NBO NC2 NC3 NC4 NC6 ..."  
NOA_recipe=$(OPSDIR)/static/XfkDisplay/recipes/NOA.par  
NAO_recipe=$(OPSDIR)/static/XfkDisplay/recipes/NAO.par  
NB2_recipe=$(OPSDIR)/static/XfkDisplay/recipes/NB2.par  
NBO_recipe=$(OPSDIR)/static/XfkDisplay/recipes/NBO.par  
NC2_recipe=$(OPSDIR)/static/XfkDisplay/recipes/NC2.par  
NC3_recipe=$(OPSDIR)/static/XfkDisplay/recipes/NC3.par  
NC4_recipe=$(OPSDIR)/static/XfkDisplay/recipes/NC4.par  
NC6_recipe=$(OPSDIR)/static/XfkDisplay/recipes/NC6.par
```

J. Fyen

5 Maintenance Activities

Activities in the field and at the Maintenance Center

This section summarizes the activities at the Maintenance Center (NMC) Hamar, and includes activities related to monitoring and control of the NORSAR teleseismic array, as well as the NORESS, ARCESS, FINESS, GERESS, Apatity, Spitsbergen and Hagfors small-aperture arrays.

Activities also involve preventive and corrective maintenance, planning and activities related to the refurbishment of the NORSAR teleseismic array.

NORSAR

Visits to subarrays in connection with:

- Cable splicing
- Replacement of AIM-24 digitizers and preamplifiers
- Installation of power modification at remote sites
- Installation of DC/DC converter cards
- Removal, repair and replacement of equipment damaged by lightning

NORESS

- Repair of Hub processor and power supply damaged by lightning

ARCESS

- The Hub, UPS and CIM units were severely damaged by overvoltage on 8 June 97. They were brought to NMC for repair, and reinstalled 28-29 August 97.
- Installation of interface unit between Hub unit and satellite modem
- Repair of UPS rectifier and replacement of batteries
- Installation of ventilation unit for the Hub room

NMC

- Repair of defective electronic equipment, including the Hub, UPS and CIM units from ARCESS.

Additional details for the reporting period are provided in Table 5.1.

P.W. Larsen

K.A. Løken

Subarray/ area	Task	Date
<i>April 1997</i>		
NORSAR	Cable splicing at SP02.	April
01A		1-2/10
NMC		April
<i>May 1997</i>		
NORSAR	<p>No data from site. The 48VDC power supply in the UPS unit was damaged by lightning. The unit was taken to NMC for repair.</p> <p>Replaced the +9V protection diode at the remote site SP05. Replaced the battery card and the -9V protection diode at the remote site SP04.</p> <p>Reinstalled the 48VDC power supply. Replaced the +9V protection diode and the preamplifier at the SP03 remote site. Replaced preamplifier at the remote site SP01. All the equipment was damaged by lightning.</p> <p>The KS-54000 broadband seismometer was found to have been damaged by lightning and was taken to the NMC for repair.</p> <p>Reinstalled the KS-54000 broadband seismometer.</p> <p>Replaced the 48VDC power supply.</p> <p>Installed power modification at the BB remote site and SP05 remote site.</p> <p>Installed power modification at the SP03, SP04 and 00 remote sites.</p> <p>Repair of defective electronic equipment.</p>	May
03C		15/5
04C		15/5
03C		16/5
03C		20/5
03C		22/5
03C		23/5
01A		28/5
01A		30/5
NMC		May
<i>June 1997</i>		
NORSAR	The 48 VDC power supply had to be reset due to spikes on the power line caused by lightning.	June
02B		17,19/6

Subarray/ area	Task	Date
01A	The CIM units had to be reset.	17/6
03C	Replaced the lightning protection card in the CTV for the remote AIM-24BB digitizer in the LPV.	19/6
06C	Replaced protection control card and Brick amplifier at SP03. A DC/DC converter card was also installed in the SP03 junction box.	25/6
ARCESS	The UPS, HUB and CIM were found to be damaged by over-voltage on the main 230 VAC line. The HUB and the CIM had to be taken to NMC for repair.	11-15/6
NMC	Repair of defective electronic equipment.	June
<i>July 1997</i>		
NORSAR		July
06C	Replaced the old well head vault lid at SP05 with a new lid made out of aluminum.	1/7
01A	Replaced 48VDC power supply	2/7
03C	The 48 VDC power supply was found to have been damaged by lightning.	2/7
	Replaced the 48 VDC power supply.	3/7
	Installed DC/DC converter card in SP03 and BB junction boxes.	
	Replaced protection control card and Brick amplifier at SP01.	
02B	Installed DC/DC converter in BB junction box.	3/7
	The CIM units had to be reset.	
02B	Installed magnetic voltage regulator on the main 230 VAC line	4/7
02B	Installed DC/DC converter card and replaced protection control card and Brick amplifier at SP02, 04 and 00.	7/7
01B	Installed DC/DC converter card in SP01, 03, 00 and BB junction boxes	8/7
01B	Replaced Brick amplifier at SP00. The cables to SP01, 02, 05 and 00 were damaged by lightning	9/7

Subarray/ area	Task	Date
04C	Installed DC/DC converter card in SP02, 04, 05 and BB junction boxes. Replaced protection control card and Brick amplifier at SP02 and 04.	10/7
01A	Installed DC/DC converter card and replaced protection control card and Brick amplifier at SP04 and 05.	11/7
02C	The KS-54000 broadband seismometer was found to have been damaged by lightning	14/7
03C	Replaced Brick amplifier at SP03	15/7
04C	Replaced Brick amplifier at SP02	17/7
06C	Installed DC/DC converter card in junction box at SP01. Replaced lightning protection card in CTV for remote site SP03	22/7
06C	Replaced Brick amplifier at SP01	28/7
NORESS	The Hub processor and power supply were found to have been damaged by lightning and had to be repaired..	24/7
NMC	Repair of defective electronic equipment. Repair and testing of Hub unit from ARCESS	July
<i>August 1997</i>		
NORSAR		August
01A	Installed DC/DC converter card at SP02 and SP04	4/8
01A	Reinstalled AIM 24 digitizer at SP02	5/8
01B	Located damage on the cable at SP02	5/8
01B	Installed DC/DC converter card at SP04	6/8
03C	Installed DC/DC converter card at SP02, SP04 and SP00	8/8
03C	Installed DC/DC converter card at SP02 and SP05 Replaced AIM 24 digitizer at SP04	11/8
02B	Located damage on the cable at SP05	13/8
02B	Cable splicing at SP05	14/8
06C	Installed DC/DC converter card at SP04	15/8
04C	Installed DC/DC converter card at SP01, SP00 and SP03	18/8

Subarray/ area	Task	Date
06C	Installed DC/DC converter card at SP00	20/8
06C	Replaced fuses on protection card at SP05. Replaced protection card at SP00. Replaced DC/DC converter card at SP04	26/8
ARCESS	Reinstalled the Hub unit	28-29/8
NORESS	Testing of the ARCESS Hub unit	15/8
NMC	Repair of defective electronic equipment.	August
<i>September 1997</i>		
NORSAR		September
06C	Replaced protection card in CTV for remote site SP00	1/9
01A	Installed power modification at SP02, SP03 and SP00	8/9
02C	Replaced Brick amplifier, protection card and control card at SP05	11/9
04C	Replaced DC/DC converter at SP03	16/9
02C	Installed power modification, replaced Brick amplifier and control cards at remote sites SP01 and SP02	19/9
02C	Installed power modification at SP03	22/9
02B	Installed power modification at SP03	29/9
01B	Cable splicing at SP02	30/9
ARCESS	A new interface unit made at NMC was installed between the Hub unit and the satellite modem	11/9
	The UPS rectifier was repaired and the batteries replaced	23-26/9
	Repaired fiber optical link to sites AD, B1, B5, C3, C4, D2 and D8	
	Installed new ventilation system for the Hub room	
NMC	Repair of defective electronic equipment	September

Table 5.1. Activities in the field and the NORSAR Maintenance Center during 1 April - 30 September 1997.

6 Documentation Developed

Baadshaug, U. & S. Mykkeltveit (1997): Status Report: Norway's participation in GSETT-3, Semiannual Tech. Summ., 1 April - 30 September 1997, NORSAR Sci. Rep. 1-97/98, Kjeller, Norway.

Fyen, J. (1997): NORSAR large array processing at the IDC testbed. Semiannual Tech. Summ., 1 April - 30 September 1997, NORSAR Sci. Rep. 1-97/98, Kjeller, Norway.

Kværna, T. (1997): Status of the global Threshold Monitoring (TM) system, Semiannual Tech. Summ., 1 April - 30 September 1997, NORSAR Sci. Rep. 1-97/98, Kjeller, Norway.

Ringdal, F. (1997): Study of low-magnitude seismic events near the Novaya Zemlya nuclear test site, submitted to *Bull. Seism. Soc. Am.*

Ringdal, F., E.O. Kremenetskaya, T. Kværna & V. Asming (1997): The seismic event near Novaya Zemlya on 16 August 1997. Semiannual Tech. Summ., 1 April - 30 September 1997, NORSAR Sci. Rep. 1-97/98, Kjeller, Norway.

Ringdal, F. (1997): P/S ratios for seismic events near Novaya Zemlya. Semiannual Tech. Summ., 1 April - 30 September 1997, NORSAR Sci. Rep. 1-97/98, Kjeller, Norway.

Schweitzer, J. (1997): HYPOSAT — A new routine to locate seismic events. Semiannual Tech. Summ., 1 April - 30 September 1997, NORSAR Sci. Rep. 1-97/98, Kjeller, Norway.

Schweitzer, J. (1997): Recommendations for improvements in the PIDC processing of Matsushiro (MJAR) array data, Semiannual Tech. Summ., 1 April - 30 September 1997, NORSAR Sci. Rep. 1-97/98, Kjeller, Norway.

Semiannual Technical Summary, 1 October 1996- 31 March 1997, NORSAR Sci. Rep. 2-96/97, Kjeller, Norway.

7 Summary of Technical Reports / Papers Published

7.1 Status Report: Norway's participation in GSETT-3

Introduction

This contribution is essentially an update for the period April - September 1997 of the three status reports Mykkeltveit & Baadshaug (1996a), Mykkeltveit & Baadshaug (1996b) and Baadshaug & Mykkeltveit (1997) which cover the periods January 1995 - June 1996, April 1996 - September 1996 and October 1996 - March 1997, respectively.

Norwegian GSETT-3 stations and communications arrangements

From the second half of 1993 until 1 October 1996, Norway provided continuous data from three GSETT-3 primary array stations: ARCESS, NORESS and Spitsbergen. The location and configurations of these three stations are shown in Fig. 7.1.1. ARCESS and NORESS are 25-element arrays with identical geometries and an aperture of 3 km, whereas the Spitsbergen array has 9 elements within a 1-km aperture. All three stations have a broadband three-component seismometer at the array center.

Data from these three stations are transmitted continuously and in real time to NOR_NDC. The NORESS data transmission uses a dedicated 64 Kbits/s land line, whereas data from the other two arrays are transmitted via satellite links of capacity 64 Kbits/s and 19.2 Kbits/s for the ARCESS and Spitsbergen arrays, respectively. From the NOR_NDC, data have been forwarded to the prototype IDC (PIDC) in Arlington, Virginia, USA, via a dedicated fiber optical 256 Kbits/s link between the two centers.

The NORESS array has been used in GSETT-3 as a temporary substitute for the NORSAR teleseismic array (also shown in Fig. 7.1.1; station code NOA), awaiting a complete technical refurbishment of the latter. This effort has now been completed, and starting 30 August 1996, data from the NORSAR array have been transmitted continuously to the PIDC. Subject to funding, the NORESS array will, however, be retained as a GSETT-3 primary station hopefully until such time that the NORSAR array data are fully used in the PIDC operational processing cycle. We are cooperating with the PIDC on the task of preparing for the processing of NORSAR data at the PIDC (see section 7.4 of this report). Some Testbed processing of NORSAR data has been performed. The purpose of the PIDC Testbed is to facilitate integration testing and therefore minimize disruption to the operational system.

On 1 October 1996 numerous changes were made worldwide to the GSETT-3 network. The purpose of these coordinated changes was to bring the GSETT-3 network in line with the seismic component of the International Monitoring System (IMS) to the extent possible. As the Spitsbergen array is an auxiliary station in IMS, this station changed its status from primary to auxiliary in GSETT-3 on that date. This involved terminating the continuous forwarding of SPITS data to the PIDC and making data from this station available to the PIDC on a request basis via the AutoDRM protocol (Kradolfer, 1993; Kradolfer, 1996). The other stations named above have continued providing continuous data to the PIDC, in agreement with their status as primary seismic stations in the IMS.

Uptimes and data availability

Figs. 7.1.2 - 7.1.4 show the monthly uptimes for the two Norwegian GSETT-3 primary stations ARCESS, NORESS and for the testbed primary station NOA, respectively, for the period April - September 1997, given as the hatched (taller) bars in these figures. These barplots reflect the percentage of the waveform data that are available in the NOR_NDC tape archives for each of these three stations. The downtimes inferred from these figures thus represent the cumulative effect of field equipment outages, station site to NOR_NDC communication outages and NOR_NDC data acquisition outages. The ARCESS downtime during June-August (Fig. 7.1.2) was due to damage caused by overvoltage. Reinstallation was completed on 28 August.

Figs. 7.1.2-7.1.4 also give the data availability for these three stations as reported by the PIDC in the PIDC Station Status reports. The main reason for the discrepancies between the NOR_NDC and PIDC data availabilities as observed from these figures is the difference in the ways the two data centers report data availability for arrays: Whereas NOR_NDC reports an array station to be up and available if at least one channel produces useful data, the PIDC uses weights where the reported availability (capability) is based on the number of actually operating channels. As can be seen from these figures, these differences in the reporting practice in particular affect the results for the NORESS and NOA arrays.

Experience with the AutoDRM protocol

NOR_NDC's AutoDRM has been operational since November 1995 (Mykkeltveit & Baadshaug, 1996a).

Between November 1995 and the network changes on 1 October 1996, only 207 requests from external users were processed.

After SPITS changed station status from primary to auxiliary on 1 October 1996, the request load increased sharply, and for the month of October 1996, the NOR_NDC AutoDRM responded to 12338 requests for SPITS waveforms from two different accounts at the PIDC: 9555 response messages were sent to the "pipeline" account and 2783 to "testbed". Following this initial burst of activity, the number of "pipeline" requests stabilized at a level between 5000 and 7000 per month. Requests from the "testbed" account show large variations.

The monthly number of requests for SPITS data for the period April - September 1997 is shown in Fig. 7.1.5.

NDC automatic processing and data analysis

These tasks have proceeded in accordance with the descriptions given in Mykkeltveit and Baadshaug (1996a). For the period April - September 1997, NOR_NDC derived information on 921 supplementary events in northern Europe and submitted this information to the Finnish NDC as the NOR_NDC contribution to the joint Nordic Supplementary (Gamma) Bulletin, which in turn is forwarded to the PIDC. These events are plotted in Fig. 7.1.6.

Data forwarding for GSETT-3 stations in other countries

NOR_NDC continues to forward data to the PIDC from GSETT-3 primary stations in several countries. These currently include FINESS (Finland), GERESS (Germany) and Sonseca (Spain). In addition, communications for the GSETT-3 auxiliary station at Nilore, Pakistan, are provided through a VSAT satellite link between NOR_NDC and Pakistan's NDC in Nilore. Data from the Hagfors array (HFS) in Sweden were provided continuously through NOR_NDC until 1 October 1996, on which date this station changed its status in GSETT-3 from primary to auxiliary, in accordance with the status of HFS in IMS. From 1 October 1996, the PIDC obtains HFS data through requests to the AutoDRM server at NOR_NDC (in the same way requests for Spitsbergen array data are handled, see above). Fig. 7.1.7 shows the monthly number of requests for HFS data from the two PIDC accounts "pipeline" and "test-bed".

Future plans

NOR_NDC will continue the efforts towards improvements and hardening of all critical data acquisition and data forwarding hardware and software components, so as to meet requirements related to operation of IMS stations to the maximum extent possible.

The PrepCom has tasked its Working Group B with overseeing, coordinating and evaluating the GSETT-3 experiment until the end of 1998. The PrepCom has also encouraged states that operate IMS-designated stations to continue to do so on a voluntary basis and in the framework of the GSETT-experiment until such time that the stations have been certified for formal inclusion in IMS. In line with this, we envisage continuing the provision of data from Norwegian IMS-designated stations without interruption to the PIDC, and later on, following certification, to the IDC in Vienna, via the new global communications infrastructure currently being elaborated by the PrepCom.

U. Baadshaug
S. Mykkeltveit

References

- Baadshaug, U. & S. Mykkeltveit (1997): Status Report: Norway's participation in GSETT-3. *Semiann. Tech. Summ.*, 1 October 1996 - 31 March 1997, NORSAR Sci. Rep. No. 2-96/97, Kjeller, Norway.
- Kradolfer, U. (1993): Automating the exchange of earthquake information. *EOS, Trans., AGU*, 74, 442.
- Kradolfer, U. (1996): AutoDRM — The first five years, *Seism. Res. Lett.*, 67, 4, 30-33.
- Mykkeltveit, S. & U. Baadshaug (1996a): Norway's NDC: Experience from the first eighteen months of the full-scale phase of GSETT-3. *Semiann. Tech. Summ.*, 1 October 1995 - 31 March 1996, NORSAR Sci. Rep. No. 2-95/96, Kjeller, Norway.
- Mykkeltveit, S. & U. Baadshaug (1996b): Status Report: Norway's participation in GSETT-3. *Semiann. Tech. Summ.*, 1 April 1996 - 30 September 1996, NORSAR Sci. Rep. No. 1-96/97, Kjeller, Norway.

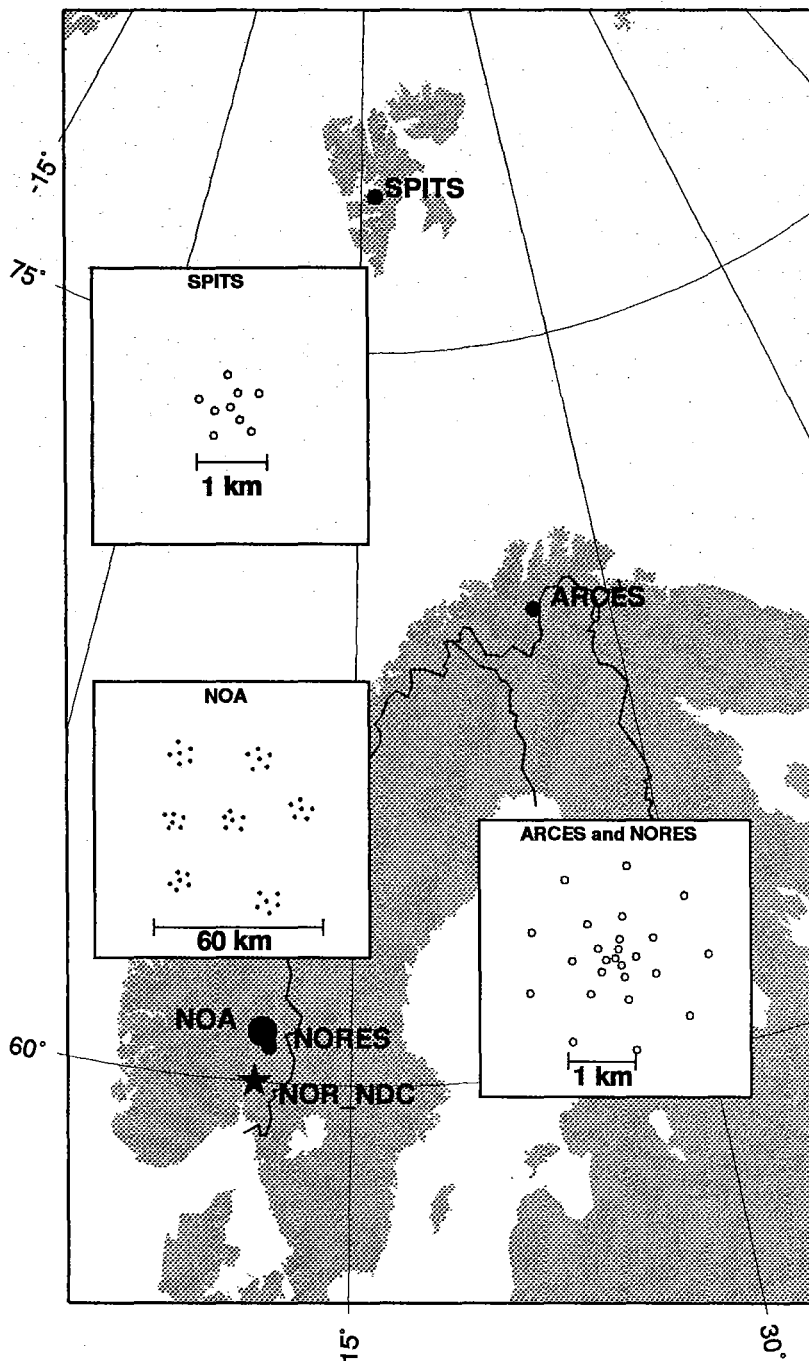


Fig. 7.1.1. The figure shows the locations and configurations of the two Norwegian GSETT-3 primary array stations with station codes NORES and ARCES. The data from these stations are transmitted continuously and in real time to the Norwegian NDC (NOR_NDC) and then on to the prototype IDC. The figure also shows the location of the testbed primary station NOA, which is soon to be fully used in GSETT-3 as a primary station. The auxiliary station SPITS is also shown in the figure.

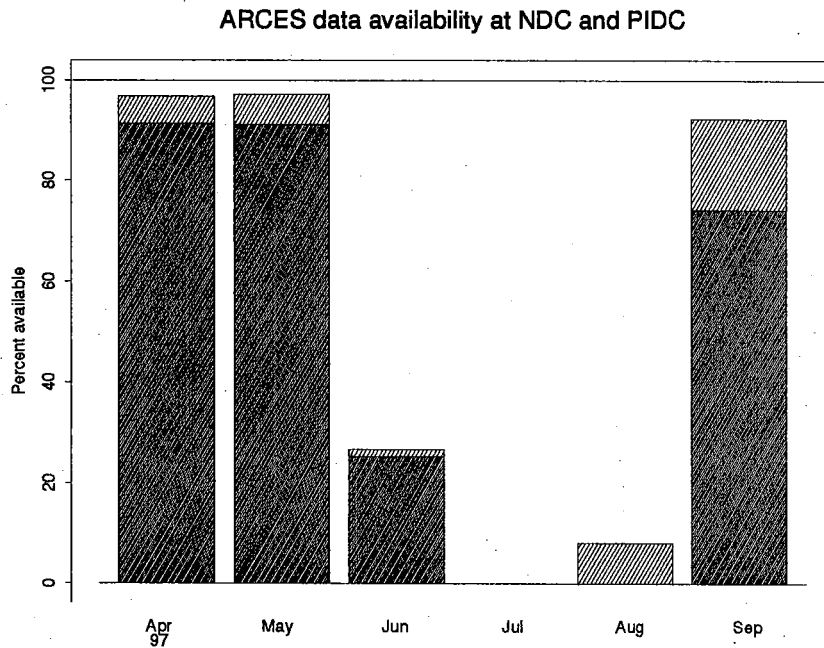


Fig. 7.1.2. The figure shows the monthly availability of ARCESS array data for the period April - September 1997 at NOR_NDC and the PIDC. See the text for explanation of differences in definition of the term "data availability" between the two centers. The higher values (hatched bars) represent the NOR_NDC data availability. The downtimes during June-August were due to overvoltage that caused severe damage to numerous components of the field system. Reinstallation was completed on 28 August.

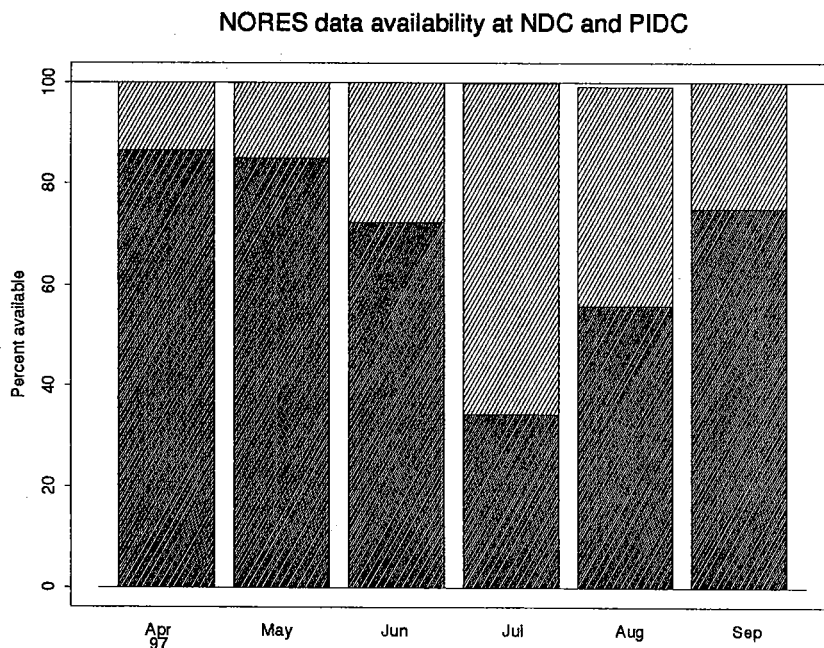


Fig. 7.1.3. The figure shows the monthly availability of NORESS array data for the period April - September 1997 at NOR_NDC and the PIDC. See the text for explanation of differences in the definition of the term "data availability" between the two centers. The higher values (hatched bars) represent the NOR_NDC data availability.

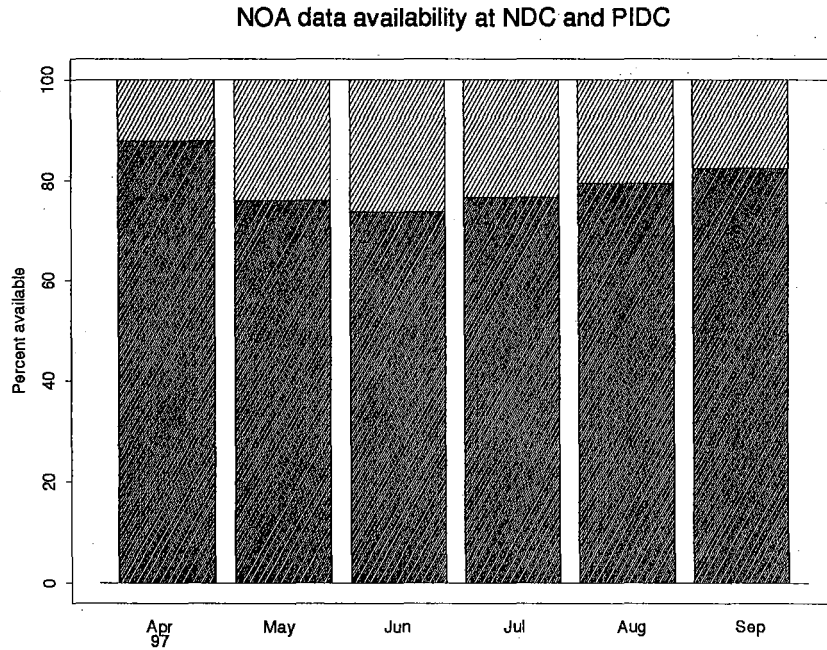


Fig. 7.1.4. The figure shows the monthly availability of NORSAR array data for the period April - September 1997 at NOR_NDC and the PIDC. See the text for explanation of differences in definition of the term "data availability" between the two centers. The higher values (hatched bars) represent the NOR_NDC data availability.

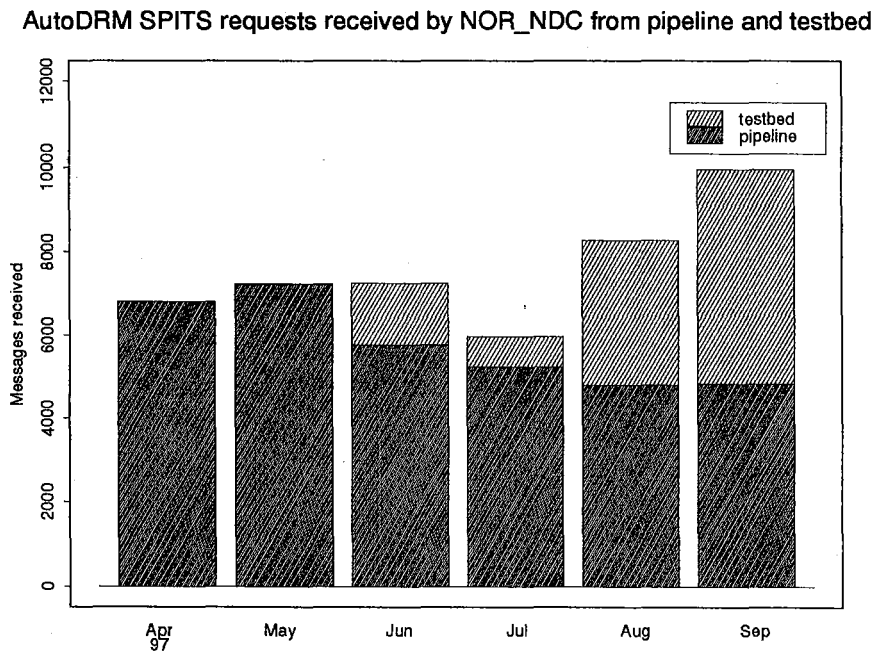


Fig. 7.1.5. The figure shows the monthly number of requests received by NOR_NDC from the PIDC for SPITS waveform segments.

Reviewed Supplementary Events

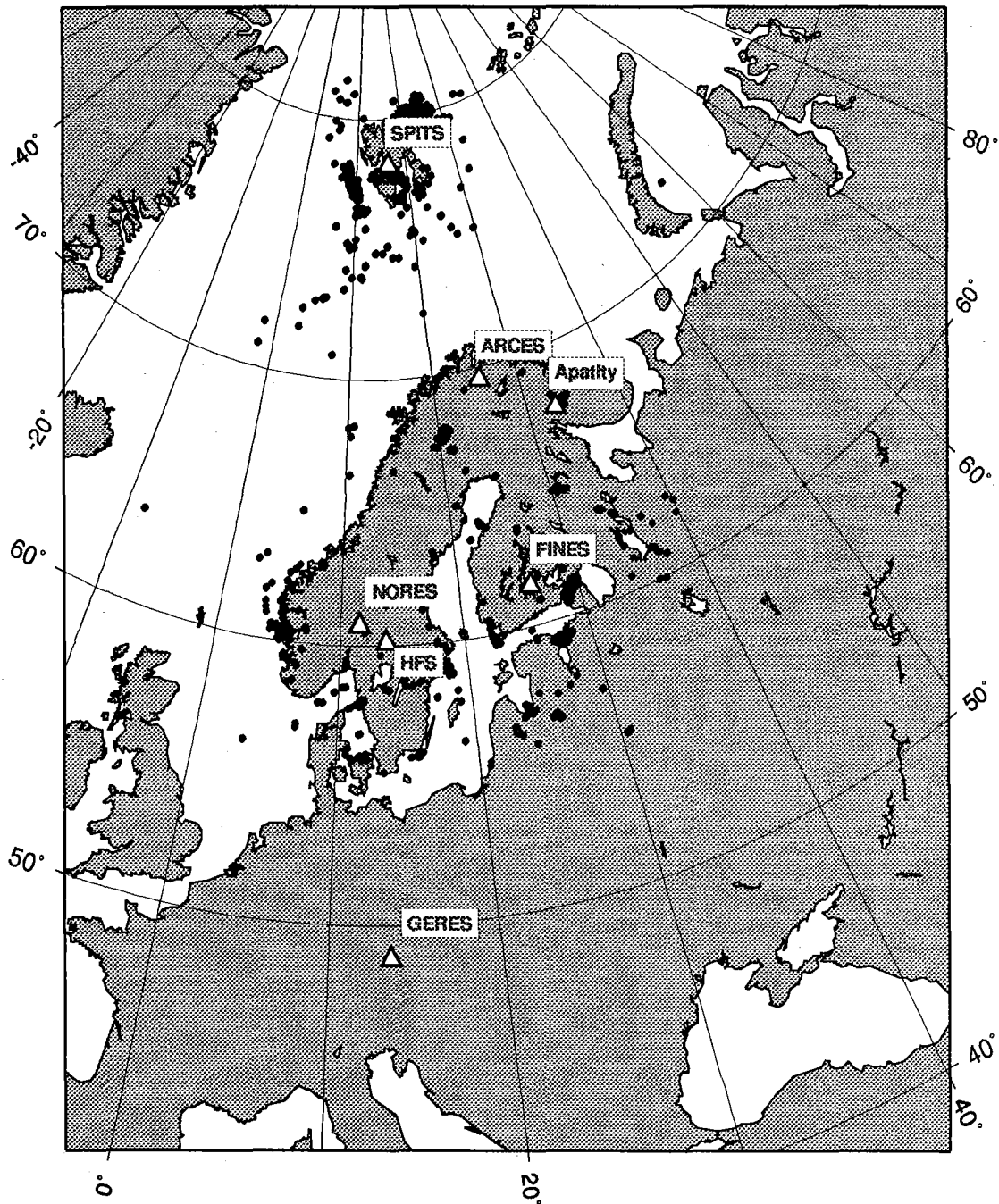


Fig. 7.1.6. The map shows the 921 events in and around Norway contributed by NOR_NDC during April - September 1997 as Supplementary (Gamma) data to the PIDC, as part of the Nordic Supplementary data compiled by the Finnish NDC. The map also shows the seismic stations used in the data analysis to define these events.

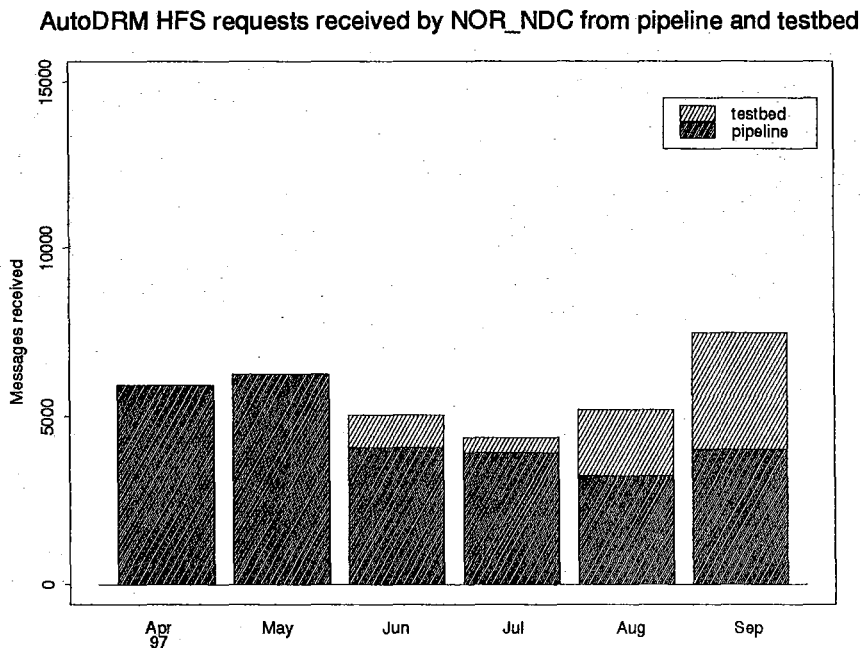


Fig. 7.1.7. The figure shows the monthly number of requests received by NOR_NDC from the PIDC for HFS waveform segments.

7.2 Status of the global Threshold Monitoring (TM) system

Introduction

Detailed descriptions of the global Threshold Monitoring (TM) system have been given in several of the latest NORSAR Semiannual Technical Summaries (Kværna et al., 1994, Ringdal et al., 1995, Kværna, 1996, 1997), and for information on the technical details we refer to these reports and the references therein. In this report we will give the status of the development and testing of the TM system at the Provisional International Data Center (PIDC), as well as outlining some of our ideas for future development of the system.

Continuous TM processes

During the 6 months of this reporting period we have been running all the basic computational processes of the TM system on the PIDC testbed. These processes are:

- Continuous calculation of short-term-averages (STAs) for all primary stations using the detection and feature extraction program (*DFX*) running in the Alpha processing pipeline. The STAs are written to cyclical files for subsequent usage. The processes in the Alpha pipeline are running as close as possible to real-time.
- Continuous calculation of the three-station detection capability of the network for a set of 2562 globally distributed target areas, using the STAs calculated by *DFX*. This program, called *tm_regproc*, is implemented in the Delta processing pipeline, running with a delay of 10 hours behind real-time.
- Interpolation and reformatting of the three-station detection capability to facilitate map displays of the results. This program, called *tm_data2rdf*, is also implemented in the Delta pipeline.

These processes have all been running without errors, and they have not caused any problems to the continuous operation of the PIDC testbed. In addition, we have verified that the computational resources available at the PIDC testbed are sufficient for keeping the TM related processes up with real-time. This shows that the basic computational processes of the TM system are now of sufficient quality to satisfy the requirements for transfer into the operational pipeline at the PIDC.

TM Products

A set of programs for generation of products from the TM system was implemented on the PIDC testbed in mid-September, but due to some problems with the operational environment, we initially faced some difficulties in getting our programs into stable operation. We now hope to have identified the main problems, and anticipate that with the latest changes to our programs, stable operation can be accomplished.

Three types of products (plots) are now available from the TM system. These products are designed to provide useful information to the international community on the performance and status of the primary seismic network used for monitoring of the Comprehensive Test Ban

Treaty (CTBT). All of these plots are created on an hourly basis and provide an overview of the characteristics of the primary seismic network during the analyzed hour.

In the following, a detailed description of the different products will be given:

Information on data availability and seismic events

There are four main factors that cause variations in the event detectability of the primary seismic network. These are:

- Fluctuations with time in the background noise level
- Changes in data quality at the PIDC caused by communications problems, station outages or other data errors like spikes and gaps
- Temporary deficiencies in the PIDC data processing
- Signals from interfering seismic events around the world.

For the first type of hourly plots, shown in Fig. 7.2.1, the color of the station symbols provide information on the availability of data for a particular 1-hour interval (1997/09/07 10:00 to 11:00). The arrays are marked by circles and three-component stations by triangles. Red symbols indicate that data were successfully recorded and processed less than 10% of the total time interval, yellow symbols indicate a success rate between 10% and 90% and green symbols indicate that for more than 90% of the time data were successfully recorded and processed.

In order to estimate the detection capability at different parts of the world for a 1 hour interval, we need to take into account the maximum travel-time of the phases possibly originating anywhere in the Earth within this time interval. This means that with the current parametrization of the TM system, we actually need to analyze about 1 hour and 22 minutes of data from each station, and the statistics shown in Fig. 7.2.1 in fact apply to this interval.

The statistics on available and processed data is derived from the short-term-averages (STAs) of the different stations, and the STAs of the cyclical files are assigned particular null values if there are gaps in the processing by DFX. Processing gaps are reported in the cases of unavailable data or processing problems at the PIDC, or if the data quality checking feature of DFX identified erroneous data so that DFX was unable to create STA traces.

Notice that for the interval reported in Fig. 7.2.1, the Australian arrays (ASAR and WRA), the GERES and FINES arrays in Europe, as well as the BGCA and partly the DBIC stations in Africa were all down. As shown later in this report, the outage of ASAR and WRA lead to a significantly reduced event detection capability for the areas within and around Australia.

When the Reviewed Event Bulletin (REB) is complete, the locations of events originating within or close to the actual time interval are introduced into these plots, and the event information are given below the map (see Fig. 7.2.1.). Notice the occurrence of a major event (m_b 4.9) and an aftershock in Pakistan.

Detailed information on station outages and processing gaps, arriving signals and fluctuations in the background noise level

The panel shown in Fig.7.2.2 provides an overview of the background noise level and the observed signals at each of the primary stations during the data interval (1 hr 22 min 20 s) used for assessing the detection capability of the 1 hour interval.

The traces shown are continuous $\log(A/T)$ equivalents derived from the STA traces. The STA traces are calculated from filtered beams for the arrays, and for the three-component stations from filtered vertical-component channels.

The fluctuations in the $\log(A/T)$ equivalents are either caused by variations in the background noise levels, calibration signals, data problems like unmasked spikes or electronic noise, or signals from seismic events. Notice in particular the signals from the m_b 4.9 event in Pakistan (origin time 10:15:24) seen at most stations of the primary network.

For each station, the cutoffs of the filter bands used for teleseismic monitoring are given below the station codes. Also given are the average values of the $\log(A/T)$ equivalents, which is an overall measure of the background noise level. Generally speaking, a low background noise level indicate a good capability to detect signals, and vice versa.

The percentages of successfully recorded and processed data are also given for each station, and the intervals with gaps in data processing are indicated in red above the time axis.

Together with the station and event information illustrated in Fig. 7.2.1, the station data panel shown in Fig. 7.2.2 provide a convenient tool for assessing the state-of-health of the PIDC primary seismic network. In addition, this information will help to explain temporary variations in the global event detectability.

Network detection capability maps

As presented in the previous Semiannual Technical Summary (Kværna, 1997), a simplified instantaneous network detection capability map can be computed by choosing the **third lowest** of the station "noise magnitudes", and then adding e.g., 0.7 m_b units to accommodate an SNR of 5.0 required for phase detection.

As a product from the global Threshold Monitoring system, we show in the upper map of Fig. 7.2.3 the average network detection capability for the 1-hour interval (1997/09/07 10:00 to 11:00). Variation from hour to hour of the average detection capability is primarily caused by long station or processing outages, by increased background noise levels at the different stations, or by signals of longer duration from large seismic events. Notice in particular the low detection capability around Australia and Africa caused by the outages of the stations ASAR, WRA, BGCA and partly DBIC.

In addition, the lower map of Fig 7.3.3 shows the poorest (lowest) detection capability for the analyzed hour. Differences from the average capability are primarily caused by signals from seismic events, shorter outages, and data errors like unmasked spikes or electronic noise.

Notice that the m_b 4.9 event in Pakistan temporarily lowers the detection capability all over the world, in particular in the neighborhood of the actual event location.

Both types of maps shown in Fig. 7.2.3 should provide important information on the capability of the primary seismic network to detect events in different parts of the world, whereas the information provided in Figs. 7.2.1 and 7.2.2 will help to explain the variations in the global event detection capability.

The products provided from the global TM system should in this way be useful for monitoring compliance with the CTBT, in particular by placing confidence on the performance of the International Monitoring System, but also by giving a warning in the case of lowered monitoring capability, e.g., caused by station outages, communication problems, data processing problems or extremely high seismic activity.

Transfer of the Global Threshold Monitoring system from the PIDC testbed to the PIDC operational pipeline

Although the testing of the different modules of the TM system are approaching its completion on the PIDC testbed, there is some work left before we are ready to move the TM system to the operational pipeline. During the next couple of months we therefore have to focus on completing the operational and users' manual as well as streamlining the different scripts and programs for operation by non-expert users. Once this is completed a proposal will be written to the PIDC Configuration Control Board (CCB) for transfer of the TM system to the PIDC operational pipeline.

Future developments

We plan in the near future to include in the TM system the bulk station magnitude corrections derived from the event station magnitudes reported in the Reviewed Event Bulletins (REBs). This will require little work, but it will significantly reduce the uncertainty associated with the estimated global detection capability.

The threshold monitoring concept was originally developed to assess the maximum magnitude of possibly hidden events in given regions, at the 90% confidence level (Ringdal and Kværna, 1989, 1992). With this approach we also obtain an estimate of the monitoring capability of the network to observe small events in different target areas using the most sensitive stations of the network. Somewhat simplified, we could say that for events below the monitoring threshold, it would be unlikely to observe signals at any stations of the network. On the other hand, for event magnitudes slightly above the monitoring threshold, it may be possible to observe signals at the most sensitive stations of the network by visual inspection or by running a detector at a low detection threshold.

The upper map of Fig. 7.2.4. shows the average monitoring threshold for the 1-hour interval (1997/09/07 10:00 to 11:00). Notice that in North America and northern Europe the average monitoring threshold is very low due to the location of sensitive array stations located in these regions, whereas the monitoring threshold around Africa and Australia is high because of station outages.

It seems that the average monitoring threshold is generally about one magnitude unit lower than the average three-station detection capability shown in Fig. 7.2.3. This means that by re-analyzing data at the stations most sensitive to events in a given region, we are able to observe signals from events with magnitudes significantly below the number given by the three-station detection capability. Notice that the color code is shifted by 0.5 m_b units between Figs. 7.2.3 and 7.2.4.

Similar to the poorest detection capability shown in the lower map of Fig 7.2.3, the lower map of Fig. 7.4.4 shows the highest monitoring threshold during the analyzed hour. Again, notice the temporary increase in monitoring threshold for large parts of the world caused by signals from the m_b 4.9 event in Pakistan.

We may at a later stage include the maps of the average and highest monitoring threshold as a product from the global TM system. The monitoring thresholds will provide information as to what extent it is possible, at a later stage, to identify signals from smaller seismic events that were not reported in the Reviewed Event Bulletin. This suggests that the low monitoring thresholds obtainable by TM system could have a significant deterrence value during a CTBT.

T. Kværna
F. Ringdal
U. Baadshaug
H. Iversen

References

- Kværna, T., F. Ringdal, H. Iversen and N.H.K. Larsen (1994): A system for continuous seismic threshold monitoring, final report, Semiannual Tech. Summ., 1 Apr - 30 Sep 1994, NORSAR Sci. Rep, 1-94/95, NORSAR, Kjeller, Norway
- Kværna, T. (1996): Tuning of processing parameters for Global Threshold Monitoring at the IDC, Semiannual Tech. Summ., 1 Apr - 30 Sep 1996, NORSAR Sci. Rep, 1-96/97, NORSAR, Kjeller, Norway
- Kværna, T. (1997): Threshold magnitudes, Semiannual Tech. Summ., 1 Oct 1996 - 31 Mar 1997, NORSAR Sci. Rep, 2-96/97, NORSAR, Kjeller, Norway
- Ringdal, F. and T. Kværna (1989): A multi-channel approach to real time network detection, location, threshold monitoring. *Bull. Seism. Soc. Am.*, 79, 1927-1940.

Ringdal, F. and T. Kværna (1992): Continuous seismic threshold monitoring, *Geophys. J. Int.*, 111, 505-514.

Ringdal, F., T. Kværna and S. Mykkeltveit (1995): Global seismic threshold monitoring and automated network processing, Semiannual Tech. Summ., 1 Oct 1994 - 31 Mar 1995, NORSAR Sci. Rep, 2-94/95, NORSAR, Kjeller, Norway

1997/09/07 10:00:00 - 1997/09/07 11:00:00

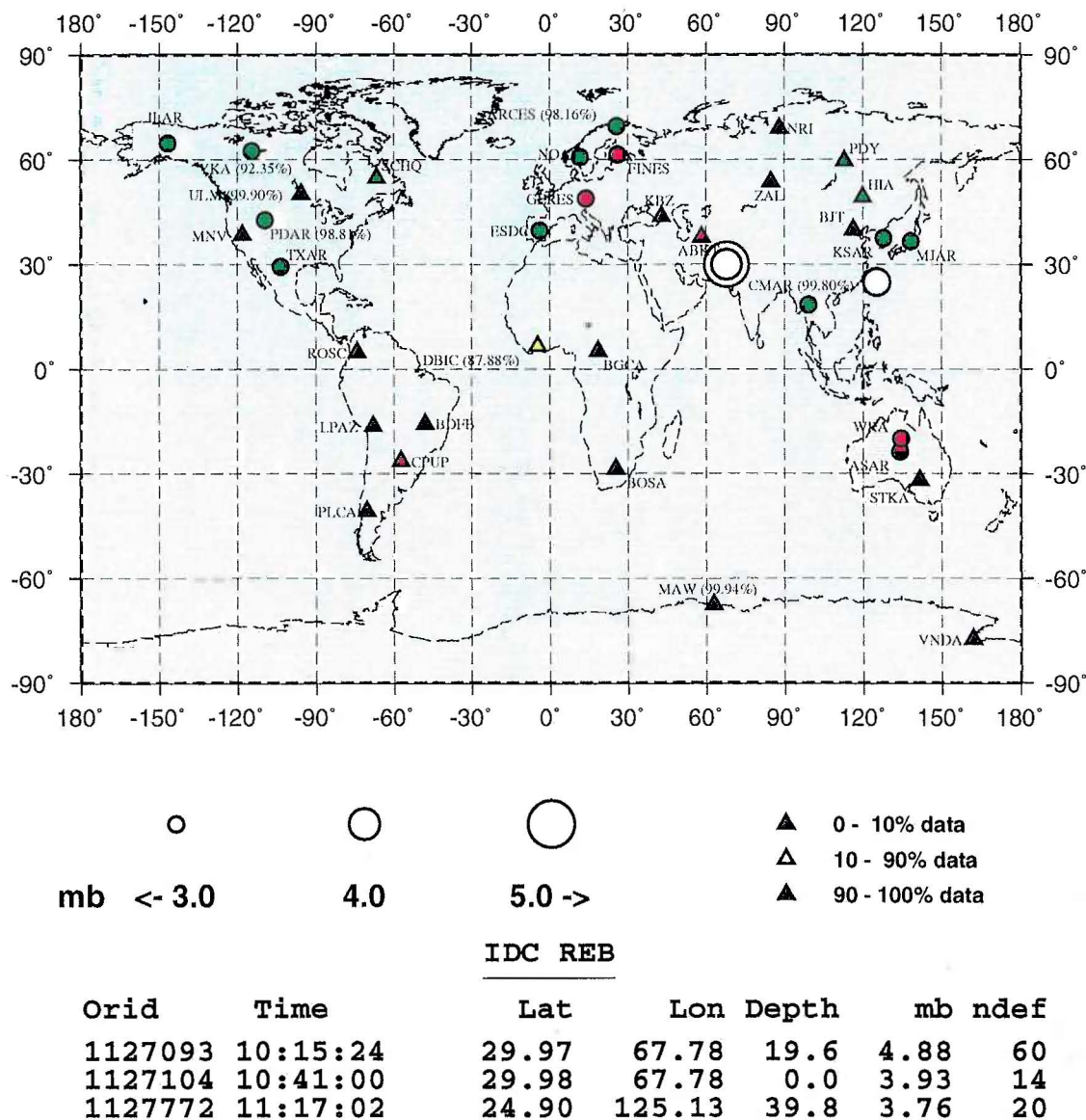
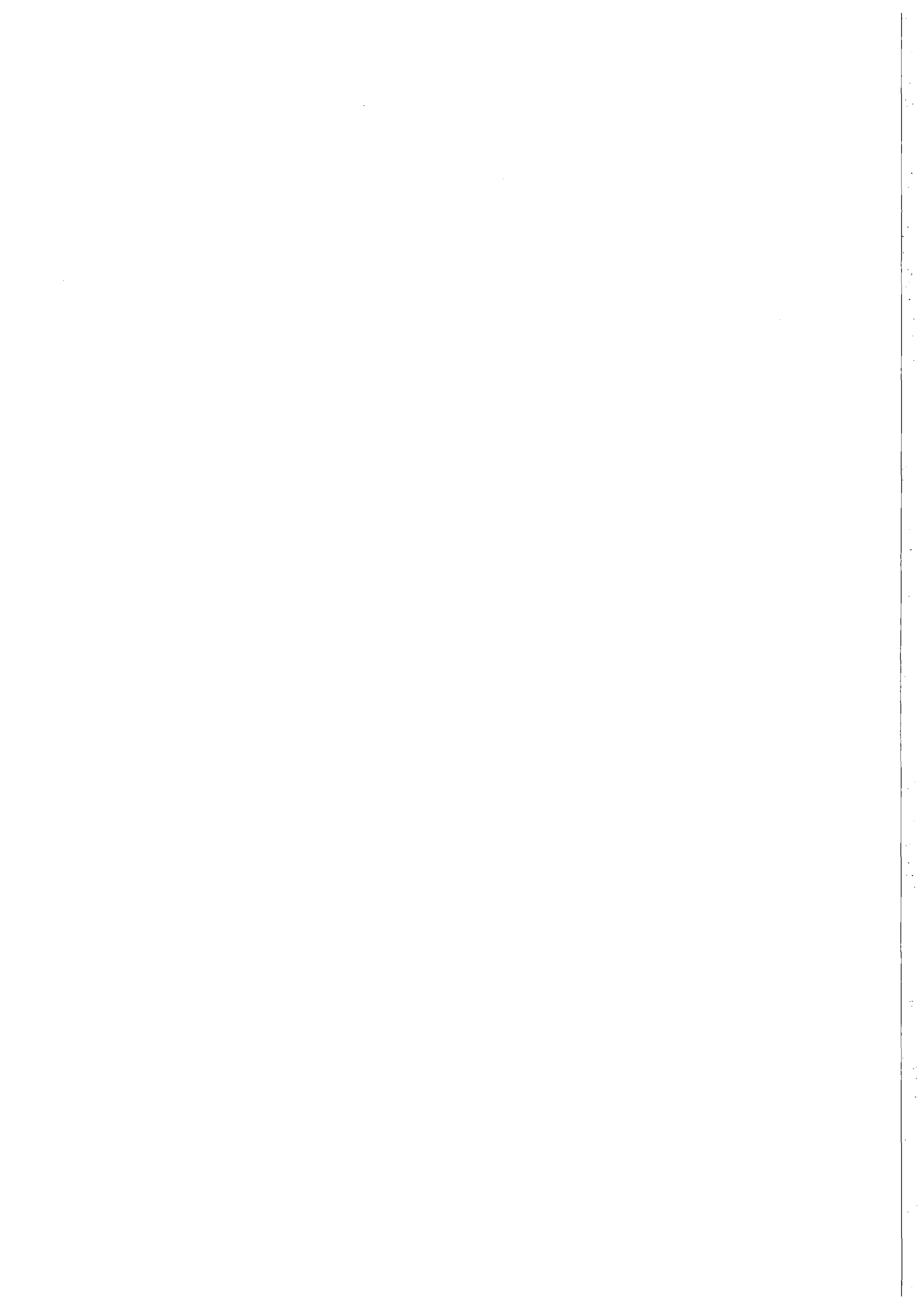


Figure 7.2.1. The color of the station symbols provide information on the availability of data for a particular 1-hour interval (1997/09/07 10:00 to 11:00). The arrays are marked by circles and three-component stations by triangles. Red symbols indicate that data were successfully recorded and processed less than 10% of the total time interval, yellow symbols indicate a success rate between 10% and 90% and green symbols indicate that for more than 90% of the time data were successfully recorded and processed.

Notice that for the interval reported, the Australian arrays (ASAR and WRA), the GERES and FINES arrays in Europe, as well as the BGCA and partly the DBIC stations in Africa were all down.

When the Reviewed Event Bulletin (REB) is complete, the locations of events originating within or close to the actual time interval is plotted, and the event information is given below the map. Notice the occurrence of a major event (m_b 4.9) and an aftershock in Pakistan.



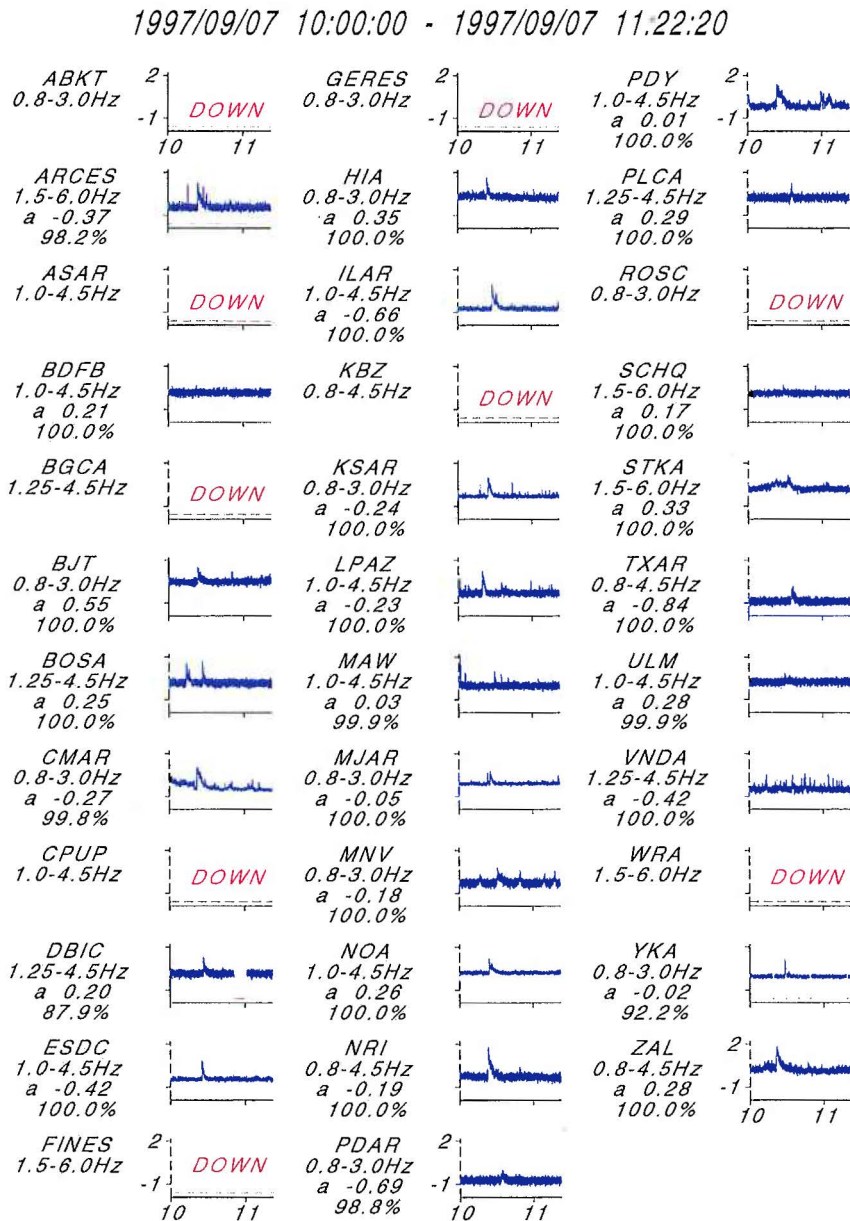
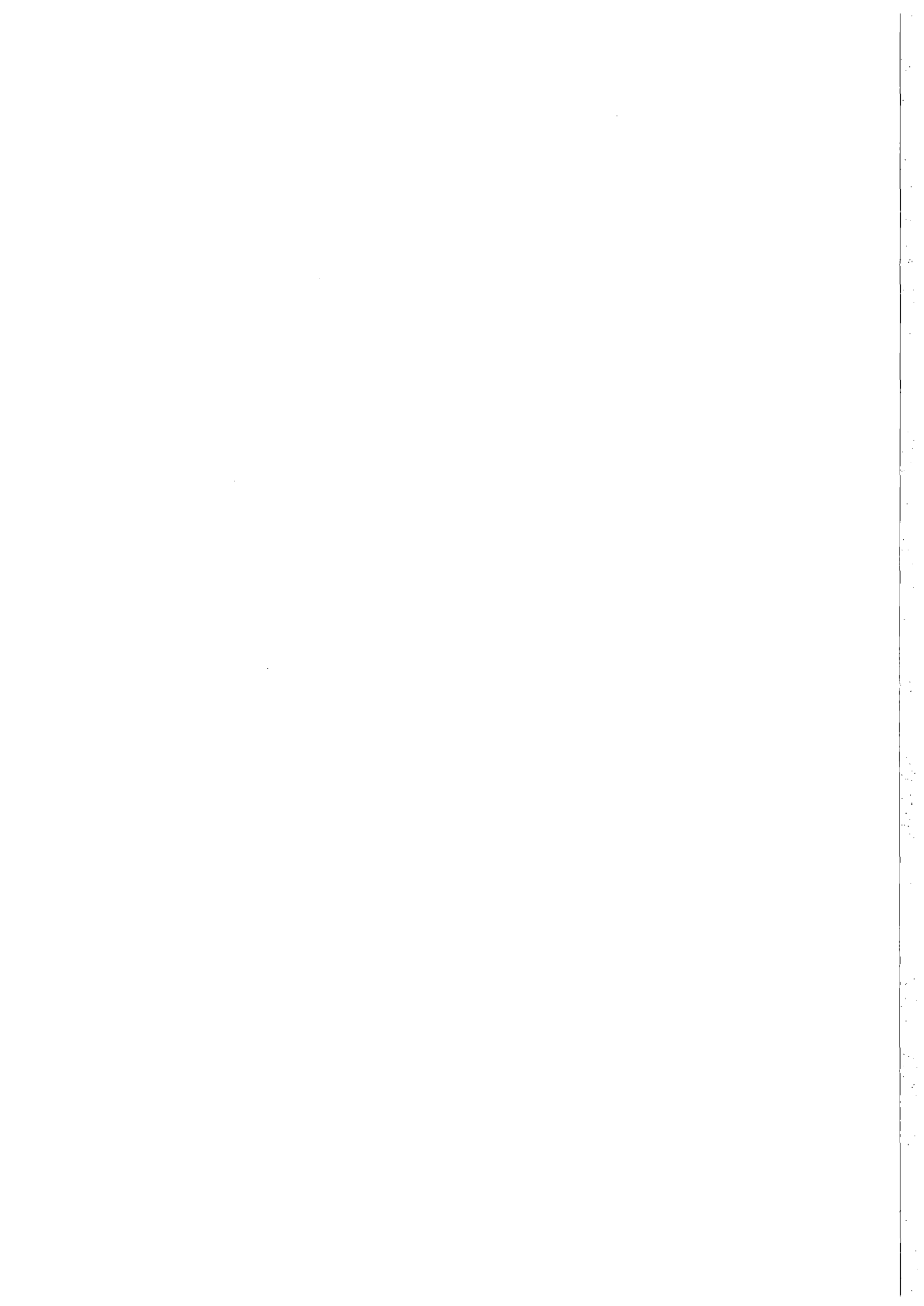


Figure 7.2.2. The panel provides an overview of the background noise level and the observed signals at each of the primary stations during the data interval (1 hr 22 min 20 s) used for assessing the detection capability of the 1 hour interval. The traces shown are continuous log(A/T) equivalents derived from the STA traces. Notice in particular the signals from the m_b 4.9 event in Pakistan (origin time 10:15:24) seen at most stations of the primary network.

The STA traces are calculated from filtered beams for the arrays, and for the three-component stations from filtered vertical-component channels. For each station, the cutoffs of the filter bands used for teleseismic monitoring are given below the station labels. Also given are the average values of the log(A/T) equivalents, which is an overall measure of the background noise level.

The percentages of successfully recorded and processed data are also given for each station, and the intervals with gaps in data processing are indicated in red above the time axis.



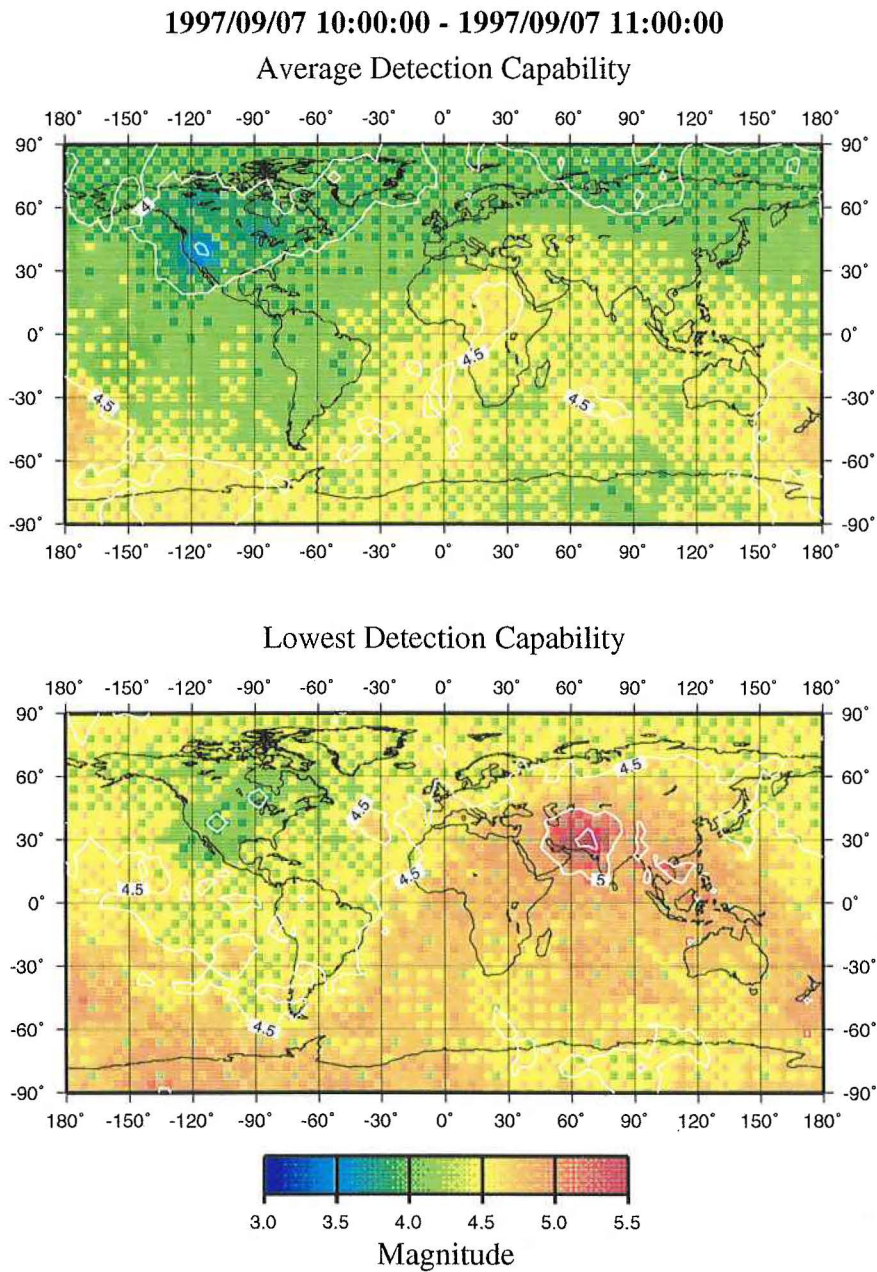
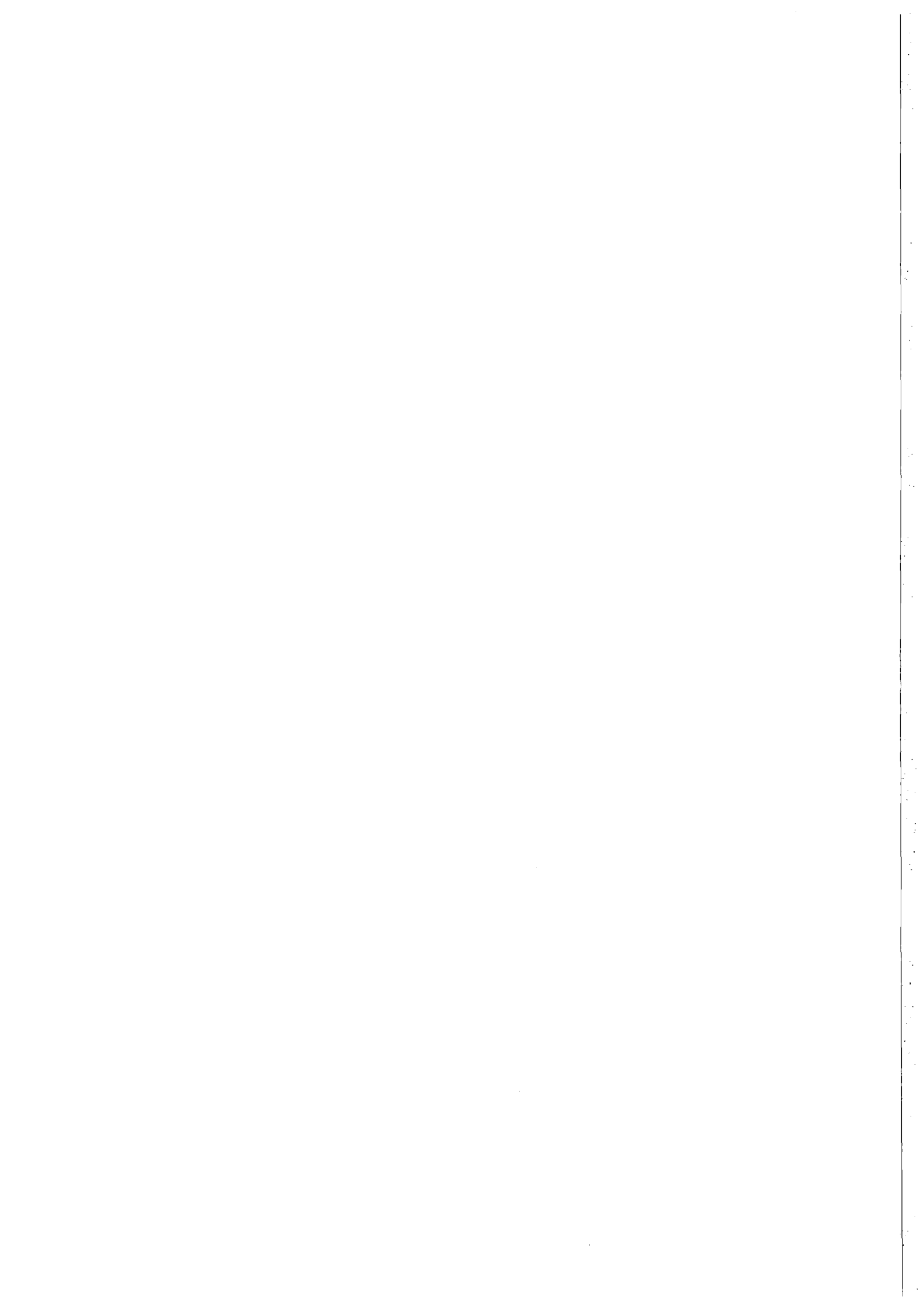


Figure 7.2.3. The the upper map of the figure shows the average network detection capability for the 1-hour interval (1997/09/07 10:00 to 11:00). Variation from hour to hour of the average detection capability is primarily caused by longer station or processing outages, by increased background noise levels at the different stations, or by signals of long duration from large seismic events. Notice in particular the low detection capability around Australia and Africa caused by the outages of the stations ASAR, WRA, BGCA and partly DBIC.

The lower map shows the poorest (lowest) detection capability for the analyzed hour. Differences from the average capability are primarily caused by signals from seismic events, shorter outages, and data errors like unmasked spikes or electronic noise. Notice that the m_b 4.9 event in Pakistan temporarily lowers the detection capability all over the world, and in particular in the neighborhood of the actual event location.



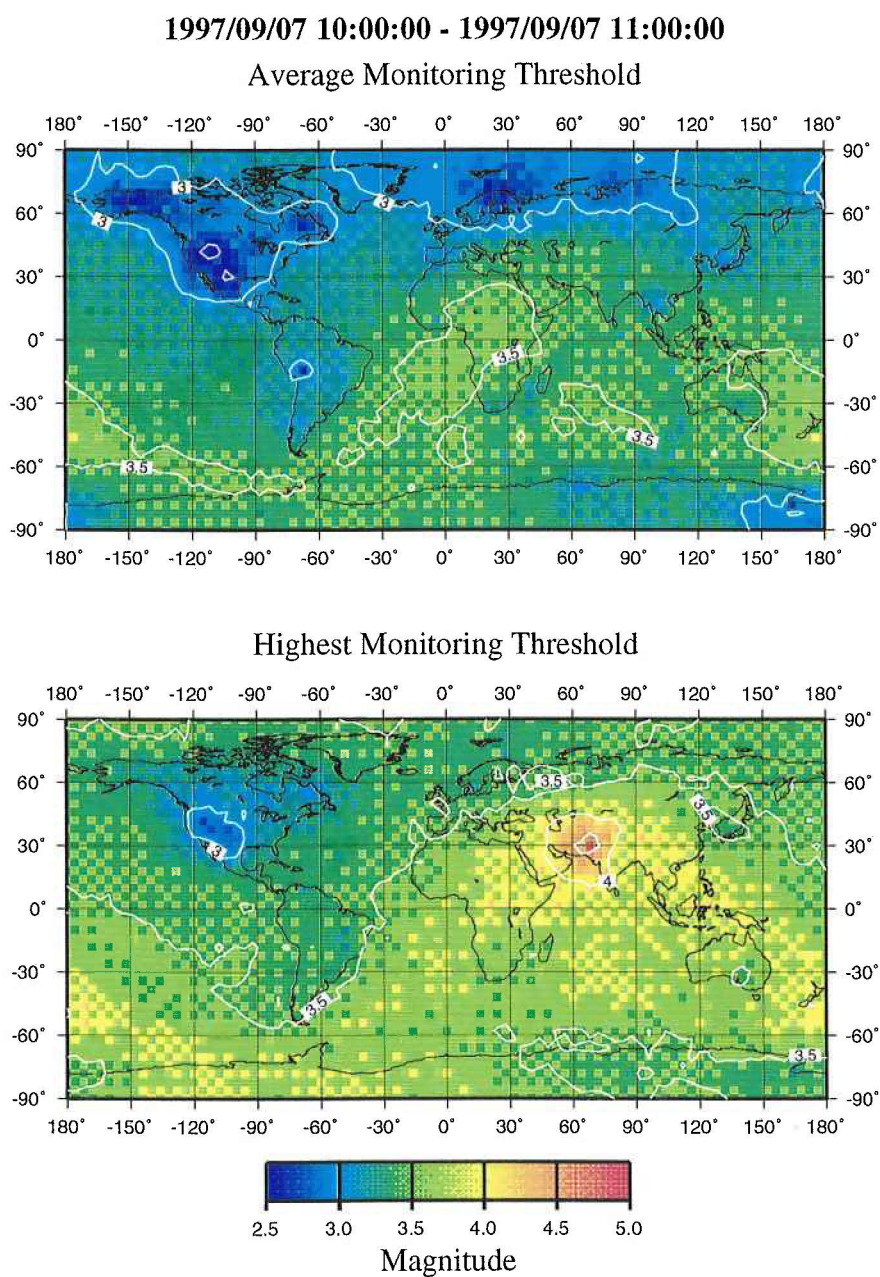


Figure 7.2.4. The upper map shows the average monitoring threshold for the 1-hour interval (1997/09/07 10:00 to 11:00). The monitoring threshold gives an estimate of the monitoring capability of the network to observe small events in different target areas using the most sensitive stations of the network.

Notice that in North America and northern Europe the average monitoring threshold is very low due to the location of sensitive array stations located in these regions, whereas the monitoring threshold around Africa and Australia is high because of station outages.

It seems that for the current primary seismic network, the average monitoring threshold is generally about one magnitude unit lower than the average three-station detection capability shown in Fig. 7.2.3. This means that by reanalyzing data at the stations most sensitive to



events in a given region, we are able to observe signals from events with magnitudes significantly below the number given by the tree-station detection capability. Notice that the color code is shifted by 0.5 m_b units between Figs. 7.2.3 and 7.2.4.

Similar to the poorest detection capability shown in the lower map of Fig 7.2.3, the lower map of this figure shows the highest monitoring threshold during the analyzed hour. Again, notice the temporary increase in monitoring threshold for large parts of the world caused by signals from the m_b 4.9 event in Pakistan.

7.3 HYPOSAT - A new routine to locate seismic events

Introduction

A new program, HYPOSAT, has been developed for the purpose of utilizing the largest possible set of available information for locating events. That means, besides the usually used travel times and eventually azimuth informations, this program also inverts for the observed ray parameters (or apparent velocities) as well as for travel-time differences between phases observed at the same station. To invert the ray parameter gives a weaker indication for the epicentral distance but the ray-parameter residual is a good criterion to identify phases and a large residual can also indicate a large azimuth error. Travel-time differences are usually used only in the case of surface reflections (pP or sP) to estimate the depth of the source or in cases where a single station alone observes P and S and an azimuth. With this program all possible travel-time differences can be used as additional observations. In the case of ideal error free data, these travel-time differences are a linear combination of the onset times and they cannot contribute new information to the inversions. But the situation changes in the case of erroneous and incomplete data (see the examples), which is usual for all location problems. All travel-time differences are dependent on the epicentral distance but not on the source time or systematic timing errors; the influence of source-depth errors and velocity anomalies below the stations is also reduced.

In the case of reflections (e.g. pP, sP, pS, sS, PmP, SmP, PcP, PcS, ScP, PcP, ScS) the travel-time difference to a direct phase is strongly influenced by the source depth. The usage of travel-time differences also decreases the influence of model uncertainties, because the travel-time differences are less sensitive for base line shifts between different models.

Intuitively, utilizing all this information for locating events should give a possibility of obtaining better location estimates (origin time, latitude, longitude, and depth). In the following, the program and its usage will be described in some detail, as well as some examples will be shown on event locations with and without the usage of travel-time differences.

Data input

The data input for this program are the models used to calculate the travel times, station informations and the observed data. The following points explain this in more detail:

- a) In this version of the program the routine supports the following Earth models prepared for the tau-spline interpolation software of Buland & Chapman (1983): Jeffreys-Bullen (1940), PREM (Dziewonski & Anderson, 1981), IASP91 (Kennett & Engdahl, 1991), SP6 (Morelli & Dziewonski, 1993), and AK135 (Kennett et al., 1995).
- b) Additionally, to locate events in local or regional distances, a model of horizontal layers eventually with discontinuities of first or second order can be defined and used for regional phases (Pg, Pb, Pn, Sg, Sb, Sn), their surface reflections (pPg, pPb, pPn, sSg, sSb, sSn), their multiples (PgPg, PbPb, PnPn, SgSg, SbSb, SnSn), and eventually their reflections from the Conrad or the Mohorovicic discontinuity (PbP, PmP, SbS, SmS).

- c) Station coordinates in a NEIC-type list and eventually a file containing local P- and S-velocities below the stations to correct onset times for station elevation and possibly for a known velocity anomaly below this station.
- d) File containing data for calculating the ellipticity corrections (Kennett & Gudmundsson, 1996).
- e) Observed arrival times of all phases as defined in the IASP91 tables or the local/regional model and their standard deviations. As an option, the travel-time differences between phases arriving at the same station are calculated internally and used during the inversion.
- f) Observed azimuth and ray parameter (apparent velocity) values from array or polarization measurements and their standard deviations.
- g) If known, an initial solution for the hypocenter can be given, including its uncertainty.

The inversion

To get a relatively well defined starting epicenter, all available azimuth observations are used to calculate a mean solution of all crossing azimuth lines. If this fails, a single S-P travel-time difference and a single azimuth observed at the same station can also be used to define an initial epicenter. If this also is not possible, a starting epicenter is guessed either at the closest station or in the center of the station net.

The initial source time is derived from all S-P travel-time differences after Wadati (1933) or derived from the earliest onset time at the closest station.

Usually the location process of a seismic event is formulated as an iterative inversion of a linearized system of normal equations (Geiger, 1910). In this program this equation system is solved with the Generalized-Matrix-Inversion (GMI) technique (e.g. Menke, 1989) using the Single-Value-Decomposition algorithm (SVD) as published in Press et al. (1992). All partial derivatives - except those given by the tau-spline software (Buland & Chapman, 1983) - are calculated in the program during the inversion process and the Jacobi matrix is recalculated for each iteration. The iteration process stops, if the change between two different solutions falls below a predefined limit. Internal procedures test the quality and stability of a solution.

The given standard deviations of the observed data (independently given for every onset, azimuth, and ray parameter observation) are used respectively to weight the corresponding equation in the equation system. The parameters to be modeled (i.e. the source parameters) are weighted initially with the given (or calculated) uncertainties and later with the standard deviations of the modeled parameters, now used as 'a priori' information for the next iteration. This will keep relatively well defined model parameters mostly unchanged in the next iteration. E.g. if the epicenter is well defined by the data, the remaining observed residuals are used mainly to resolve source time and depth. In this version of the program the final standard deviations of the modeled parameters are given as the uncertainties of the estimated source. The calculation of 90% confidence error ellipses is planned for the next upgrade of the program.

All calculations are done for the spherical Earth; internally all latitudes are transformed into geocentric latitudes (Gutenberg & Richter, 1933). The input and output are always in geographic latitudes and longitudes; all standard deviations of the inverted coordinates are given in

degrees. An output of the resolution, the correlation and the information-density matrix for the last iteration is optional.

The system of equations to be solved has the following form:

$$\begin{bmatrix}
 1 & \frac{\partial t_1}{\partial lat} & \frac{\partial t_1}{\partial lon} & \frac{\partial t_1}{\partial z_o} & \dots \\
 1 & \frac{\partial t_i}{\partial lat} & \frac{\partial t_i}{\partial lon} & \frac{\partial t_i}{\partial z_o} & \\
 0 & \frac{\partial dt_1}{\partial lat} & \frac{\partial dt_1}{\partial lon} & \frac{\partial dt_1}{\partial z_o} & \dots \\
 0 & \frac{\partial dt_j}{\partial lat} & \frac{\partial dt_j}{\partial lon} & \frac{\partial dt_j}{\partial z_o} & \\
 0 & \frac{\partial p_1}{\partial lat} & \frac{\partial p_1}{\partial lon} & \frac{\partial p_1}{\partial z_o} & \dots \\
 0 & \frac{\partial p_k}{\partial lat} & \frac{\partial p_k}{\partial lon} & \frac{\partial p_k}{\partial z_o} & \\
 0 & \frac{\partial azi_1}{\partial lat} & \frac{\partial azi_1}{\partial lon} & 0 & \dots \\
 0 & \frac{\partial azi_l}{\partial lat} & \frac{\partial azi_l}{\partial lon} & 0 &
 \end{bmatrix}
 \begin{bmatrix}
 \delta t_o \\
 \delta lat \\
 \delta lon \\
 \delta z_o
 \end{bmatrix}
 =
 \begin{bmatrix}
 \Delta t_1 \dots \\
 \Delta t_i \\
 \Delta dt_1 \dots \\
 \Delta dt_j \\
 \Delta p_1 \dots \\
 \Delta p_k \\
 \Delta azi_1 \dots \\
 \Delta azi_l
 \end{bmatrix}$$

where

- $t_{1,i}$ - i travel times and their residuals $\Delta t_{1,i}$
- $dt_{1,j}$ - j travel-time differences between two phases observed at the same station and their residuals $\Delta dt_{1,j}$
- $p_{1,k}$ - k observed ray parameters (or apparent velocities) observations and their residuals $\Delta p_{1,k}$
- $azi_{1,l}$ - l observed azimuth (from station to epicenter) observations and their residuals $\Delta azi_{1,l}$
- δt_o - the calculated change in the source time for one iteration
- δlat - the calculated change in the latitude for one iteration
- δlon - the calculated change in the longitude for one iteration
- δz_o - the calculated change in the source depth for one iteration (if not fixed)

Test examples

The following examples should illustrate the advantages of using travel-time differences as an additional parameter in the inversion. In the case of error-free onset observations, the travel-time differences are not independent from the absolute travel times and therefore they do not change the results of the inversions. But in the case of erroneous or insufficient data, the usage of travel-time differences can improve the result.

To demonstrate this, a synthetic example was chosen. The coordinates of the event are listed in the first row of Table 7.3.1. The travel times calculated for model AK135 (Kennett et al., 1995) to the stations ARCES, FINES, and NORES are listed in Table 7.3.2. These data were inverted to reestimate the theoretical source using different approaches. The results of these inversions are listed in Table 7.3.1. The solution and especially the depth estimation of this example is depending on the initial epicenter because of the disadvantageous geometry of source and observing stations. The initial epicenter for all further inversions was set to latitude 54.5° and longitude 21.5° ; azimuth or ray parameter values and station corrections were not used for this test. In the first two inversions the original data were inverted once with and, once without the usage of travel-time differences (TTD). The solution in both cases is within some numerical limits the same. The differences between the two solutions and the differences to the theoretical location can be partly explained by the truncation of the input onset times to 1/100 s, partly by the usage of a finishing convergence criterion for defining a solution, and partly by the disadvantageous geometry. In a next step, the absolute onset times at FINES were disturbed by adding 1 s for both phases (Pn and Sn) to simulate a systematic timing error. Because the source depth was not longer resolvable in this case, it was fixed at 10 km (S1). In the next simulation (S2) the theoretical travel times were kept originally at FINES and NORES, but a 3 s delay was added for all onsets at ARCES. This was done to simulate a station at a larger distance with a weak onset leading to late picks for both Pn and Sn. In a last test (S3) all these effects were combined: the onsets at ARCES were 3 s delayed, for FINES Sn was 1 s delayed and Pn comes 1 s too early, and both onsets at NORES come 1 s too early.

In all cases with erroneous data (S1 - S3) the inversion with travel-time differences gives a solution closer to the 'true' source and the corresponding quality parameters (i.e. standard deviations and the rms values) are smaller, as it can be expected for a least squares fit with more data. This example clearly shows that the usage of travel-time differences helps to define the best location.

The 16 August 1997 event in the Kara Sea

Finally, the new program was used to locate the seismic event of 16 August 1997 in the Kara Sea. For this event the readings of the first P and the first S onsets were precisely picked at many stations in Fennoscandia and northern Russia. Table 7.3.3 contains all readings used to locate this event; included are also assumed reading errors for these onsets. One problem to locate seismic events in this region is that the appropriate model for the upper-mantle structure in the Barents Sea is not well known. Therefore this event was located with several global and regional models; all inversions used travel-time differences as additional data. The results for the different inversions are listed in Table 7.3.4. Also given are the locations published by the IDC (REB) and the NEIC (PDE, weekly). Note that the very small rms value for the IDC solution is due to the very small number of defining onset times (5), the other 6 defining data are

azimuth and ray-parameter observations at the stations FINES, HFS, and NORES. Common for all solutions is that this event clearly occurred off-shore of Novaya Zemlya in the Kara Sea. But all different solutions including their given confidence regions span a region of about 2000km², which is double of the uncertainty assumed necessary for verifying compliance with the CTBT.

In this study the global models PREM, IASP91 and AK135 and the regional models KCA (King & Calcagnile, 1976), NORSAR (Mykkeltveit & Ringdal, 1981), and FIN (as used in Helsinki for the Nordic Bulletin, e.g. Uski & Pelkonen, 1996) were used to calculate the epicenter either with a fixed depth at 0 km or at 10 km or to calculate the hypocenter of this event. Models KCA and NORSAR were only developed for P velocities, therefore the corresponding S velocities were calculated with a v_P/v_S ratio of $\sqrt{3}$.

Another open question of this event is its depth. PDE fixed the depth at 10 km and the IDC gave a fixed depth of 0 km, which means that both data centers were not able to invert the depth from their data with their model. Except for model KCA, which had been developed mostly for the lower part of the upper mantle, all solutions show smaller uncertainties for a fixed depth of 10 km than for 0 km. Finally the inversion also included the source depth. No stable solution could be found in this case for models IASP91 and KCA. The large depth of 112 km for model FIN is clearly wrong and for model AK135 the depth could only be determined with a wrong longitude. However, the two other solutions (for models PREM and NORSAR) prefer a hypocenter deeper than 10 km. In conclusion, all these results may indicate a depth of this event in the middle crust, although reservations must be made due to the low SNR and the lack of station specific calibration data at many stations.

In all cases, the uncertainties using the NORSAR model are the smallest, i.e. this model describes quite well the regional upper mantle for events in the Novaya Zemlya region observed in Fennoscandia and northern Russia. This confirms earlier work by Ringdal et al. (1997) about the advantages of this regional model.

Remark

The program HYPOSAT is available including all necessary data files, examples, a manual, and the source code. The newest version can always be found on the ftp-server of NORSAR (ftp.norsar.no) under /pub/johannes/hyposat.

J. Schweitzer

References

- Buland, R. & Chapman C.H. (1983). The computation of seismic travel times. *Bull. Seism. Soc. Am.* **73**, 1271-1302.
- Dziewonski, A.M. & Anderson, D. L. (1981). Preliminary reference Earth model. *Phys. Earth Planet. Inter.* **25**, 297-356.

- Geiger, L. (1910): Herdbestimmung bei Erdbeben aus den Ankunftszeiten. Nachrichten der K. Gesellschaft der Wissenschaften zu Göttingen, math.-phys. Klasse, 331-349.
- Gutenberg, B. & Richter, C.F. (1933): Advantages of using geocentric latitude in calculating distances. *Gerlands Beiträge zur Geophysik* **40**, 380-389.
- Jeffreys, H. & Bullen, K.E. (1940). Seismological tables, British Association for the Advancement of Science, London.
- Kennett, B.L.N. & Engdahl, E.R. (1991). Traveltimes for global earthquake location and phase identification, *Geophys. J. Int.* **105**, 429 - 466.
- Kennett, B.L.N., Engdahl, E.R. & Buland, R. (1995). Constraints on seismic velocities in the Earth from traveltimes, *Geophys. J. Int.* **122**, 108 - 124.
- Kennett, B.L.N. & Gudmundsson, O. (1996). Ellipticity corrections for seismic phases, *Geophys. J. Int.* **127**, 40 - 48.
- King, D.W. & Calcagnile, G. (1976). P-wave velocities in the upper mantle beneath Fennoscandia and western Russia. *Geophys. J. R. astr. Soc.* **46**, 407 - 432.
- Menke, W. (1989). Geophysical data analysis: discrete inverse theory - revised edition. *International Geophysics series* **45**, Academic Press.
- Morelli, A. & Dziewonski, A.M. (1993). Body-wave traveltimes and a spherically symmetric P- and S-wave velocity model, *Geophys. J. Int.* **112**, 178-194.
- Mykkeltveit, S. & Ringdal, F. (1981). Phase identification and event location at regional distance using small-aperture array data. In: Husebye, E.S. & Mykkeltveit, S. (eds.), 1981: *Identification of seismic sources - earthquake or underground explosion*. D. Reidel Publishing Company, 467 - 481.
- Press, W.H., Teukolsky, S.A., Vetterling, W.T. & Flannery, B.P. (1992). *Numerical recipes in FORTRAN, the art of scientific computing* - second edition. Cambridge University Press.
- Ringdal, F., Kremenetskaya, E., Asming, V., & Filatov, Y. (1997). Study of seismic travel-time models for the Barents region. In: *NORSAR Semiannual Tech. Summ. 1 Oct 96 - 31 Mar 97*, NORSAR Sci. Rep. **2-94/95**, Kjeller, Norway, 102-114.
- Uski, M. & Pelkonen E. (1996). Earthquakes in northern Europe in 1995. University of Helsinki, Institute of Seismology, Report R-102, 63.
- Wadati, K. (1933). On the travel time of earthquake waves. Part. II. *Geophys. Mag. (Tokyo)* **7**, 101 - 111.

Table 7.3.1: Theoretical and inverted source coordinates either with travel-time differences (TTD) or without. The cases S1 - S3 have more or less biased onsets, for further details see text.

Time	Latitude [°]	Longitude [°]	Depth [km]	Location Error [km]	RMS [s]	Remarks
00:00:00.000	55.0000	22.0000	10.00			theoretical source
23:59:59.988 ±0.015	55.0022 ±0.0026	21.9990 ±0.0011	9.67 ±0.39	0.41	0.002	with TTD
23:59:59.985 ±0.018	55.0027 ±0.0030	21.9989 ±0.0012	9.60 ±0.46	0.51	0.002	without TTD
00:00:00.417 ±0.416	55.0016 ±0.0265	21.9244 ±0.0390	10.0 fixed	4.85	0.363	S1, with TTD
00:00:00.500 ±0.781	55.0069 ±0.0518	21.9171 ±0.0573	10.0 fixed	5.37	0.367	S1, without TTD
00:00:00.684 ±1.518	54.9728 ±0.0967	21.9053 ±0.1424	10.0 fixed	6.78	1.341	S2, with TTD
00:00:00.378 ±2.902	54.9516 ±0.1909	21.9063 ±0.2132	10.0 fixed	8.07	1.348	S2, without TTD
23:59:59.148 ±1.875	54.8996 ±0.1194	21.8362 ±0.1766	10.0 fixed	15.35	1.439	S3, with TTD
23:59:58.785 ±3.542	54.8752 ±0.2328	21.8489 ±0.2608	10.0 fixed	16.95	1.447	S3, without TTD

Table 7.3.2: The theoretically estimated onset times for the inversion tests of Table 7.3.1.

Station	Distance [°]	Phase	Onset Time
NORES	8.003	Pn	00:01:56.15
NORES	8.003	Sn	00:03:26.58
FINES	6.810	Pn	00:01:39.80
FINES	6.810	Sn	00:02:57.27
ARCES	14.676	Pn	00:03:27.28
ARCES	14.676	Sn	00:06:09.74

Table 7.3.3: The observed onsets of the 16 August 1997 Kara Sea event.

Station	Phase	Onset Time	Time Error	Azimuth	Azimuth Error
APA0	Pn	02:13:18.0	2.0		
APA0	Sn	02:15:00.0	2.0		
FINES	Pn	02:14:46.3	1.0		
HFS	P	02:15:42.5	0.5	24.0	15.0
JOF	Pn	02:14:09.9	1.0		
JOF	Sn	02:16:29.1	2.0		
KAF	Pn	02:14:39.4	1.0		
KBS	Pn	02:13:57.5	1.0		
KBS	Sn	02:16:08.1	2.0		
KEF	Pn	02:14:42.8	1.0		
KEV	Pn	02:13:25.2	0.5		
KEV	Sn	02:15:07.9	2.0		
KJN	Pn	02:14:12.7	1.0		
NORES	P	02:15:44.2	0.5	38.0	15.0
NRI	Pn	02:13:31.4	1.0		
NRI	Sn	02:15:19.1	2.0		
NUR	Pn	02:15:02.3	1.0		
PKK	Pn	02:15:07.1	1.0		
SDF	Pn	02:13:45.2	1.0		
SDF	Sn	02:15:44.7	2.0		
SPITS	Pn	02:13:44.3	0.5	106.0	15.0
SPITS	Sn	02:15:44.8	2.0	100.0	15.0
SUF	Pn	02:14:34.3	1.0		
VAF	Pn	02:14:41.4	1.0		

Table 7.3.4: Calculated hypocenters for the 16 August, 1997 Kara Sea event. Listed are the results of the international bulletins PDE (weekly) and REB and the solutions of this study for several models and source depth tests. The given uncertainties for the IDC and NEIC are 90% confidence limits and for the HYPOSAT solutions standard deviations. Additionally given is the number of defining data (#) and the rms-values for the used onset times.

Model	Origin Time	Latitude	Longitude	Depth [km]	#	RMS [s]
Data center solutions						
IDC (REB)	02:10:59.9 ±0.72 s	72.648° ±10.0 km	57.352° ±5.7 km	0.00 fixed	11	0.20
NEIC (PDEw)	02:10:59.77 ±1.03 s	72.835° ±17.0 km	57.225° ±10.3 km	10.00 fixed	7	1.4
Source fixed at 0.0 km						
PREM	02:11:01.695 ±1.304 s	72.4730 ±0.1102°	56.9182 ±0.3443°	0.00 fixed	33	5.844
IASP91	02:10:59.338 ±1.371 s	72.5256 ±0.1172°	56.9143 ±0.3662°	0.00 fixed	33	6.305
AK135	02:10:59.247 ±1.239 s	72.5181 ±0.1060°	56.9676 ±0.3308°	0.00 fixed	33	5.682
FIN	02:11:03.139 ±0.982 s	72.5176 ±0.0873°	57.2926 ±0.2724°	0.00 fixed	33	3.181
KCA	02:10:59.968 ±0.360 s	72.4594 ±0.0317°	57.4922 ±0.0940°	0.00 fixed	30	1.327
NORSAR	02:11:00.404 ±0.309 s	72.4439 ±0.0274°	57.4362 ±0.0835°	0.00 fixed	31	1.164
Source fixed at 10.0 km						
PREM	02:11:02.894 ±1.202 s	72.4691 ±0.1017°	56.9573 ±0.3173°	10.00 fixed	33	5.397
IASP91	02:11:00.561 ±1.300 s	72.5250 ±0.1114°	56.9451 ±0.3477°	10.00 fixed	33	5.967
AK135	02:11:00.481 ±1.183 s	72.5184 ±0.1014°	56.9931 ±0.3162°	10.00 fixed	33	5.409
FIN	02:11:04.315 ±0.915 s	72.5154 ±0.0814°	57.3269 ±0.2536°	10.00 fixed	33	2.897
KCA	02:11:00.969 ±0.382 s	72.4589 ±0.0337°	57.5118 ±0.1000°	10.00 fixed	30	1.435
NORSAR	02:11:01.536 ±0.276 s	72.4442 ±0.0245°	57.4672 ±0.0748°	10.00 fixed	31	1.075
Free depth						
PREM	02:11:06.182 ±1.280 s	72.4937 ±0.0874°	56.4632 ±0.3180°	25.42 ±17.87	32	3.780
AK135	02:11:10.753 ±2.150 s	72.6046 ±0.0523°	54.7204 ±0.4121°	28.05 ±23.92	30	2.377
FIN	02:11:10.179 ±0.591 s	72.5538 ±0.0493°	57.4424 ±0.1511°	112.02 ± 9.42	33	2.147
NORSAR	02:11:02.152 ±0.630 s	72.4443 ±0.0247°	57.4840 ±0.0767°	15.43 ± 5.19	31	1.080

7.4 NORSAR Large Array Processing at the IDC Testbed

Introduction

Beginning September 1, 1996, large array NORSAR (NOA) data have been continuously transmitted to the IDC. Already in April 1996, a new function, "*compute-beamform-fk*" (Fyen 1996), to be used for large array slowness vector estimation was implemented into the DFX in cooperation with SAIC staff. IDC testbed operation of this version for NOA data was initiated on October 9, 1996 and initial results from DFX processing of NOA was reported in NORSAR Sci. rep. No 2-96/97.

NOA processing at the testbed

It has earlier been found that DFX processing of the large primary array station NOA is functioning satisfactorily (see NORSAR Sci. rep. No 2-96/97). During the current reporting period, efforts have been made to find useful setup for the analysts to use ARS and XfkDisplay. ARS is used at the IDC for waveform analysis and phase picking. XfkDisplay is used to perform F/K analysis on array data, and prepare new beams for analysis.

The standard way of IDC processing is that for each origin, an array *origin beam* is prepared using the predicted slowness vector. Additionally, a beam using the DFX estimated slowness vector is prepared, called *fk beam*. After refinement of the location, the analyst may prepare either a new origin beam using ARS and with slowness vector predicted from the new location, or a new *fk beam*, using results from supplementary F/K analysis. The latter option is extensively used by the analyst.

During a visit to SAIC, La Jolla, we used ARS to find whether large array NOA analysis demanded changes to ARS or XfkDisplay. It was found that station NOA can be implemented and used for analysis just like any other array in IMS. Origin beams are prepared that make use of time delay corrections. XfkDisplay was able to perform standard F/K analysis on NOA data, and surprisingly good results were obtained.

In addition, the NOA array has features that make it possible to introduce subarray processing, but these features have not yet been tested extensively.

We have continued additional review and analysis of NOA detection processing at the testbed. In particular, we have analyzed in detail detection statistics for the period 21 August-3 September 1997, and compared them to results obtained for the earlier period 11 January-19 February 1997 (see NORSAR Sci. rep. No 2-96/97). In general, the results were similar, but some problems from the earlier period were found to have been corrected. This concerns in particular the reliability and stability of the automatic testbed processing. Details from both of these analysis periods have been reported in the CCB memo discussed below.

Operational implementation of NOA at the IDC

In cooperation with SAIC staff, we have submitted to the IDC Configuration Control Board (CCB) a memorandum proposing the inclusion of NOA as a primary station in the GSETT-3 network. This memorandum consists of a main text with general discussion of the objective,

expected benefits, possible risks and dependencies, suggested procedures and testing results. It is supplemented by three appendices, describing in detail an evaluation of the testbed processing, the overall structure of the configuration files and the detailed contents of these files.

A summary of the CCB memorandum is included as an appendix to this chapter.

Recommendations for the IDC

There are two features with the NOA array that impose demands on the software developers to do signal processing correctly. The array is large and thus sensitive to correct use of slowness and azimuth in beamforming. All seismometers have large DC offset which requires that filter processes include mean removal ("demean") and tapering. We will here list some points that we think are important for all IMS station processing.

Demean, taper, filter

For any process involving a filter operation, the data segment should be demeaned and tapered before filtering. The demean function must be based on the average value of all samples in the data segment. Sample masking from the QC operation should be included. After demean, the data should be tapered. Tapering must be applied to the start of the segment and after all known data gaps. NORSAR has submitted a code for smooth tapering to the SAIC staff. The effect of ignoring tapering is particularly exposed when using ARS. However, it is recommended that any filter operation should use tapering.

ARS

For the analyst to be able to view data with large offset, it is essential that demeaning be applied to the data. For almost all data, it is also essential that tapering be applied before filtering.

Origin beams

During the testing of ARS, it was noted that NOA origin beams had significantly smaller SNR as compared to beams formed at NORSAR. The reason for this was found to be that a fixed slowness parameter is used in the origin beam recipes. All origin beam recipes for all arrays have parameters that tell the DFX-beamer to use predicted azimuth and a fixed slowness of 0.125 sec/km (8.0 km/sec velocity). The fixed slowness is used instead of predicted slowness. For large arrays, the effect of using fixed slowness rather than predicted is a clear degradation of the beam. For a small-aperture array like Spitsbergen, the effect is not so dramatic. However, even for arrays like ARCES, the degradation of the beam is significant. When origin beams are formed for ARCES, the D-ring is excluded. This makes the array smaller, and the effect of a fixed slowness is therefore reduced. At the same time, the exclusion of the D-ring means a degradation of the noise suppression.

The reason for using fixed slowness has been that the origin may be wrong. However, in addition to origin beams, the analyst may use "fkb" beams, i.e., beams formed by using the DFX estimated slowness and azimuth. If the origin is incorrect, then this detection beam would be a better choice than forming beams with fixed slowness and azimuth predicted from the origin.

For NOA it is absolutely necessary to use predicted slowness rather than fixed slowness for origin beams, and we strongly recommend that predicted slownesses be use also for other arrays.

XfkDisplay

For NOA, the "beamform-fk" option may be used to perform time domain f/k analysis. The first implementation of this option works very well, but the possibility to switch between the time domain and frequency domain analysis is limited. We have noted that experienced analysts at CMR use XfkDisplay very often, and also use the options for change of filter bands, etc., quite extensively. We propose that this analyst tool be further enhanced to include interactive switching between standard and other types of f/k -type processing. The "beamform-fk" can be developed further by including an option to do incoherent in addition to conventional beamforming. This may be useful for all arrays, if the analyst has an easy way to switch between these methods. If such options are included, it will be necessary to extend the text on the contour plots to include a list of parameters describing the method used.

J. Fyen

B. Paulsen

References

Fyen, J. (1996): Improvement and Modifications, NORSAR Sci.Rep. No. 2-95/96.

Appendix A

Summary of a memorandum to the CCB on including NOA as a primary station in the GSETT-3 network

Statement of Objective

To include the large array NOA as a primary station in the PIDC operations pipeline. The station will replace NORES.

Summary of Proposed Change

The large NORSAR array (NOA) is designated as one of the IMS primary seismic stations. So far during GSETT-3, the small NORES array, which is located within the NOA aperture, has been used as a substitute, awaiting finalization of NOA refurbishment. NOA processing has now been extensively tested on the testbed and is ready for operational implementation. It is therefore proposed to remove station NORES from operations and install NOA.

At the moment, both NOA and NORES data are transmitted continuously to the PIDC. Subject to funding, we propose to continue transmitting NORES data to the PIDC to permit continued use of both NOA and NORES data at the testbed. Depending on testbed and operational experience, and funding, the NORES array may be included as an additional NOA subarray.

Although NOA consists of 7 (and possibly 8) subarrays, the NOA station processing with DFX will result in one arrival and one station for a detected seismic phase arrival. For analyst review, one array beam representing NOA will be used for teleseismic events.

Expected Benefits

The large NOA array has a superior capability in providing very accurate azimuth/slowness estimates as compared to the small NORES array (see Appendix A of the CCB memo).

Furthermore, NOA, which is comprised of 7 subarrays, will provide the possibility for subarray-based processing, which could take advantage of the significant signal focusing effects in improving detectability. In a longer term, it may be decided to use NORES as an additional NOA subarray to retain the regional capability. An evaluation of possible improvement in detection capability using subarray detection (by defining subarray groups using same reference as NOA), can be performed when both operations and testbed detection results are available for comparison.

A summary of testbed experience with NOA processing is presented in Appendix A of the CCB memo.

The NOA array has 7 three-component broadband instruments over an aperture of 60 km. The use of array processing techniques (F/K analysis) using broadband data is has been very useful for determining slowness vectors of surface waves.

Possible Risks and Dependencies

The use of NOA instead of NORES will mean a possible risk of reduced capability for processing of regional events in Fennoscandia. However, an update of the detection recipes to include regional phases may to some extent compensate for this. Moreover, we propose to continue transmitting NORES data to the PIDC, such that continued testbed operations using NORES and/or NOA data may be continued.

For GA processing we propose to use the same slowness/azimuth association parameters as are used for NORES. Although NOA array will show smaller azimuth residuals as compared to NORES, we do not at this stage propose to use smaller azimuth limits for NOA. Note also that the estimated slowness vector for NOA is compensated for azimuth residuals through the use of time delay corrections in the DFX "*beamform-fk*" process.

It has been demonstrated that DFX detections obtained at the PIDC testbed are in very good correspondence with detections obtained at Norway NDC. Moreover, Appendix A show that the slowness vector estimation is by far better than the one used at the NDC.

Since testbed DFX processing of NOA data started in October 1996, there has been periods where detections have been missing and false detections have been reported. This has been identified as problems with data transfer from operations to testbed, and wrong use of parameters. Since November 97, the operations data availability for NOA has been 97-99%, and the detection processing at the testbed has shown no such failures.

Summary of Testing Results

It has been demonstrated that DFX processing results for NOA are comparable to the results obtained at the NDC, and that the azimuth residuals using "*beamform-fk*" process are significantly better than those obtained by traditional beampacking (NDC process). Moreover, it has been shown that ARS analysis of NOA data can be performed just like for any other array.

Analyst Review

One NOA\cb origin beam and one NOA\fk detection beam is formed by DFX using time delay corrections, which should give the analyst nearly optimal beams for NOA arrivals. This has been verified by experienced analysts at CMR. NOA data may be sent to XfkDisplay for further analysis using standard F/K analysis, and create new NOA\fk beams. This has also been verified using ARS and XfkDisplay. New NOA\cbtmp origin beams can also be formed by ARS, and this has been verified.

For the operation of NOA as one array station, all standard analysis procedures like forming new origin beams, sending data to XfkDisplay, calculate FK and form new beams have been verified to function correctly.

Optional Analyst Review using Time-Domain F/K

XfkDisplay patch release PIDC_5.0.44 has the ability to use the "beamform-fk" process. This process is initiated if the /nmrd/ops/net/idc/static/XfkDisplay/recipe/NOA.par includes the following parameter settings:

- fk_timedelay_file= /nmrd/ops/net/idc/static/DFX/fk/fkgrid/NOA.BMFK.maxslow0.1
- max_slow=0.1
- nslow=51
- beam_timedelay_file=/nmrd/ops/net/idc/static/DFX/beam/tdcorr/NOA.tdcrr

By default, these parameters will be set in the NOA.par file, but these parameters may be set interactively by the analyst using the edit parameter option of XfkDisplay. The use of this option for many cases gives a better estimate of the slowness vector when compared to the standard F/K. Also, an SMR has been submitted to extend the capabilities of this option to include interactive switching between standard and other types of F/K processing.

Optional Analyst Review using Subarrays

The large array NOA has large amplitude variations across the array. In some areas, 2-3 subarrays have clear signals, whereas the rest of the array has no signal. In some of these cases, the full array beam will not detect the signal, and it can be useful to inspect a single subarray for a signal. Each one of the 7 subarrays has at least one region where it is clearly best.

If there are missed detections, or detections with bad slowness vector estimate, the analyst may use ARS to form subarray origin beams for inspection. In this way, if the origin is correct, the subarrays can be inspected for possible signals.

Another approach is to inspect individual sensors for signals, and then use XfkDisplay to calculate F/K and prepare subarray beam(s). For weak signals, an estimate of slowness from one good subarray may be better than full array F/K.

The basic operational concept for NOA is to use full array beams just like any other array. The use of readings from subarrays is optional as help for the analyst. If the analyst include readings from e.g. subarray NC6, the parameter files are specified such that postprocessing can be performed for station NC6. Station code NC6 will then appear in the REB, and the quality control should make sure that for the same phase, only one station from affiliation NOA should be represented in the REB. It is the authors experience that analysts have very good understanding of the use of subarrays, and problems with both subarray (e.g. NC6) and full array (NOA) station readings for same phase may not occur. Moreover, the use of a subarray rather than full array will be used only in cases where readings from the full array beam is impossible.

Configuration Files

The configuration files from the testbed necessary to implement NOA processing in operations are all listed in Section 4. They should be installed in the corresponding subdirectories in the OPS tree.

Database Tables

In order to process NOA and its subarrays, new entries need to be made in the affiliation, sensor, site, instrument and sitechan relations of the operational databases. In Appendix C to the CCB memo a list of the necessary values for the new tuples can be found.

Plan and Schedule for Implementation

We recommend implementation as soon as possible.

The following steps are necessary to implement the installation:

1. Enter necessary tuples into **site**, **sitechan**, **affiliation**, **sensor**, and **instrument** relations to allow automated and interactive processing to utilize NOA and its subarrays.
2. Install all listed configuration files from the testbed into the OPS tree.
3. Install new DFXdefault.scm file and DFX executable into operations.
4. Initiate new station NOA as a part of the automated operational pipeline.

Costs and Resources Required for Implementation

Installation of the configuration files and the Scheme and executable file should not take more than a few hours. It should be implemented by PIDC operations staff.

7.5 The seismic event near Novaya Zemlya on 16 August 1997

Introduction

On 16 August 1997, the CTBT prototype International Data Center in Arlington, Va. reported a small seismic disturbance located near the Russian nuclear test site on Novaya Zemlya. Initial IDC analysis indicated that this event could have taken place on land, and that the seismic signals had characteristics similar to those of an explosion.

The event caused significant concern in the United States and several other countries, because it was seen as a possible violation of the treaty that was signed in September 1996. Russian authorities claimed that it was a small earthquake, and not an explosion.

The 16 August 1997 event provides a very useful case study of what might happen if an unusual seismic event is detected after a CTBT enters into force. In this paper, we briefly recollect the sequence of analysis carried out at the Norwegian National Data Center for this event, including our interaction with the IDC and other countries in this analysis.

Data analysis at the prototype IDC

The PIDC located this event very well already in their Automatic Event List (AEL), which was published only hours after the event occurred. The AEL location was 72.79N, 57.37E, which turned out to be only a few tens of kilometers away from the best location that we eventually were able to calculate. Furthermore, the automatic algorithm to retrieve auxiliary data worked according to the specifications, so that Spitsbergen array data was retrieved and included in the subsequent automatic processing.

The excellent IDC performance is particularly noteworthy since only three primary stations (NORES, FINES and NRI) detected the 16 August 1997 event. Unfortunately, the key primary station for this region (ARCES) was not available due to repair work at that site. The processing and subsequent interactive analysis of the event clearly suffered from this absence, but the redundancy of seismological stations in the Fennoscandian region nevertheless contributed to alleviate this situation to some extent.

The Reviewed Event Bulletin (REB) location was published a few days later, in general accordance with the IDC time schedule. This location (72.6484N, 57.3517E) was again quite good, and did not differ much from the initial automatic location. However, the IDC used only P-phases as defining phases, due to the well-known problem of IASPEI91 vs Fennoscandian model travel times. Thus, the need to include regionally calibrated travel-time curves was accentuated by this experience.

Data analysis at the Norwegian NDC

In cooperation with colleagues in the United States, Scandinavia, Finland and Russia, NORSAR scientists carried out a detailed analysis of the 16 August 1997 event, even before the REB solution became available. To assist in this analysis, we collected considerable additional data from stations not forming part of the IMS. In particular, the entire Finnish network was made available to us, as well as data from the Apatity array in the Kola Peninsula. Station KEV in Finland had particularly high SNR, and provided a good replacement for ARCES. Some of the stations in the Northern European Network are shown in Figure 7.5.1.

Although most of these additional data were in principle available in near real-time, it took some time to collect it, because the appropriate mechanisms for on-line retrieval had not been implemented. This is clearly an area in which improved procedures are required for the future.

NORSAR and Kola Regional Seismological Centre (KRSC) worked together on locating this event, each carrying out independent analysis. Since some phase onsets were very difficult to read, this was quite useful, and the results were very consistent. We were very quickly able to confirm beyond doubt that the 16 August 1997 event was located in the Kara Sea, at least 100 km from the Novaya Zemlya nuclear test site.

Subsequent analysis resulted in only minor adjustment of the location. Our "best" result so far, using all available P and S phases and applying the Fennoscandian travel-time model, is as follows:

72.51N, 57.55E Depth = 0 km (fixed)

The error ellipse is about 10km (major semi-axis), but it is of course uncertain how well it represents the actual error. Figure 7.5.2 shows the estimated location and error ellipse, and also shows for comparison Marshall et al's (1989) location of the 1 August 1986 earthquake, which is the only confirmed earthquake previously recorded near Novaya Zemlya.

The depth of the 16 August 1997 event can, in our opinion, not be resolved on the basis of the available data. While it is true that the RMS residuals are smaller if a greater than zero depth is assumed, the available travel-time calibration and the accuracy of the phase readings are insufficient to give a confident depth estimate (See also the discussion in Section 7.3 of this report).

As is well known, epicentral location using P-phases only is less sensitive to possible errors in the regional travel-time model than locations using both P and S phases. If the SNR is sufficient, the P-phase readings can also be made with much higher accuracy than those of later phases. For illustration purposes, we have located the epicenter using the P-phases from three stations with very high SNR. These stations (Spitsbergen,

Kevo and Amderma) have well separated azimuths to the epicenter. The result is shown in Figure 7.5.3, and is in fact quite consistent with our "best" estimate, although slightly to the southwest.

The size of the 16 August 1997 event is about two orders of magnitude smaller than e.g. the underground nuclear explosion of 24 October 1990 (which was close to 50 kilotons), and is also considerably less than the nearby earthquake of 1 August 1986. The Richter magnitude is estimated to 3.5.

We have no evidence, based on our recordings, that would classify this event as an explosion. We have not been able to find Rayleigh waves corresponding to this event, and have therefore been unable to apply the Ms:mb discriminant. The P/S ratio is in our opinion inconclusive, as detailed in Section 7.6 of this report. The offshore location suggests that it was a natural earthquake. Other explanations could be forwarded, but the data does not enable us to reach a firm conclusion.

Searching for aftershocks

Perhaps the best indication of an earthquake source would be the presence of several aftershocks, if such could be found. We have carried out a detailed search for aftershocks of the 16 August 1997 event, using both Spitsbergen array data and data that later have become available at KRSC from the Amderma station south of Novaya Zemlya.

Our search of Spitsbergen data, which was conducted by detailed visual inspection of the array beam, enabled us to find a second (smaller) event from the same site a little more than 4 hours after the main event. This second event had Richter magnitude 2.6, and could be quite clearly seen to originate from the same source area (Figure 7.5.4).

This conclusion was supported when Amderma data became available at KRSC some weeks later. Figures 7.5.5 and 7.5.6 show Amderma 3-component recordings of the two events. The recordings are very similar, but as can be seen by the scaling factor in front of the traces, they differ in size by about an order of magnitude. Note the high SNR even for the smallest of the two events. The P-wave spectrum of the largest event (Fig. 7.5.7) shows that there is significant signal energy from 1 Hz up to the Nyquist frequency of 20 Hz, with maximum SNR at frequencies above 5 Hz.

In spite of very careful analysis of both Spitsbergen and Amderma data, we have not been able to identify additional aftershocks during the two weeks following the main event.

Although we were confined to carry out the search for aftershocks by visual inspection, the development currently in progress at NORSAR on establishing a method for optimized site-specific threshold monitoring (Kværna & Ringdal, 1997) holds promise to provide a simple interactive tool to aid the analyst in such searches in the future.

Conclusions

The 16 August 1997 event provides a particularly interesting case study for the Novaya Zemlya region. It highlights the fact that even for this well-calibrated region, where numerous well-recorded underground nuclear explosions have been conducted, it is a difficult process to reliably locate and classify a seismic event of approximate m_b 3.5. It is also shown that supplementary data from national networks can provide useful constraints on event location, especially if the azimuthal coverage of the monitoring network is inadequate. It thus serves to confirm the conclusions of Ringdal (1997) in this regard.

It is clear from this study that more research is needed on regional travel-time calibration, regional signal characteristics and application of $M_s:m_b$ and other discriminants at regional distances. In applying the latter criterion, it would be particularly useful to estimate an upper confidence limit on M_s for events with marginal or non-detected surface waves.

It would be a particularly useful exercise to carry out a small chemical calibration explosion in the Kara Sea, in order to improve the travel-time tables for this region. Such an explosion, even if not recorded teleseismically, would provide valuable additional information for future studies. It is well worth noting that even though many nuclear explosions have been conducted at Novaya Zemlya in the past, the value of these for such calibration is limited, since very few of the IMS stations were in operation during that time.

While the IDC processing functioned very well for this event, it should be taken due note of the fact that a second (smaller) event, not satisfying the current IDC event definition criteria, could be clearly singled out by detailed analysis of the IMS station at Spitsbergen. It might be useful to consider, for future processing, the possibility of the IDC carrying out routine searches for aftershocks in such cases of events of special interest. The optimized threshold monitoring technique could provide a useful tool to help the analyst undertake such searches efficiently and easily.

Another lesson learned from this event is the need to organize rapid retrieval of supplementary data from available national seismic stations. Such data, although not being part of the IMS, could nevertheless provide increased confidence in the IMS solutions, and thus be valuable in national CTBT monitoring.

F. Ringdal, NORSAR

T. Kvaerna, NORSAR

E.O. Kremenetskaya, KRSC

V.E. Asming, KRSC

References

- Kværna, T. & F. Ringdal (1997): Threshold Monitoring of the Novaya Zemlya Test Site, Manuscript in preparation, NORSAR, Kjeller.
- Marshall, P.D., R.C. Stewart and R.C. Lilwall (1989): The seismic disturbance on 1986 August 1 near Novaya Zemlya: a source of concern? *Geophys. J.*, 98, 565-573.
- Ringdal, F. (1997): Study of low-magnitude seismic events near the Novaya Zemlya nuclear test site, Submitted to *Bull. Seism. Soc. Am.*, Feb. 1997.

Station network

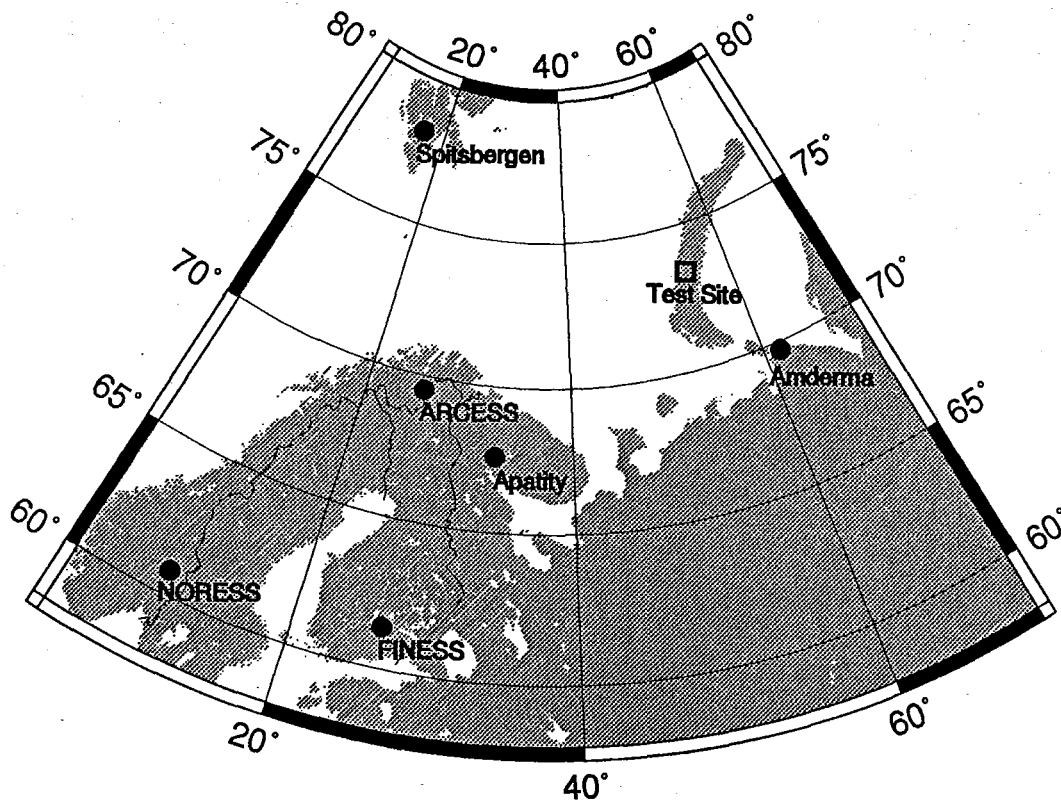


Fig 7.5.1. Map showing the locations of regional arrays in Northern Europe. The location of the northern Novaya Zemlya nuclear test site is also shown.

Location of 16 August 1997 event

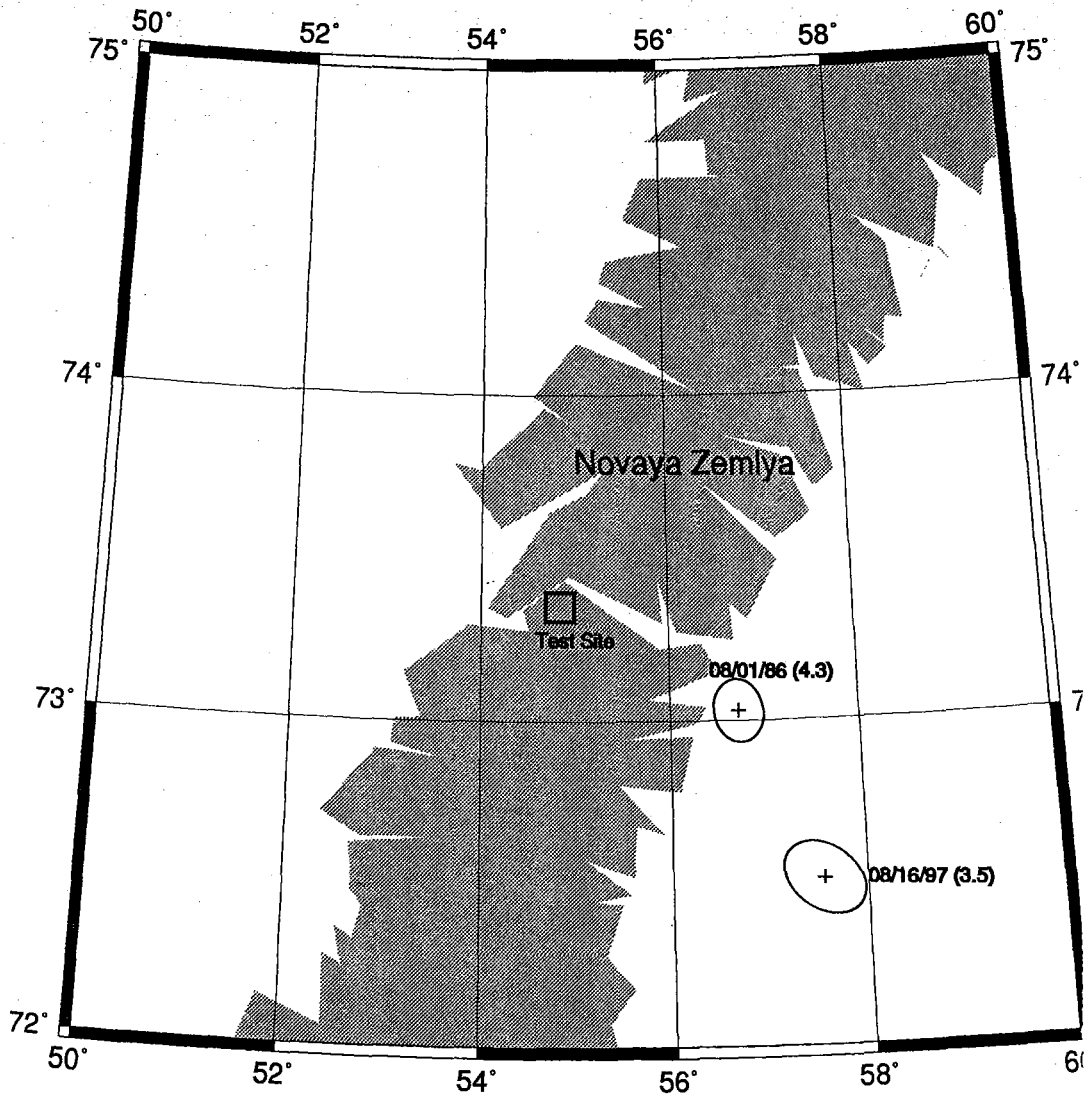
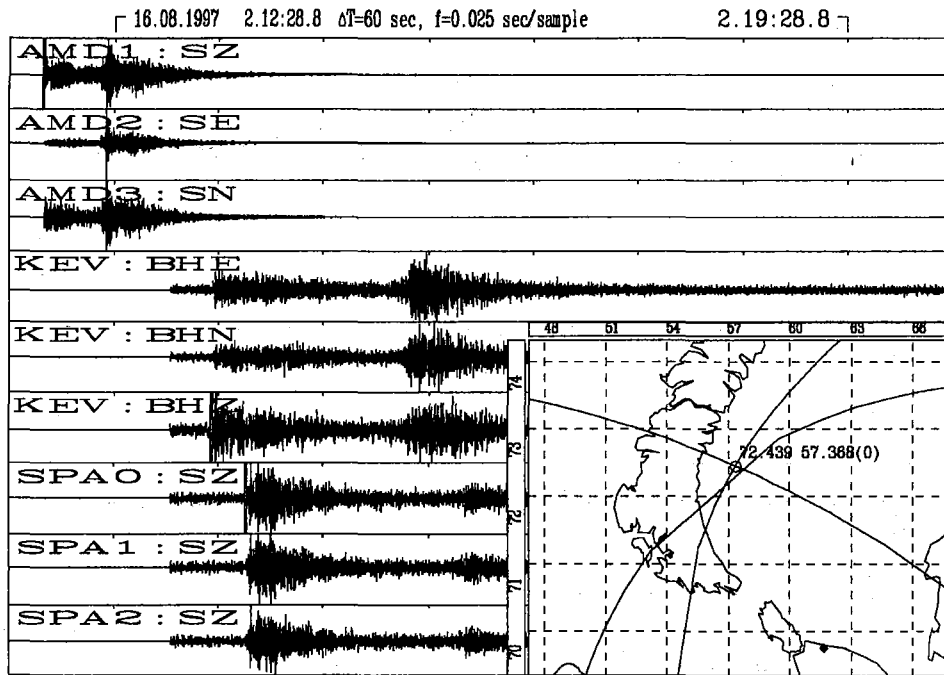


Fig 7.5.2. NORSAR's location estimates of the 16 August 1997 seismic event, together with the estimated location of the 1 August 1986 earthquake (Marshall et al, 1989). The error ellipses (90% confidence) are based on assumed prior uncertainties in the regional travel-time tables and onset time readings, and must be taken as only a tentative indication of the actual epicentral accuracy.



By P only, Depth=0

Fig 7.5.3. Illustration of the location of the 16 August 1997 seismic event using P-phases only from three stations (Anderma, Kevo, Spitsbergen). See text for comments.

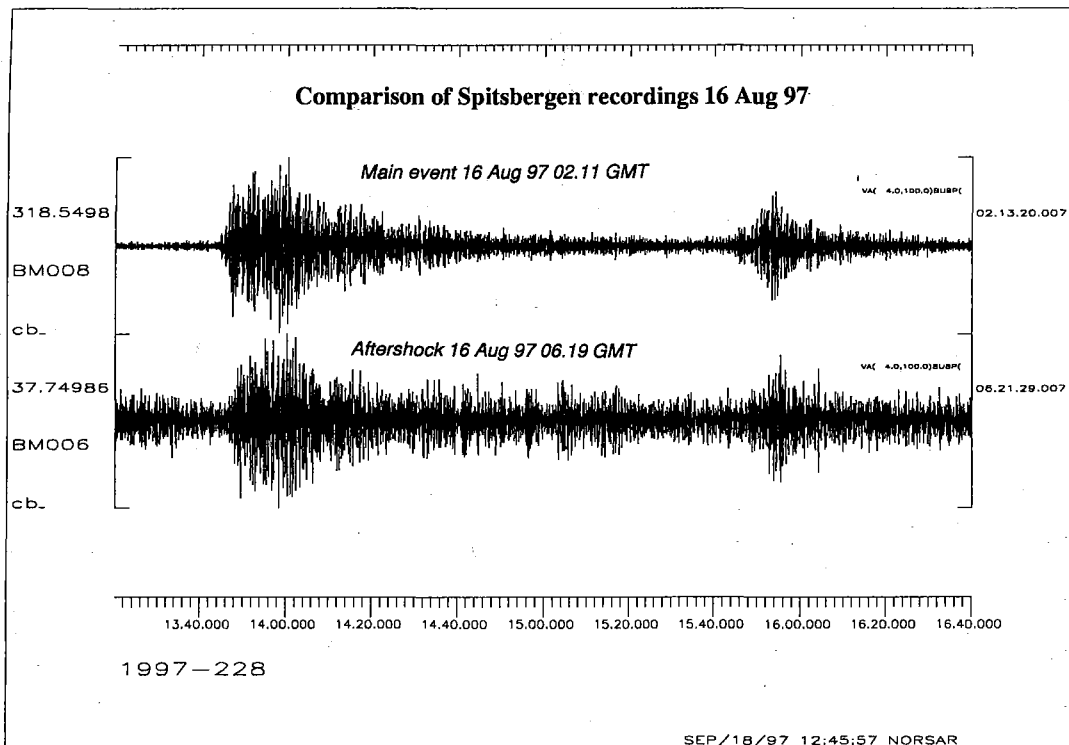


Fig 7.5.4. Recordings by the Spitsbergen array of the two events on 16 August 1997. The traces are array beams steered towards the epicenter, and with an S-type apparent velocity in order to enhance the S-phase. The traces are filtered in the 4-8 Hz band. Note that the traces are very similar, although not identical. The scaling factors in front of each trace is indicative of the relative size of the two events.

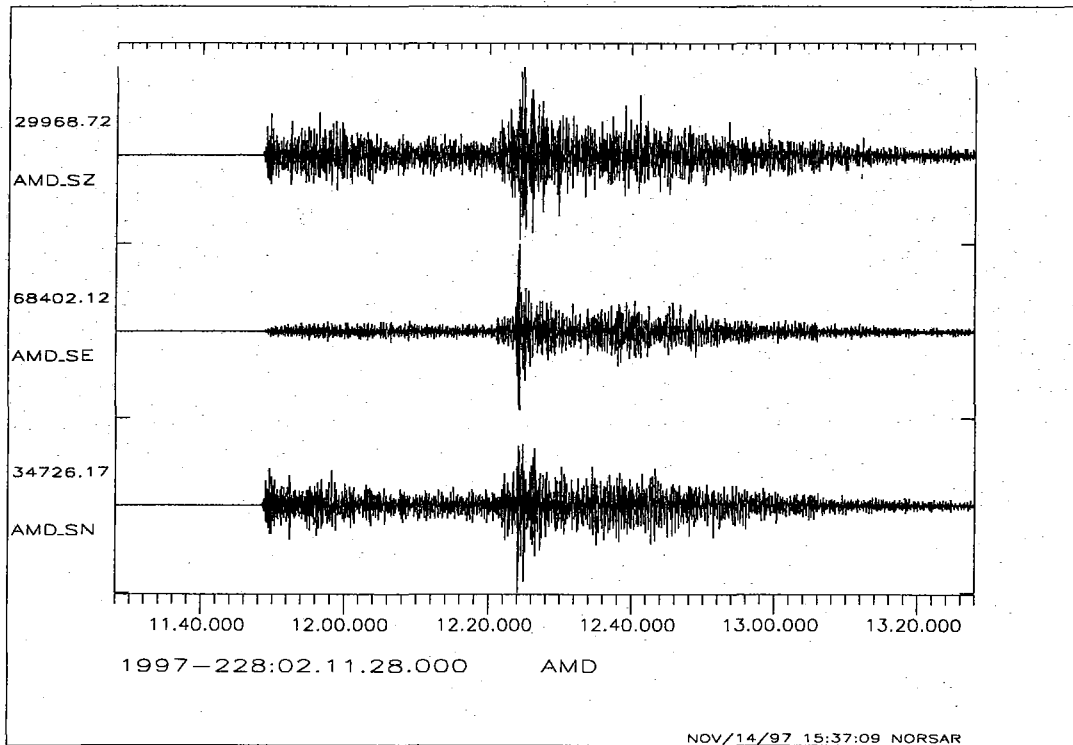


Fig 7.5.5. Recordings by the Amderma 3-component center station of the first event on 16 August 1997. The traces are filtered in the 2-16 Hz band. The scaling factor in front of each trace is indicative of the event size.

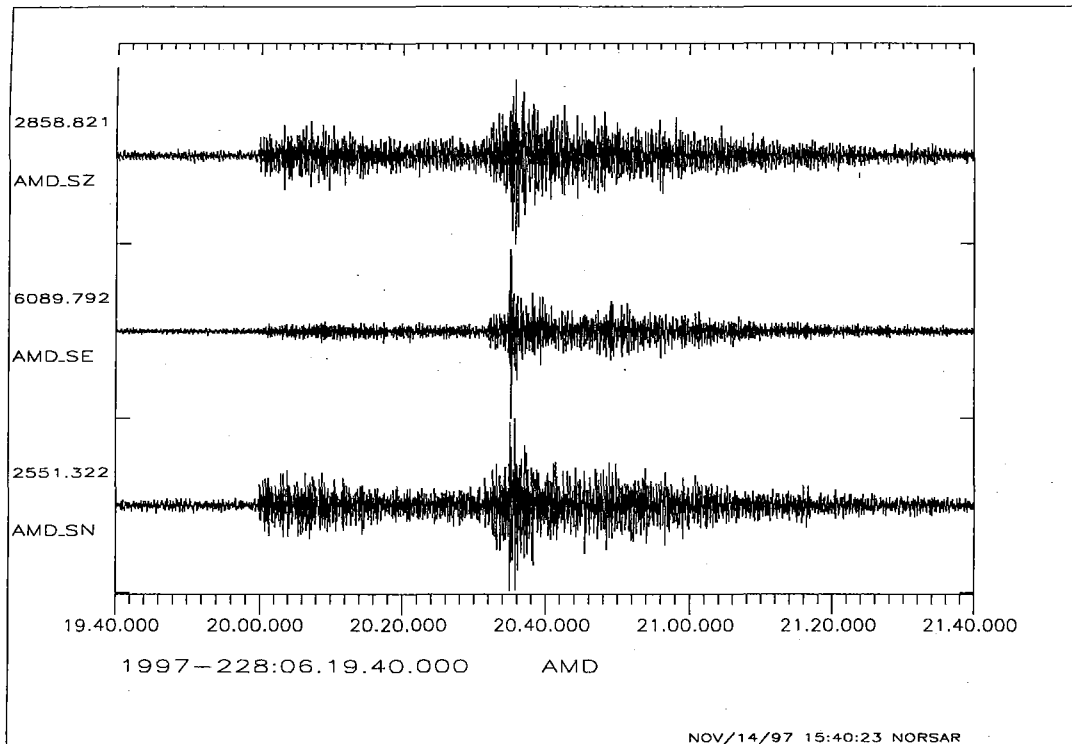


Fig 7.5.6. Recordings by the Amderma 3-component center station of the second event on 16 August 1997. The traces are filtered in the 2-16 Hz band. The scaling factor in front of each trace is indicative of the event size. Note the similarity to Figure 7.5.5.

AMD 16 Aug, 1997, 02:11 GMT

Signal and noise spectra

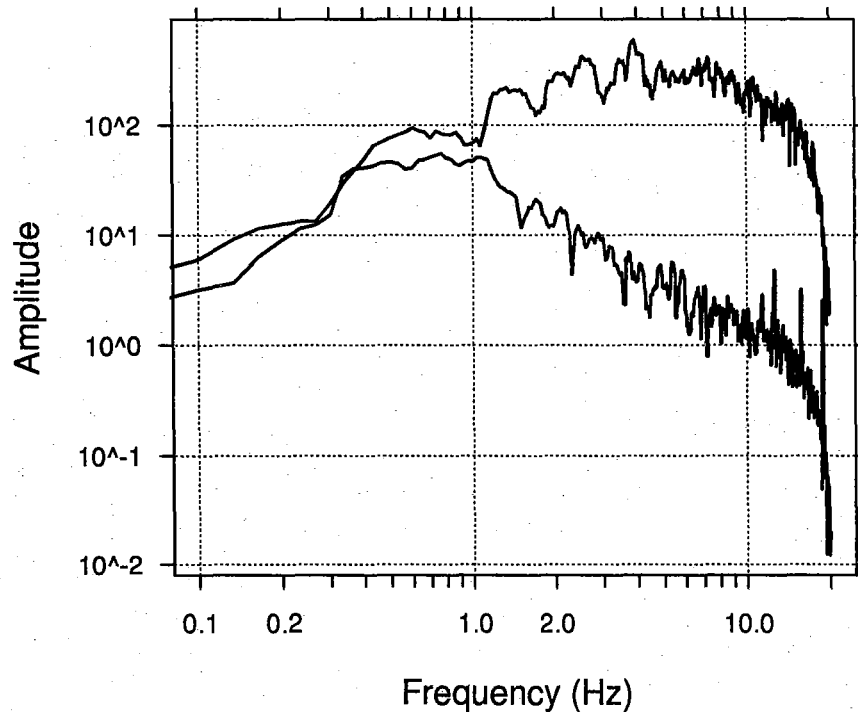


Fig. 7.5.7. P-wave and noise amplitude spectra for the Kara Sea event of 16 August 1997, 02.11 GMT as recorded by the AMD SPZ center seismometer. The spectra represent 30-second windows for both the P-phase and the noise preceding P onset. The spectra have not been corrected for system response.

7.6 P/S ratios for seismic events near Novaya Zemlya

Introduction

The seismic event near Novaya Zemlya on 16 August 1997 at 02.11 GMT has been the subject of extensive analysis in order to locate it reliably and classify the source type. Because it was detected with high signal-to-noise ratio only by stations in Fennoscandia, NW Russia and Spitsbergen, the azimuthal coverage of the recordings is insufficient to obtain a good picture of the seismic field. Nevertheless, there has been suggestions that the recorded signals at some stations show characteristics similar to those that could be expected from an explosion. On the other hand, there has also been arguments forwarded to the extent that this event could be confidently classified as an earthquake, especially based on observed P/S ratios. In this paper we consider some of this evidence in light of previous recordings of nuclear explosions.

The NORSAR large array has an extensive database of recordings from events near Novaya Zemlya, including some nuclear explosions of magnitudes similar to those of the 16 August event and the nearby earthquake of 1 August 1986 (Ringdal, 1997). It is therefore of interest to compare the P/S ratios for these events, as recorded by individual sensors in the array. In this paper, we give some comments on these observations as well as observations from other available stations at regional distances.

Before going into detail on this analysis, we note that the IDC processing of this low-magnitude event was remarkably accurate and in full accordance with the procedures envisaged for the future International Monitoring System. Even though one of the key arrays (ARCESS) was out of operation due to repairs, the IDC successfully provided an automatic location and magnitude estimate that turned out to be quite close to the solution obtained through more extensive analysis at a later processing stage.

The earthquake of 1 August 86 and the nuclear explosion of 9 October 77

Figs. 7.6.1 and 7.6.2 show recordings at five NORSAR subarrays (center sensors) for the earthquake of 1 August 1986 and the nuclear explosion of 9 October 1977. These events have similar magnitudes (4.3 and 4.5) and are also at similar epicentral distance (~20 degrees) and azimuth. The data has been filtered in the band 1.0-3.0 Hz. The following observations can be made:

- The P/S ratios show very large variability across the array for both events.
- For each sensor pair, the P/S ratios are quite similar, although P/S is slightly smaller on average for the earthquake
- The variability in the P/S ratios are dominated by strong P-wave focusing effects across NORSAR

While it is seen that the P/S for the earthquake is generally slightly smaller than for the explosion (as might be expected), it is in fact *larger* for one of the sensors (NBO00).

It must be concluded from these two figures that P/S in this frequency band is not a very powerful discriminant when using data recorded at a single array or station. Clearly, a better perfor-

mance might be expected if data from a large range of azimuths are available, but the overall performance of this discriminant is still questionable. Recent studies for Central Asia (Hartse et al, 1997), has shown that the P/S discriminant for that region appears effective at frequencies above 4 Hz, but has a poor performance for frequencies below 4 Hz. At NORSAR, there is almost no significant S-wave energy above 4 Hz, so we are confined to consider the lower frequencies.

Comparison of recordings at the same NORSAR seismometer sites

Figs. 7.6.3 and 7.6.4 show recordings of 4 events near Novaya Zemlya at NORSAR sites 02B00 and 04C00 respectively. These two sites are representative in the sense that one has a fairly large P/S ratio and the other has a fairly weak such ratio. The four events are (shown from top to bottom on the figures):

- 16 August 1997 (m_b 3.5)
- 1 August 1986 (earthquake, m_b 4.3)
- 26 August 1984 (nuclear explosion, m_b 3.8)
- 9 October 1977 (nuclear explosion, m_b 4.5)

The data has been filtered in the band 1.5-3.0 Hz, in order to maximize the SNR.

In both figures, it is very difficult to see any appreciable S-wave energy for the 16 Aug 97 event, because the noise preceding the P-phase is of the same order as the signal recorded in the S-phase window. In fact, we have been unable to find a filter band in which the S-wave of the 16 Aug 97 event is clearly defined. This of course means that the amplitude of the S-wave for this event as seen on the plots must be considered an "upper limit", making any firm conclusion rather difficult.

Nevertheless, it seems fair to state that the S-wave of the 16 August 1997 event (relative to P) is probably weaker than for the earthquake on 1 August 1986. On the other hand, the difference between the 1 August 1986 earthquake and the two nuclear explosions is not large, which is consistent with the general statements made above. Thus, the data are rather inconclusive as far as source classification of the 16 August 1997 event is concerned.

Kevo and Finess P/S ratios for NZ events

We have looked at recent data from Kevo and Finess, and compared the 16 August 1997 event to the nuclear explosion at Novaya Zemlya on 24 October 1990. The two figures that follow are descriptive of the situation:

Fig. 7.6.5 shows Kevo data (BBZ) for the two events. The data have been filtered in the band 3-5 Hz, which should be one of the more useful bands for source identification. It is obvious that the P/S ratio for the 16 August 1997 event is much smaller than for the nuclear explosion. Similar results have been obtained when comparing to other nuclear explosions in the magnitude range 5.5-6.0 (Richards and Kim, 1997).

Fig. 7.6.6 shows a similar plot (1.5-3.0 Hz) for the Finess center sensor (SPZ). At the time of the 1990 explosion, we had only the temporary Finesa configuration deployed, and the figure shows the low-gain channel from that configuration for the 1990 event. (All the other channels were severely clipped). The seismometer (Geotech S-13) and the instrument location are, however, identical for the 1990 and 1997 events, so in spite of the change of digitizer, the filtered channels should be quite comparable.

The S-phase at Finess for the 1997 event is not very distinct, but does appear to exceed the background noise. The P/S ratio in this filter band seems to be close to 1.0. For the 1990 explosion, the S phase is likewise difficult to see, but because of the strong P-phase, it is clear that the P/S ratio is well above 1. Thus, the P/S criterion as applied to Finess gives a similar result as for Kevo.

Unfortunately, we do not have data for Kevo or Finess for nuclear explosions of a magnitude similar to the 16 August 1997 event. The comparison of this event with past nuclear explosions which are two orders of magnitude larger cannot be considered conclusive, without taking into account the possibility of source scaling differences. This is discussed in more detail below.

Source scaling of the P/S ratio

To our knowledge, only one station at a regional distance, the NORSAR array, has available digital recordings of both large and small nuclear explosions from Novaya Zemlya. It may be instructive to study the P/S pattern of these explosions as a function of the event size.

In order to accomplish this, we have used the one NORSAR sensor (01A01) that has dual gain recording (the usual high-gain channel and a channel that is attenuated by 30dB). The attenuated channel has been available since 1976, and therefore provides a good data base of unclipped short period recordings of Novaya Zemlya explosions.

Fig. 7.6.7 shows a selection of nuclear explosions recorded at 01A01, with magnitudes ranging from 3.8 (26 August 1984) to 6.0 (10 August 1978). The data have been filtered in the band 1.0-3.0 Hz. There is a remarkable and systematic increase in the P/S ratio with increasing magnitude. This demonstrates that comparing the P/S ratios of large and small events could easily give misleading conclusions.

An illustration, in an expanded scale, for two of these explosions is shown in Fig. 7.6.8. The difference between these two explosions is in fact rather similar to the differences seen for the Kevo recordings shown earlier, which likewise compares a large and a small seismic event. Admittedly, the Kevo recordings are in a higher frequency band, but there is clearly reason for caution in interpreting the Kevo plots based on the results discussed above.

Because of the large epicentral distance of NORSAR from the test site, there is no appreciable high-frequency energy in the NORSAR recordings. Consequently, we have not been able to assess the possible source scaling of the P/S ratio for frequencies of 3 Hz and above. It would seem reasonable that such a source scaling might in fact be present also at these higher frequencies, but this needs to be further studied.

Conclusions

The P/S ratio as recorded by NORSAR and other available stations does not give sufficient evidence to provide a confident classification of the 16 Aug 97 event. This is mainly due to the lack of recordings of earthquakes and explosions in the Kara Sea of magnitudes similar to this event. It would be very desirable to carry out a chemical calibration explosion (in water) near the epicenter of the event. Besides contributing to improved seismic velocity models for the Barents region, such a calibration explosion would also help providing more confident classification of the 16 August 97 event, including constraints on the source depth.

The 16 August 97 event is certainly a very interesting case study for defining the potentials and limitations in classifying a low-magnitude seismic event, especially taking into account that it occurred near a known nuclear test site for which at least some calibration data exists. We will continue our analysis of this event as more data becomes available.

F. Ringdal

References:

- Hartse, H.E., S.R. Taylor, W.S. Phillips and G.E. Randall (1997). A preliminary study of regional seismic discrimination in Central Asia with emphasis on western China, *Bull. Seism. Soc. Am.* 87, 551-568
- Richards, P.G. and Won-Young Kim (1997). Test-ban Treaty monitoring tested, *Nature*, 23 Oct. 1997
- Ringdal, F. (1997): Study of low-magnitude seismic events near the Novaya Zemlya nuclear test site, *Bull. Seism. Soc. Am.* (in press)

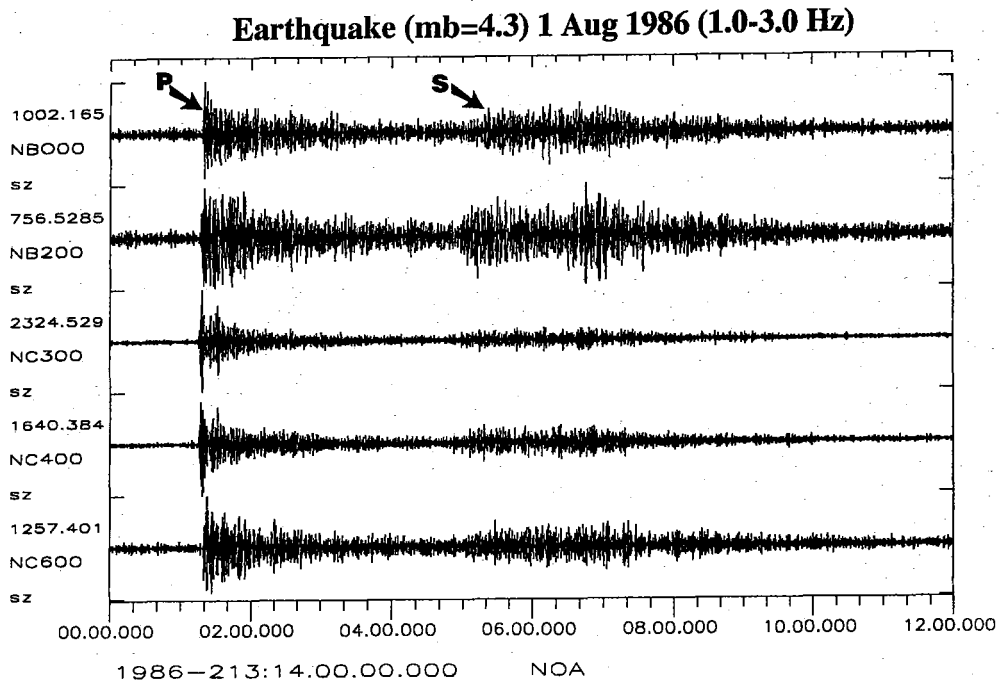


Fig. 7.6.1. Selected NORSAR SP seismometer recordings for the Novaya Zemlya earthquake of 1 August 1986. Note the strong variation in relative strength of the P and S phases across the array.

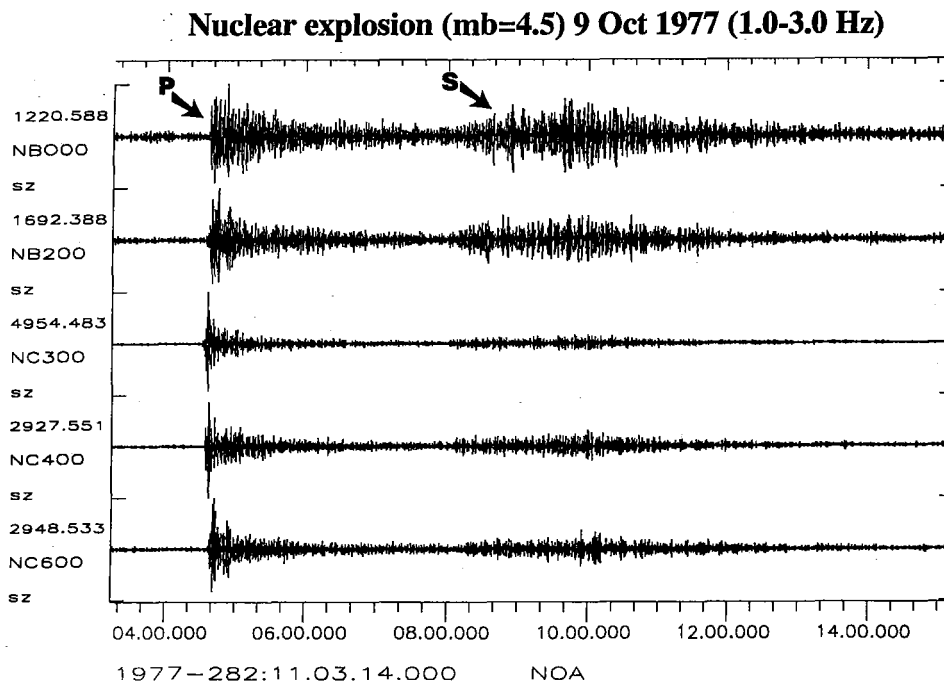
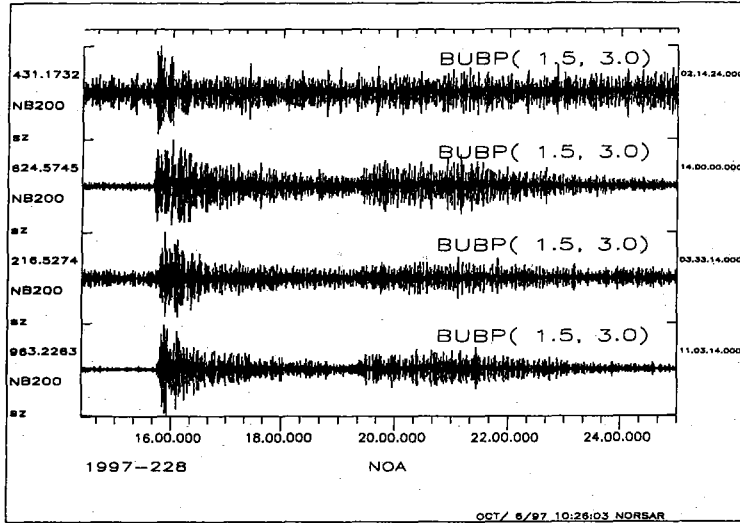


Fig. 7.6.2. Selected NORSAR SP seismometer recordings for the Novaya Zemlya nuclear explosion of 9 October 1977. Note the similarity to Fig. 7.6.1 as to the relative strength of P and S phases pairwise for the same instruments, as well as the similarity in variation across the array.

NORSAR 02B00



16 Aug 97
mb=3.5

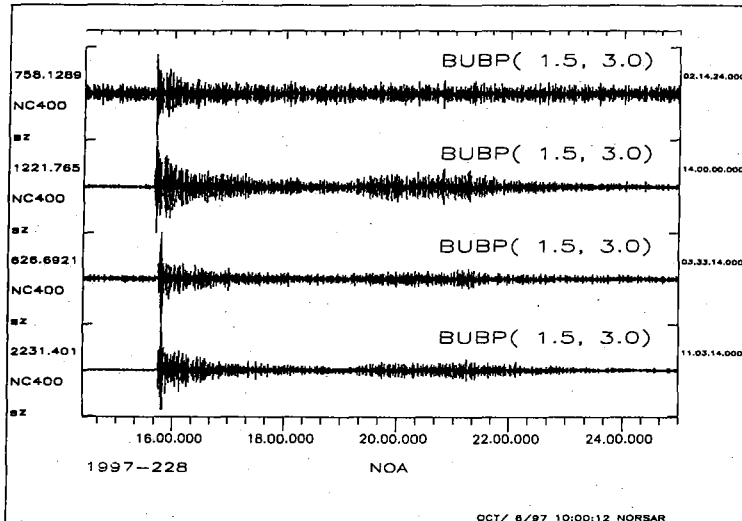
1 Aug 86
mb=4.3 (earthquake)

26 Aug 84
mb=3.8 (UNE)

9 Oct 77
mb=4.5 (UNE)

Fig. 7.6.3. Comparison of P and S recordings for four seismic events near Novaya Zemlya, as recorded by seismometer 02B00 of the NORSAR array.

NORSAR 04C00



16 Aug 97
mb=3.5

1 Aug 86
mb=4.3 (earthquake)

26 Aug 84
mb=3.8 (UNE)

9 Oct 77
mb=4.5 (UNE)

Fig. 7.6.4. Comparison of P and S recordings for four seismic events near Novaya Zemlya, as recorded by seismometer 04C00 of the NORSAR array.

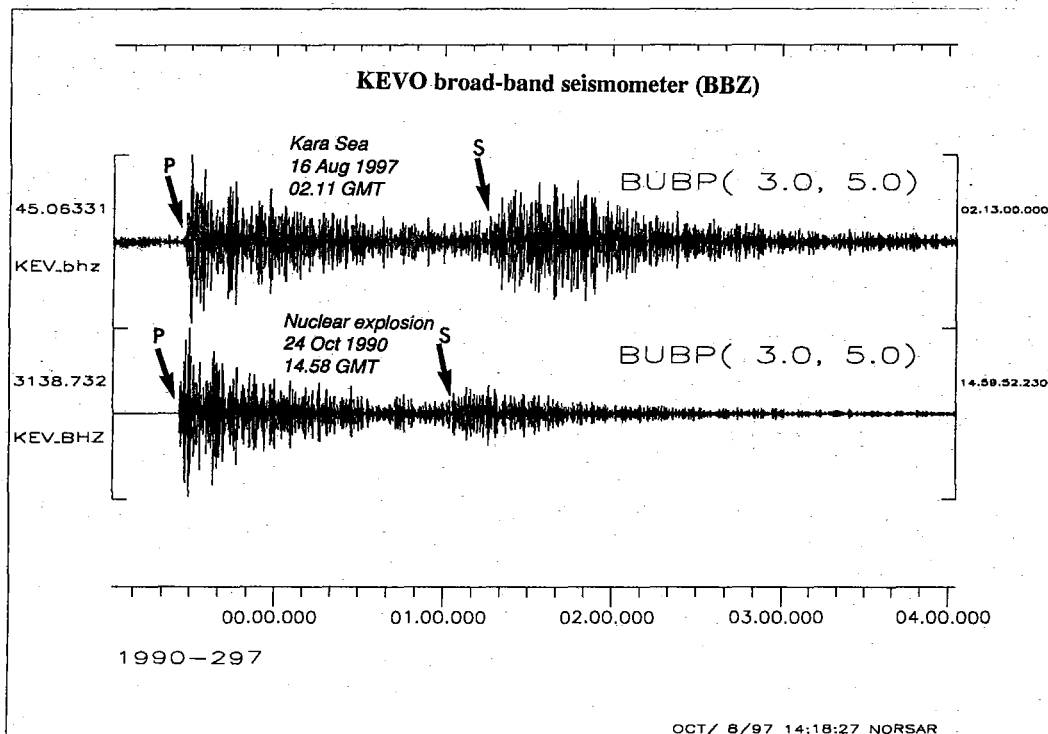


Fig. 7.6.5. Waveforms recorded by the Kevo station in Finland for the 16 August 1997 event and the nuclear explosion of 24 October 1990. Note the relatively much stronger S-phase for the first event, but also note that these two events differ in size by two magnitude units.

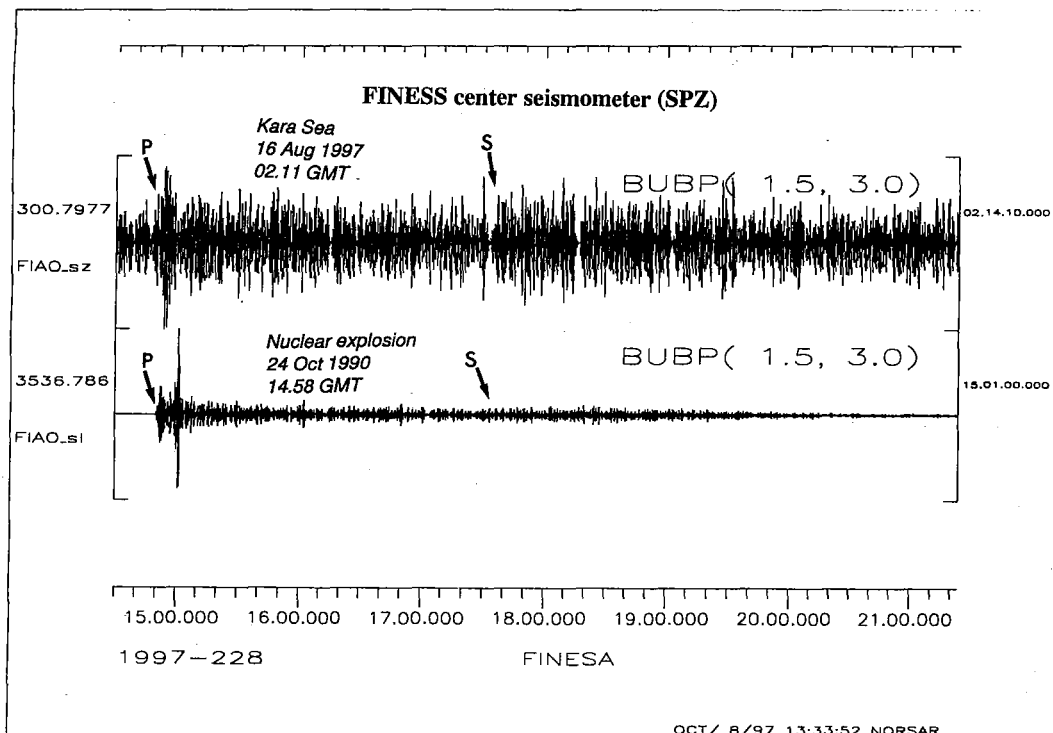


Fig. 7.6.6. Waveforms recorded by the center sensor of the Finess array in Finland for the 16 August 1997 event and the nuclear explosion of 24 October 1990. In this case, the S-phases are barely above the noise level, but it appears that the data are consistent with the picture for Kevo.

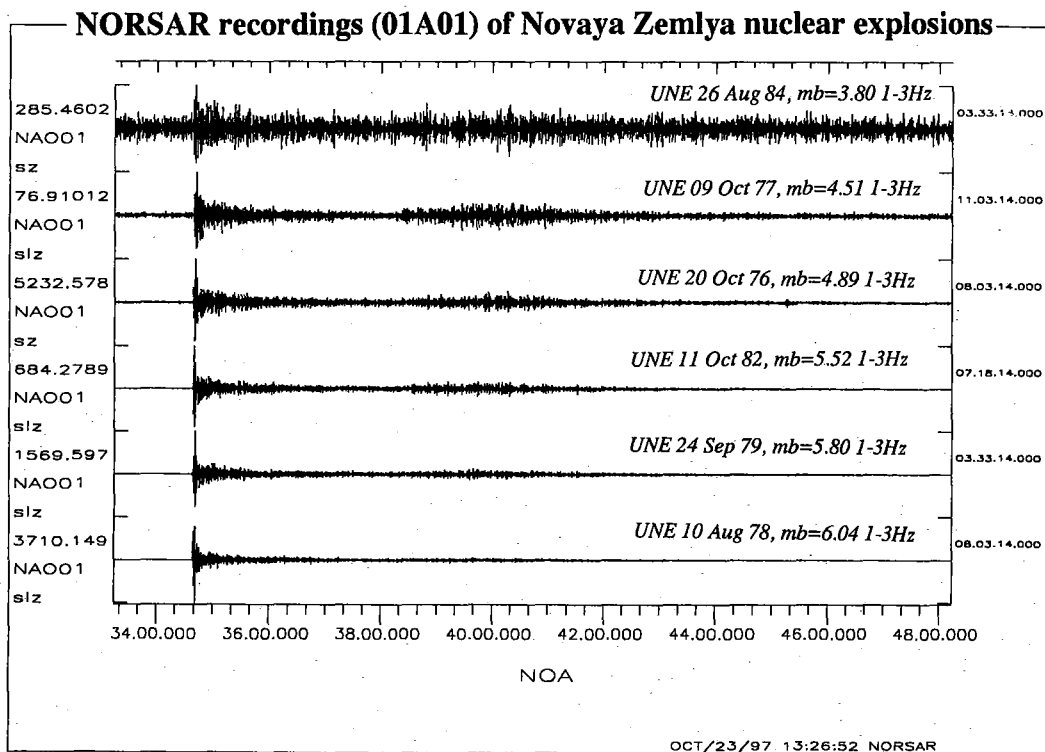


Fig. 7.6.7. NORSAR recordings (seismometer 01A01) of six Novaya Zemlya nuclear explosions of varying magnitudes. The data have been filtered in the 1-3 Hz band. Note the systematic increase in PIS ratio with increasing magnitude.

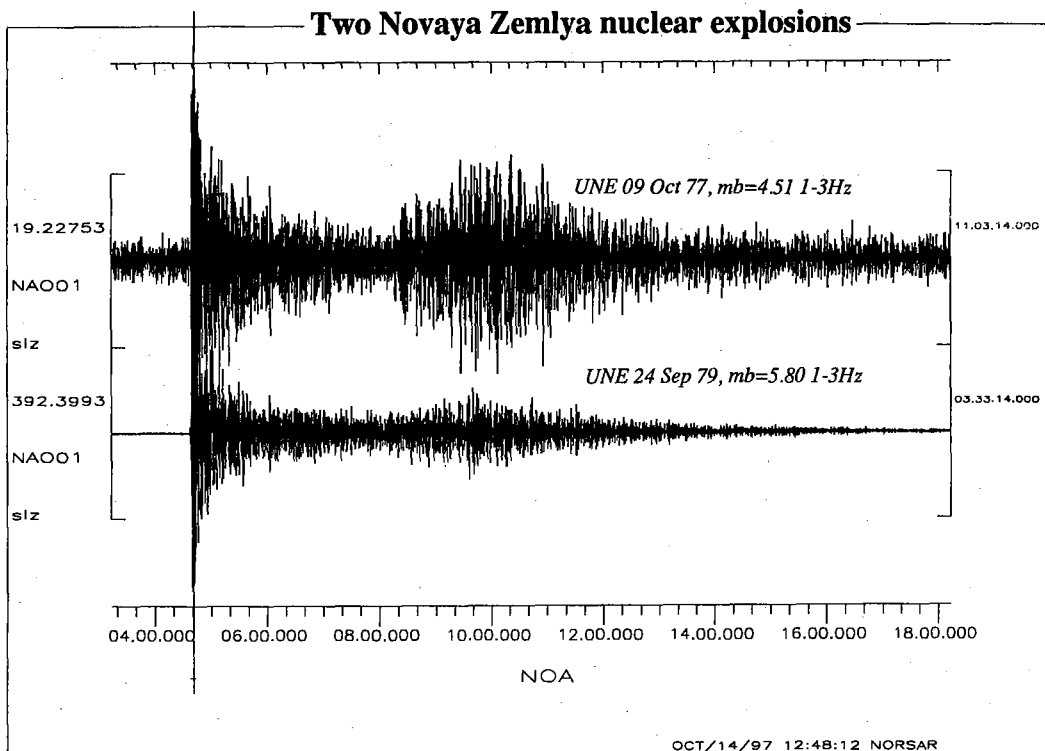


Fig. 7.6.8. NORSAR recordings (seismometer 01A01) of two of the Novaya Zemlya nuclear explosions shown in Fig. 7.6.7. The top trace shows a small explosion ($m_b=4.5$), whereas the bottom trace shows a large explosion ($m_b=5.8$). The vertical scale has been amplified to highlight the difference in PIS ratio between the two events.

7.7 Recommendations for improvements in the PIDC processing of Matsushiro (MJAR) array data

Introduction

The seismic arrays participating in the International Monitoring System (IMS) to monitor compliance with the Comprehensive Test Ban Treaty (CTBT) play an important role not only in detecting but also in defining and locating seismic events. In particular the measurements of azimuth (i.e. back azimuth, from the station to the epicenter) and ray parameter (or apparent velocity) of observed signals are used to name the onsets and to associate them to form events. Therefore all such measurements should be made as exact as possible to make them usable for all automatic data processing at the Prototype International Data Center (PIDC).

The estimates of the slowness vector of an observed seismic wave (i.e. azimuth and ray parameter) are often associated with errors. First of all the aperture and geometry of the seismic arrays limit the resolution and precision in measuring these parameters; generally spoken: the larger the aperture and the more array elements, the better the resolution capability of an array. These limits defined by the configuration of an array are additionally influenced by the actual background noise, which can distort the results, especially in the case of signals with low signal-to-noise ratios (SNR). One way to avoid (or better: to reduce) this problem is to concentrate the signal analysis in the frequency range with the best SNR. In addition, prefiltering of the data before *fk*-analysis (Schweitzer, 1994a) has been shown to be helpful to reduce the leakage of especially longer period noise into the frequency band analyzed.

Since the beginning of array seismology it has been well known that all arrays show more or less pronounced deviations of their measured azimuths and ray parameters from the theoretically estimated ones. Such deviations are commonly attributed to lateral heterogeneities of different size and structure beneath the arrays. Many studies have been undertaken to derive such deviations and to have a set of correction values available to obtain better estimates of the event location (e.g. for the arrays analyzed at the NORSAR data center the following studies can be mentioned: NORSAR (Berteussen, 1974; Fyen et al., 1995), ARCES, FINES, GERES, and NORES (Schweitzer, 1994b; Schweitzer, 1995; Schweitzer & Kväerna, 1995), and SPITS (Schweitzer, 1994b)).

The results from array measurements of onsets observed for the Matsushiro array (MJAR) in Japan show a large scatter and are thus difficult to handle by the data processing at the PIDC. Therefore the contributions of MJAR to the Reviewed Event Bulletins (REBs) were investigated in more detail to obtain as reported in this contribution recommendations for the data processing at the PIDC.

Evaluation of PIDC phase measurements; comparison of MJAR with other arrays

The results provided in the PIDC Reviewed Event Bulletins (REBs) from the GSETT-3 experiment form the basis for the investigation of mislocation vectors at different arrays. In the time period January 1, 1995 to May 27, 1997, the REBs were searched for first P-arrivals corresponding to arrivals associated by the NEIC to events in its bulletins (monthly or weekly). The azimuth and slowness estimates given in the REBs were then compared to the theoretical val-

ues for P-phases from the NEIC event locations using the IASP91 model (Kennett & Engdahl, 1991) and the tau-spline software (Buland & Chapman, 1983). In order to reduce the influence of less accurate hypocenter estimates only events were considered which were located by the NEIC with observations from at least 20 stations.

To minimize the influence of erroneous phase associations and other obvious measurement problems, the following set of acceptance criteria was introduced:

- The travel-time residual of the first onset must be less than 4 seconds.
- The reported signal period used for magnitude estimation must be larger than 0.25 seconds for teleseismic onsets (phases with theoretical ray parameter less than 10 s°).
- The length of the mislocation vector (slowness-error vector) must be less than 5 s° .

If for a given array, there is a large percentage of phases falling outside the limits given above, this gives us a hint that there may be a problem with the data processing of this array at the PIDC.

To obtain an overview of the quality of the estimated azimuths and ray parameters, the mean azimuth errors, the mean ray-parameter errors and the corresponding standard deviations were calculated. Some of the arrays were operational only for a short time period during the time interval for which the REBs were searched, and thus provided few observations, which often showed a large scatter. For further analysis it was therefore required that at least 1000 observations were available. The results are listed in Table 7.7.1 and discussed in the following.

- Table 7.7.1 clearly shows that at some arrays specific problems exist. E.g., the percentage of P-arrivals with travel-time residuals exceeding 4 seconds is high (exceeding 4.9%) for CMAR, ESDC, GERES, KSAR, MJAR and TXAR. This can be caused both by structural heterogeneities beneath the arrays or by data processing problems at the PIDC.
- The relatively high percentage of high-frequency teleseismic onsets at ARCES, NORES and SPITS is clearly due to the data processing at the PIDC. It should be noticed that the frequency analyzed in this study is **not** the frequency providing the highest SNR, but the frequency associated with the amplitude used for estimation of m_b . The standard attenuation curves for calculating event magnitudes are not calibrated for amplitudes measured at such high frequencies.
- The arrays having a large number of arrivals with large mislocation vectors are generally those with a small aperture, as evidenced by the results for FINES, HFS, and SPITS in particular. The MJAR array, however, stands out as an exception to this pattern. This array has an aperture of about 10 km, but still has a large number (22%) of arrivals with large mislocation vectors. This is an indication that there are problems with the MJAR data processing at the PIDC.
- For the number of onsets remaining after outlier rejection (#U in Table 7.7.1), the mean onset-time residual, the mean azimuth residual, the mean ray-parameter residual and the mean slowness error were calculated for each station. The positive mean travel-time residuals for all stations in Table 7.7.1 are due to the use of NEIC source times (calculated with the Jeffreys-Bullen model (1940)) and prediction of the arrivals using the IASP91 model. In

general there exists a well-known base-line shift of about 2 seconds between the IASP91 and the Jeffreys-Bullen model, so from Table 7.7.1 it cannot be concluded that any of the arrays show anomalous travel-time behavior.

- Concerning the estimates of mean azimuth and ray-parameter residuals after rejecting the outliers, there is a good correlation with the array aperture, as the two largest arrays, WRA and YKA, show the smallest deviations from the theoretical values. The scatter in the azimuth and ray-parameter measurements is mostly due to systematic mislocations or noisy data. However, some arrays like PDAR, SPITS and TXAR show very large azimuth errors and/or scatter, which is believed to be caused by the influence of dipping structures beneath the arrays. After removal of the outliers, the azimuth measurements at MJAR show no specific trend. Concerning the mean ray-parameter residuals, only PDAR and SPITS stand out as clearly having a larger scatter than the other arrays. When comparing the mean length of the mislocation vectors (rightmost column of Table 7.7.1), MJAR is one of the arrays having the largest value.

In conclusion, MJAR shows an unexpectedly large amount of "bad" azimuth and slowness estimates which cannot be explained by systematic effects caused by heterogeneities beneath the array site only.

The MJAR data

To investigate the statistics reported above for the MJAR array in more detail, a data base of MJAR recordings was created. The search criteria used were the same as those described above. The original MJAR data and associated onset parameters were retrieved from the PIDC for 294 onsets between May 1 and July 1, 1997. Fig. 7.7.1 shows the error vectors, given as the difference in this ray parameter versus azimuth space, between the PIDC slowness values and the theoretically estimated ones. The symbol (small circle) used in this figure represents the theoretical value, and the end of the line represents the PIDC estimate. As expected from the former paragraph, the amount of erroneous estimates is large quite large, but on the other hand many slowness estimates are quite good. It is also seen that for some source regions systematic shifts can be observed, which is an indication for lateral heterogeneities beneath the MJAR site. The problematic slowness estimates are not those associated with such systematic effects, but the large amount of erroneous estimates with error-vector lengths of more than 5 s° . These errors are not associated with a specific source region, epicentral distance, nor azimuth; since all slowness values are affected similarly.

The processing parameters used to analyze the data for MJAR at the PIDC were also retrieved and used in the NORSAR analysis program EP to reproduce the results of the PIDC. This did not work perfectly, although the amount of 'bad' estimates, as well as the mean features of the reported values were in general confirmed. The differences found between the PIDC and the EP results can be explained partly by different realizations of filters, fk-analysis and onset-time handling, but it also became clear that the results were strongly dependent on parameter settings such as frequency range used, analysis time window, and slowness range for the fk-analysis.

Improving the MJAR analysis

The MJAR array consists of six sites approximately situated on a circle plus one central site. The aperture of the array is about 10 km and the mean distance between neighbouring sites is about 5 km (see Fig. 7.7.2). This geometry defines the characteristic parameters of this array, which influence the results of the slowness measurements. For a monochromatic wavefront the minimum distance D_{min} between neighbouring array sites defines the maximum wavenumber K_{max} , which can be resolved by this array without distortions due to aliasing effects:

$$D_{min} = 1 / (2 \cdot K_{max})$$

The wavenumber K_{max} is related to the minimum apparent velocity V_{min} , for which a monochromatic wave with the frequency ν can be resolved:

$$K_{max} = \nu / V_{min}$$

Combining the two equations with the mean distance between neighbouring sites at MJAR of about 5 km, one gets:

$$V_{min} = 10 \cdot \nu$$

This means, e.g., that for a signal with a frequency of 1 Hz the slowness can only be correctly estimated, if the apparent velocity is higher than 10 km/s (or the ray parameter lower than 11.12 s°). Results of the fk-analysis for local or regional onsets with lower apparent velocities can be distorted by aliasing, and one may obtain a slowness solution, which actually is on a side lobe of the array transfer function. The fk-analysis as implemented at the PIDC and at NORSAR is applied to a frequency band and not to a single frequency. Results of the fk-analysis are usually presented in the form of observed energy vs. slowness. The observed energy should have its maximum at the same slowness value for all frequencies represented in the signal. But the position of the side lobes in this form is different for each frequency. Superimposing the results of all frequencies will amplify the correct slowness and reduce the side lobes. However, if the frequency pass band is relatively narrow, a side lobe may have the largest energy, and erroneous results will occur. Therefore all fk-analysis should be done with a frequency band that is chosen to be as wide as possible.

So the first attempt at solving the problem of the large amount of erroneous fk-results from analysis of MJAR data was to limit the analysis to the maximum slowness values that can be resolved for the reported dominant frequency of the onset. The parameters used in the fk-analysis at the PIDC and also the parameters chosen in this study are given in Table 7.7.2. The statistical results for this first trial - here referred to as method 'AD-HOC I' - are listed in Table 7.7.3, and Fig. 7.7.3 shows a plot of the new error vectors. Table 7.7.3 also contains the statistical values for the original PIDC results: The improvements are obvious.

Fig. 7.7.2 also gives the relative elevation of the single MJAR sites. The elevation difference between the single stations is up to 825 m. The travel-time difference for a plane wave due to this difference is up to 0.18 s for vertical incidence and an assumed mean velocity beneath the array of 4.5 km/s. This is an effect which cannot be neglected, as usually done for other arrays. To investigate the influence of the site elevation on the quality of the fk-results for MJAR data, a test called 'AD-HOC II' was performed, taking the elevation differences also into account

during the fk-analysis. A plot of the error vectors from this test can be seen in Fig. 7.7.4 and the mean errors are also given in Table 7.7.3. Again, the improvement is significant, and up to 50% (with respect to the PIDC solution) of the erroneous fk-results now disappear. But also the non-erroneous results became clearly more stable; note in particular the more consistent results for events from the same source regions and the clear decrease of the median of the slowness errors from 2.25 to 1.94 s°. The reason for the relatively large mean slowness error of MJAR (see rightmost column in Table 7.7.1) in the PIDC processing could just be the fact that the PIDC does not take the elevation differences between the single sites into account in its fk-analysis.

From the formula given above for V_{min} , it is clear that low apparent velocities are better resolved the lower the analysis frequency. Additionally, the coherency for signals above 3 Hz is relatively low, because of the large distance between the single sites of the MJAR array. Therefore a scheme to obtain the 'best' frequency range was developed and applied for the MJAR data set. The principles of this procedure can be seen in the flow chart in Fig. 7.7.5. Firstly, the detection beam is recalculated and the frequency range with the highest SNR is searched for. This frequency range is shifted as far as possible to lower frequencies because the best resolution and best signal coherence can be expected for low frequencies. Especially smaller amplitudes are often disturbed by local noise. Therefore the fk-analysis is not done for the first part of the onset, but for the part of the signal for which the SNR has its highest value. This alone contributes positively to obtaining more stable fk-results, but the best fk-parameters are found, when in an iterative process firstly the lower frequency limit and secondly the higher frequency limit are systematically modified by small steps of 0.15 Hz around the original values. For each modification of the frequency band the fk-analysis is redone. Then the final and 'best' estimate of the slowness is chosen as the one, for which the fk-quality parameter attained its highest value. This procedure adapts more precisely the frequency band to the characteristics of the actual onset. In all cases the site elevations were taken into account in the fk-analysis. Fig. 7.7.6 shows the results for the 'BEST' solution, for which the statistical values can be found in Table 7.7.3. A reduction of erroneous onsets by about 66% and a decrease of the mean length of the slowness-error vector by about 48% (compare values in the first and the last rows of Table 7.7.3) clearly demonstrate the advantages of this procedure.

Conclusions

The anomalous amount of erroneous slowness estimates for onsets at MJAR is the result of several factors. First of all, the mean minimum distances between the single sites (about 5 km) is too large for resolving the slowness of higher frequency signals. This is due to the array transfer function and the lack of signal coherency. The small number of sites makes the array additionally very sensitive to noise and other complications at any one site, since the array has practically no redundancy in its data. Applying some simple plausible changes to the parameters to estimate the slowness, a reduction of the erroneous estimates by about 30% can be achieved. A specific problem with the PIDC processing is that it does not take into account the different elevations of array sites in the fk-analysis. With a special search for the best frequency range to use in the fk-analysis for each onset, the erroneous onsets can be reduced to about 30% and all other slowness estimates are very stable. However, because of the inherent problem of the array configuration the erroneous estimates cannot be removed totally (see Fig. 7.7.6).

Recommendations for the PIDC processing of MJAR data

To stabilize the MJAR data analysis at the PIDC in the short term, the above mentioned changes in the data processing are strongly recommended:

- 1) The parameters to be used in the fk-analysis of MJAR data should be calculated in accordance to the actual frequency content of each signal, as shown in Table 7.7.2 (case AD-HOC I).
- 2) The fk-analysis routine should be modified so that elevation differences between the array sites can also be taken into account (Table 7.7.2, AD-HOC II).
- 3) A further improvement of the results can be obtained by an iterative search for the best frequency band, by choosing the analysis window around the maximum SNR value, and calculating the other parameters as shown in Table 7.7.2 (case BEST).

In a longer perspective, a modification of the MJAR array configuration (i.e. minimum distance between sites, number of sites) would be the better solution, especially in order to improve the capability for resolving also larger slowness values in a higher frequency range. The definition of additional and well analyzed S onsets would contribute to improving the location of seismic events in the whole region surrounding MJAR.

J. Schweitzer

References

- Berteussen, K.-A., 1974. NORSAR location calibration and time delay corrections. In: NORSAR Semiannual Tech. Summ. 1 Oct 73 - 31 Mar 74, NORSAR Sci. Rep. 2-73/74, Kjeller, Norway.
- Buland, R. & Chapman C.H., 1983. The computation of seismic travel times. Bull. Seism. Soc. Am. 73, 1271-1302.
- Fyen, J., Ringdal, F. & Paulsen B., 1995. Development of improved NORSAR time delay corrections. In: NORSAR Semiannual Tech. Summ. 1 April - 30 September 94, NORSAR Sci. Rep. 1-95/96, Kjeller, Norway.
- Jeffreys, H. & Bullen, K.E., 1940. Seismological tables, British Association for the Advancement of Science, London.
- Kennett, B.L.N. & Engdahl, E.R., 1991. Traveltimes for global earthquake location and phase identification, Geophys. J. Int. 105.
- Schweitzer, J. 1994a. Some improvements of the detector / SigPro - system at NORSAR. In: NORSAR Semiannual Tech. Summ. 1 Oct 93 - 31 Mar 94, NORSAR Sci. Rep. 2-93/94, Kjeller, Norway.

Schweitzer, J. 1994b. Mislocation vectors for small aperture arrays - a first step towards calibrating GSETT-3 stations. In: NORSAR Semiannual Tech. Summ. 1 April - 30 September 94, NORSAR Sci. Rep. 1-94/95, Kjeller, Norway.

Schweitzer, J. 1995. An assessment of the estimated mean mislocation vectors for small-aperture arrays. In: NORSAR Semiannual Tech. Summ. 1 April - 30 September 95, NORSAR Sci. Rep. 1-95/96, Kjeller, Norway, 128-139.

Schweitzer, J. & Kværna, T., 1995. Mapping of azimuth anomalies from array observations. In: NORSAR Semiannual Tech. Summ. 1 Oct 1994 - 31 March 95, NORSAR Sci. Rep. 2-94/95, Kjeller, Norway.

Table 7.7.1: The table gives the results from analysis of P-phase measurements at the different GSETT-3 arrays. #T is the total number of analyzed phases. NRES gives the number and percentage of phases rejected from analysis due to travel-time residuals exceeding 4 seconds. NPER gives the number and percentage of phases rejected from analysis in accordance with the requirement that the largest onset of a teleseismic phase must have a period larger than 0.25 seconds. NSLOW gives the number and percentage of phases rejected from analysis due to the length of the mislocation vector exceeding 5 s/°. #U is the number of phases remaining after the rejection of outliers, as defined by the three criteria found in the text. DT gives the mean onset-time residual and the associated standard deviation. DPHI gives the mean azimuth residual and the associated standard deviation. DR gives the mean ray-parameter residual and the associated standard deviation. DS gives the mean length of the mislocation vectors.

ARRAY	#T	NRES # %		NPER # %		NSLOW # %		#U	DT [s]	DPHI [°]	DR [s/°]	DS [s/°]
ARCES	6367	77	1.2	81	1.3	426	6.7	5783	0.59±1.35	3.51±19.82	0.62±1.32	1.64
ASAR	7238	181	2.5	22	0.3	278	3.8	6757	1.42±1.06	0.70±11.22	-0.14±1.12	1.12
CMAR	5737	471	8.2	4	0.1	124	2.2	5138	2.14±1.18	1.48±18.15	-0.56±1.33	1.85
ESDC	3429	255	7.4	0	0.0	165	4.8	3009	1.48±1.24	-2.02±17.98	0.17±1.04	1.36
FINES	6993	109	1.6	31	0.4	769	11.0	6084	0.63±1.20	3.98±25.85	0.31±1.55	1.99
GERES	6322	446	7.1	21	0.3	365	5.8	5490	1.43±1.19	6.43±26.61	-0.29±1.25	1.55
HFS	4680	105	2.2	20	0.4	804	17.2	3751	0.86±1.71	5.69±27.28	-0.38±1.86	2.35
ILAR	1374	16	1.2	0	0.0	29	2.1	1329	0.30±1.24	2.43±20.67	-0.68±1.18	1.85
KSAR	1024	57	5.6	0	0.0	37	3.6	930	1.84±1.05	1.42±12.93	0.28±0.95	1.20
MJAR	4470	261	5.8	10	0.2	979	21.9	3220	1.29±1.21	3.52±18.21	-0.11±1.24	2.19
NORES	5262	125	2.4	77	1.5	387	7.4	4673	0.63±1.57	3.39±19.02	0.37±1.48	1.76
PDAR	5109	176	3.4	1	0.0	750	14.7	4182	1.63±1.07	-8.35±40.03	-1.18±2.21	2.94
SPITS	2482	43	1.7	84	3.4	1262	50.9	1093	0.86±1.39	19.43±40.09	-0.30±2.33	3.17
TXAR	5723	282	4.9	8	0.1	256	4.5	5177	1.95±1.17	-11.28±38.59	-0.29±1.63	2.32
WRA	5633	121	2.2	13	0.2	203	3.6	5296	1.07±1.58	2.61±8.54	0.24±0.80	0.85
YKA	3403	54	1.6	1	0.0	116	3.4	3232	0.78±1.15	1.60±6.90	-0.07±0.58	0.59

Table 7.7.2: Processing parameters to estimate slowness values at MJAR. FP1 and FP2 are the lower and upper cut-off frequencies of the prefilter, respectively. FREQ is the signal frequency as measured during the detection process. FK1 and FK2 define the frequency range for the broadband-fk analysis. SMAX is the largest slowness for the fk-analysis. T1 is the lead time before the detection time or the lead time before the time of the maximum SNR value. T1 thus defines the start time of the time window for the fk-analysis; T2 is the length of this time window. The column Z indicates whether the station elevations were taken into account in the fk-analysis. For further details see the text.

METHOD	PREFILTER LOWER CUT-OFF FP1 [Hz]	PREFILTER UPPER CUT-OFF FP2 [Hz]	FK1	FK2	SMAX [s/km]	LEAD TIME T1 [s]	WINDOW LENGTH T2 [s]	Z
PIDC	0.75	8.0	FREQ*2/3	2*FK1	0.36	1.1	2.4	no
AD-HOC I	as FK1	as FK2	FREQ*2/3	2*FK1	0.1/FREQ (≥ 0.1)	10*SMAX	1 / FREQ + 20*SMAX (≥ 4.0)	no
AD-HOC II	as FK1	as FK2	FREQ*2/3	2*FK1	0.1/FREQ (≥ 0.1)	10*SMAX	1 / FREQ + 20*SMAX (≥ 4.0)	yes
BEST	0.95*FK1	1.05*FK2	best, see text	best, see text	0.1/FP1	1/FK1 before the max SNR	2 / FK1 + 2 / FP1 + 1 (≥ 5.0)	yes

Table 7.7.3: Results of the different slowness estimates of MJAR data. DS is the length of the slowness-error vector, listed both as mean value and as a median of all estimates. NUMBER OF DS > 5 (or 10) gives the number of slowness estimates for which the observed error is larger than the given value. Listed are also the mean values of the lower and upper limit of the frequency range for the broadband-fk analysis (FK1 and FK2, respectively) and the largest slowness (SMAX) for which the fk-analysis is performed.

METHOD	NUMBER OF PHASES	MEAN DS [s ²]	MEDIAN DS [s ²]	NUMBER OF DS > 10 [s ²]	NUMBER OF DS > 5 [s ²]	MEAN FK1 [Hz]	MEAN FK2 [Hz]	MEAN SMAX [s/km]
PIDC	294	5.15	2.37	45	53	0.99	1.98	0.36
Ad-Hoc I	294	3.90	2.25	30	41	0.86	1.86	0.10
Ad-Hoc II	294	3.32	1.94	24	38	0.86	1.86	0.10
BEST	294	2.66	1.84	13	18	0.66	1.45	0.18

OBSERVED RAY PARAMETER AND AZIMUTH VALUES (REBs)
 MJAR 1997, 121 - 1997, 182

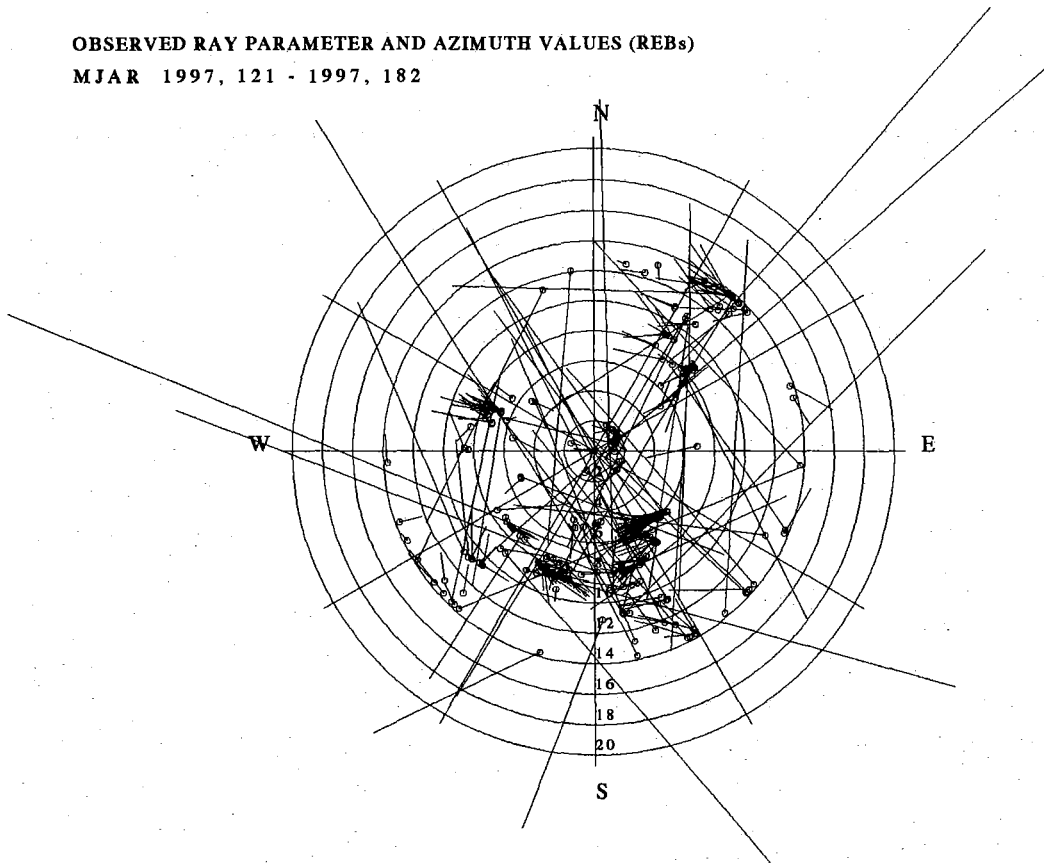


Fig. 7.7.1. Theoretical azimuth and ray-parameter values for the 294 onsets investigated are given by small circles. The corresponding values as reported by the PIDC in its final bulletins (REBs) are given as the end points of the lines.

MJAR CONFIGURATION

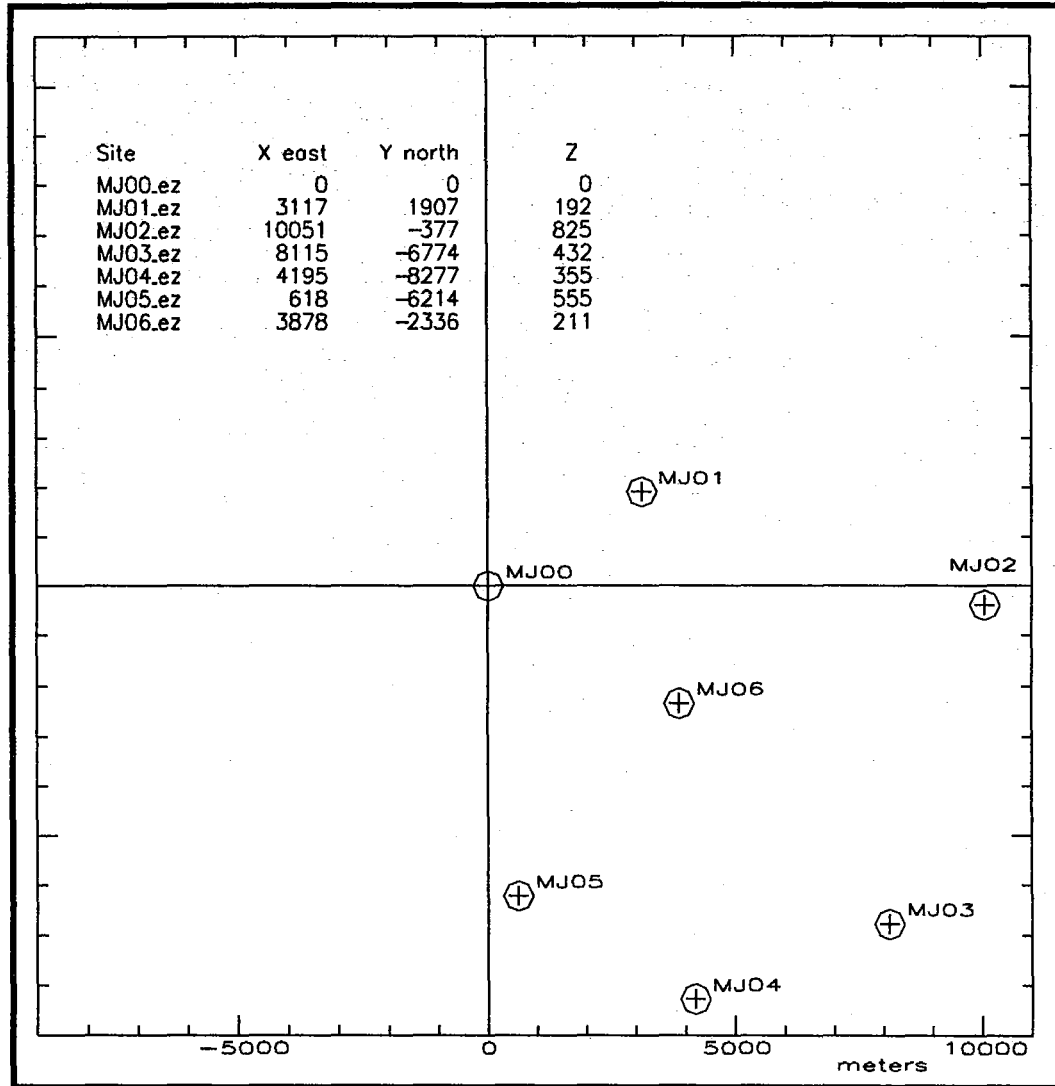


Fig. 7.7.2. The configuration of the MJAR array, with all coordinates given in m. The coordinates are relative to the array reference site MJ00. Note the large differences in the site elevations.

OBSERVED RAY PARAMETER AND AZIMUTH VALUES (AD-HOC I)
 MJAR 1997, 121 - 1997, 182

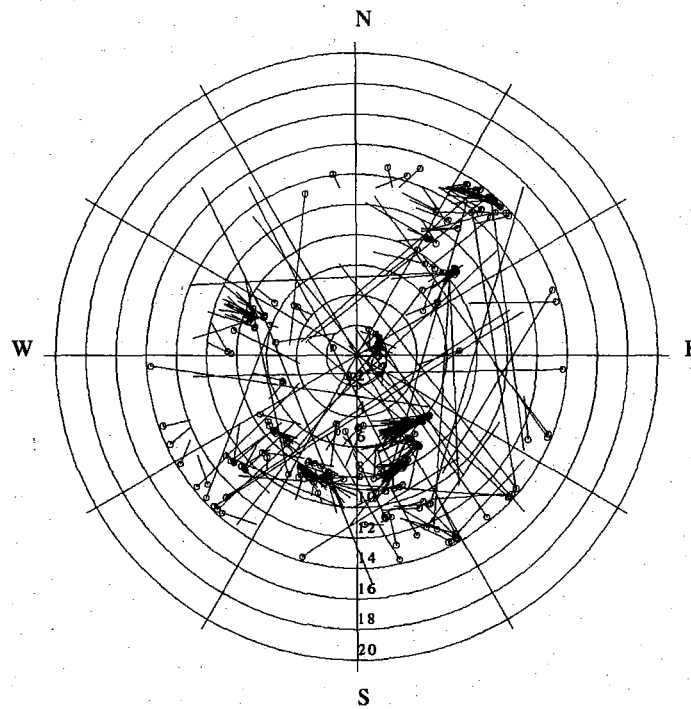


Fig. 7.7.3. Same as Fig.7.7.1 but here corresponding to parameters selected for the 'Ad-Hoc I' test to improve the fk-results, see Table 7.7.3 and the text.

MJAR 1997, 121 - 1997, 182

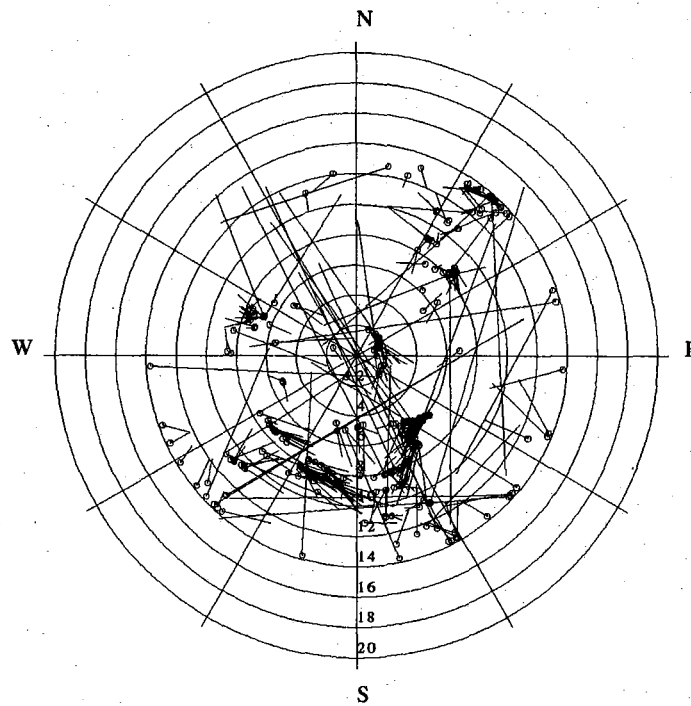


Fig. 7.7.4. Same as Fig. 7.7.3, but here the elevation differences are also taken into account in the fk-analysis.

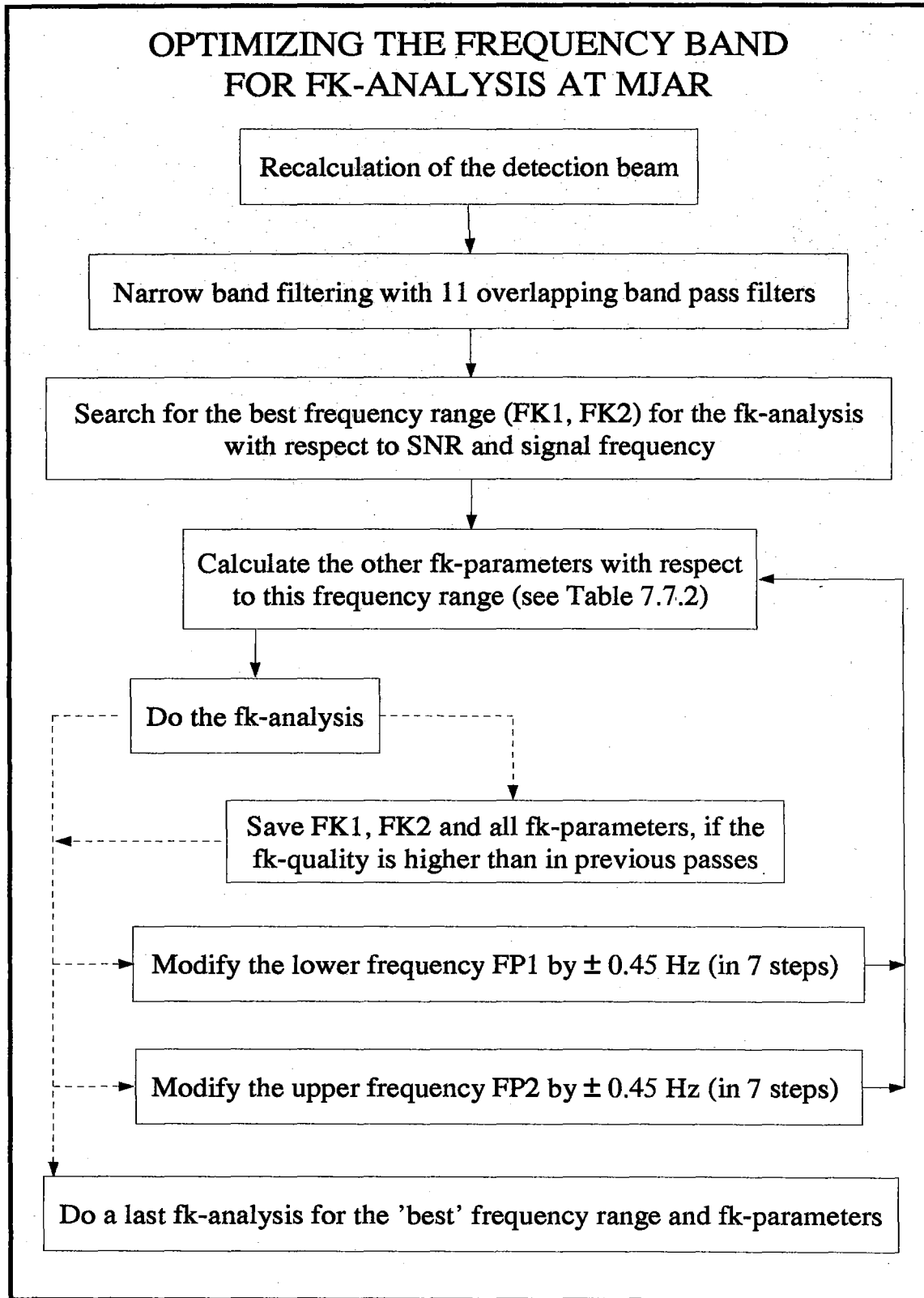


Fig. 7.7.5. This flow chart provides the details for an optimized MJAR fk-processing.

OBSERVED RAY PARAMETER AND AZIMUTH VALUES (BEST)
 MJAR 1997, 121 - 1997, 182

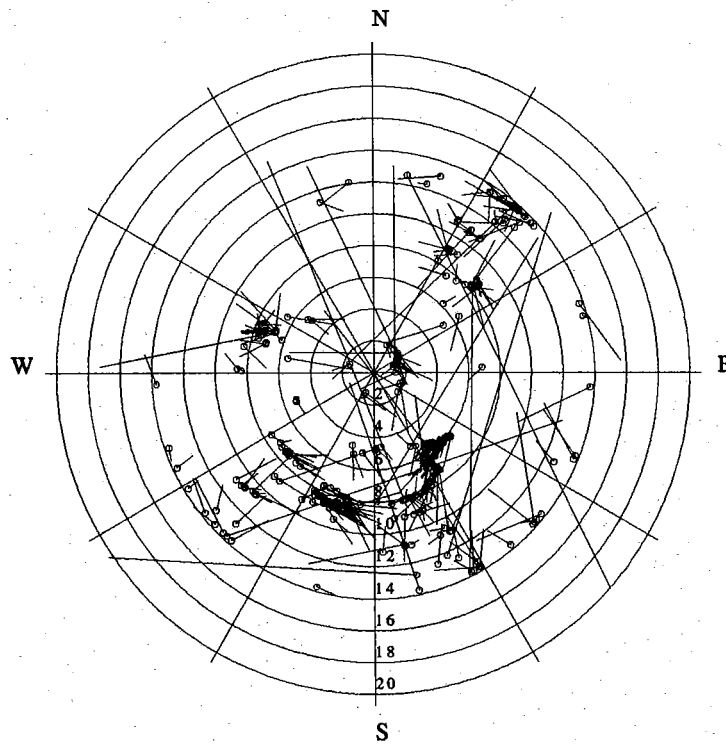


Fig. 7.7.6. Same as Fig.7.7.1, but here corresponding to parameters selected for the 'BEST' test to improve the fk-results, see Table 7.7.3 and the text.

